This is to certify that the

dissertation entitled

THE FORMATION, STRUCTURAL DYNAMICS, AND SURFACE PROPERTIES OF THIOL/GOLD SELF ASSEMBLED MONOLAYERS

presented by

David Stephen Karpovich

has been accepted towards fulfillment
of the requirements for

Ph.D. degree in Chemistry

Major professor

Date October 7, 1996

THE FORMATION, STRUCTURAL DYNAMICS, AND SURFACE PROPERTIES OF THIOL/GOLD SELF ASSEMBLED MONOLAYERS

By

David Stephen Karpovich

A DISSERTATION

Submitted to
Michigan State University
in partial fulfillment of the requirements
for the degree of

DOCTOR OF PHILOSOPHY

Department of Chemistry

1996

ABSTRACT

THE FORMATION, STRUCTURAL DYNAMICS, AND SURFACE PROPERTIES OF THIOL/GOLD SELF ASSEMBLED MONOLAYERS

By

David Stephen Karpovich

This thesis reports on the molecular-level organization and dynamical behavior of alkanethiol/gold self-assembled monolayers. The fundamental understanding developed here will allow greater preparative control and predictability in designing and building interfaces. The mass uptake associated with the formation of alkanethiol/gold monolayers was measured *in-situ* and in real time using a quartz crystal microbalance. By modeling the data using the Langmuir isotherm, thermodynamic parameters for monolayer formation were obtained. Kinetic data show that mass equilibrium is achieved in less than one minute. The formation process is not complete with initial adsorption, but includes annealing of the aliphatic chains to an ordered, all-*trans* conformation. External reflectance FTIR studies show that the time-course of this annealing process takes hours to days, and the initial adsorption conditions greatly affect the extent of the annealing.

The fluorescence response of pyrene was studied for possible use as a spectroscopic probe of alkanethiol/gold monolayer properties. The relative emission band intensities of pyrene were found to be governed by the extent of vibronic coupling between the weakly allowed first excited singlet state and the strongly allowed second

excited singlet state. This was the first fundamental photophysical explanation for the pyrene "*py*" polarity scale.

Probe molecule reorientation experiments were performed on tethered pyrene in an alkanethiol/gold monolayer. These experiments indicated that the local environments near the aliphatic chains are rigid, and the tilt angle of the aliphatic chains is 26° with respect to the surface normal. These results are fully consistent with known properties of alkanethiol/gold monolayers lending credibility to this new measurement scheme.

The mass and thickness of adsorbed layers of organic molecules on gold and thiol-modified gold were measured *in-situ*. These measurements showed no chemical specific interactions between the adsorbates and substrates. Instead it was found that the interactions of the adsorbates with the substrates are dominated by their polarizabilities. The mass versus thickness data yielded the densities of adsorbed layers which were higher than corresponding bulk liquid densities. The packing densities of the adsorbed layers are consistent with site specific adsorption indicating the importance of substrate organization on the packing of adsorbed molecules.

To My Family

ACKNOWLEDGMENTS

I wish to thank Professor Gary Blanchard, my thesis advisor and friend, for his encouragement, motivation, and advice. I am also grateful to my other committee members: Professors Kris Berglund, Marcos Dantus, and James Jackson for the invaluable professional and intellectual advice they have given me. Thanks to the Blanchard group members who were always willing to discuss ideas, listen to practice talks, and lend a hand. Heather Schessler and Saean Longiaru deserve special thanks for the great job they did on their research projects which contributed to this thesis. In addition, I wish to thank the guys in the electronics shop, the glass shop, and the machine shop. They were always willing to work with me to design and build the many unique items critical for my experiments. I especially want to thank my parents and my wife Tonya for their unconditional love and support.

Finally, I would like to thank the National Science Foundation for support of this research through grants CHE-92-11237 and CHE-95-08763.

TABLE OF CONTENTS

LIST OF TABLES

LIST OF FIGURES

Chapter 1

Introduction

Self-assembled monolayers (SAMs) were discovered in the 1980s by researchers at Bell Laboratories.[1,2] The first SAMs studied were composed of *n*-alkanoic acids adsorbed onto aluminum oxide surfaces. These monolayers formed spontaneously upon immersion of the aluminum oxide surface into an *n*-alkanoic acid in hexadecane solution. Investigation of these SAMs showed them to be very stable, chemisorbed structures. These systems were also found to be highly oriented and crystalline in nature and therefore have been thought to be ideal substrates for studying basic interfacial phenomena associated with chemical separations, molecular recognition and microdevice patterning. The widespread applicability of SAMs spawned further investigation into this field which resulted in SAMs being formed from many different chemical systems including carboxylic acids, thiols and disulfides as adsorbates and silica, silver oxide and gold as substrates.[3-6] Of these systems, one of the most widely investigated has been thiol/gold monolayers because of the facile nature of their formation and the intrinsic order available with metal substrates. [3-18]

Because of the different nature of the "head" and "tail" groups, the study of organization in these systems has been effectively separated into examinations of structure of each group. Studies of alkanethiol/gold monolayers have included investigation of aliphatic chain structure by external reflectance FTIR spectrometry.[9,19] The arrangement of the alkanethiols on the gold was studied by atomic scale microscopy.[20-23] Helium diffraction was used to study the aliphatic group arrangement

of the SAMs.[16,20] In general, it was found that the aliphatic chains resided in a very ordered, crystalline environment. The alkanethiols were found to exhibit a packing arrangement that was determined by the gold structure. The degree of ordering of alkanethiol/gold monolayers varied greatly depending on the length of their aliphatic chain.[15] For example, alkanethiols with less than ten carbons in length exhibited less aliphatic chain ordering than longer alkanethiols. From this information it is clear that interactions between adsorbates play an important role in the organization of the aliphatic functionalities.

Contact angle measurements of liquid drops on alkanthiol/gold monolayers were used to study surface properties.[3,8] These studies indicated that alkanethiol gold monolayers were hydrophobic when compared to clean metallic gold surfaces. Thiol/gold monolayers formed using carboxylic acid or hydroxyl terminated aliphatic thiols were shown to be more interactive with water than the corresponding alkane terminated monolayer. These simple yet informative measurements indicated that the surface properties of the thiol/gold monolayers could be altered significantly using thiols with functionalized terminal groups. Eventually, studies of the interaction of substances with thiol/gold monolayers focused around specific chemical recognition.[24-27]

While the average equilibrium properties of alkanethiol/gold monolayers have been studied extensively, comparatively little is understood about the formation of these SAMs. Before more elaborate SAM systems can be synthesized, knowledge of the details of alkanethiol/gold formation are needed. The few early formation studies used FTIR, optical ellipsometry, advancing contact angle measurements, and radio isotope labeling to monitor (*ex-situ*) the formation of alkanethiol/gold monolayers.[28-31] The

conclusions of these formation studies centered around optimal thiol solution composition and time of exposure of the gold surface to that solution for proper monolayer formation. A limitation of these formation studies was that the time resolution of the *ex-situ* techniques was on the order of several minutes at best so that any shorter time processes could not be resolved.

When the research for this thesis began, there were certain important concerns remaining about alkanethiol/gold monolayers despite the apparent maturity of the field. Most of the existing information on SAMs involved their equilibrium structures. More specific information about alkanethiol/gold formation was needed, especially due to the demand for tailor-made monolayers. More information was also needed regarding their structure on molecular length scales, which would play an important role in determining the utility of these systems for molecular recognition applications. Although the average mesoscopic structural properties of the monolayers had been well studied,[8,18,19,21,32] information was needed regarded the local rigidity of the aliphatic chains. Finally, more information was needed on how alkanethiol/gold monolayers, as well as interfaces in general, interact with vapor phase molecules, data which could be relevant to chemical sensing and molecular recognition. These chemical issues are addressed in this thesis using a host of measurement techniques developed during the course of this work.

In Chapter 2 the formation kinetics of alkanethiol/gold monolayers were measured *in-situ* and in real time using a quartz crystal microbalance for direct solution measurements.[33,34] This technique allows monolayer formation to be studied gravimetrically with sub-second time resolution. The formation process of alkanethiol gold monolayers was found to occur in two steps, and over two widely different time-

scales. The first step of formation, occurring in seconds, is the adsorption of thiols from solution onto the gold. The second step, occurring in hours to days, is the annealing of the aliphatic chains to ordered, crystalline-like structures. From the gravimetric data, the equilibrium constants and the free energies of formation for alkanethiols onto gold were found. It is concluded in this chapter that the alkanethiol/gold monolayer systems were not "brick-like" structures as previously thought, but rather the alkanethiols exhibited mobility across the gold surface.

Chapter 3 reports on the temperature dependence of the free energies of formation of *1*-octadecanethiol/gold monolayers.[35] From the temperature dependence of the equilibrium constants, the enthalpy of formation was determined. The entropy of formation was then found from the enthalpy and the free energies. These quantities serve to provide a measure of the robustness of the monolayers. This chapter includes a detailed discussion on the adsorption and desorption reactions involved in alkanethiol/gold formation.

Chapter 4 is a fundamental study of the spectroscopy of pyrene.[36] The study of pyrene was necessary for this research since pyrene was to be used as a probe molecule to investigate the dynamic properties of the SAMs on a short timescale (described in Chapter 5). The study described in this chapter is also useful for the general scientific community. Pyrene has been used as a probe for local polarity because its emission spectrum varies predictably with the polarity of the environment in which it resides. While this behavior of pyrene and some other PAHs has been well documented, little was known about the spectroscopic mechanism for this behavior. The mechanism is outlined in this chapter.

Chapter 5 describes a study of the structure of the local environment around the aliphatic chains on short, picosecond time-scales.[37] These studies were done by performing orientational relaxation dynamics experiments on tethered pyrene chromophores within alkanthiol/gold monolayers. The hindered rotor model was used to describe the motion of the tethered pyrene. It was found that the local environments formed by the aliphatic chains are very rigid. The results, while intuitive, demonstrate a new measurement scheme for probing molecular dynamics within interfacial films and unify the notion of structurally rigid films..

Chapters 2, 3, and 5 focus on answering the fundamental question regarding formation and structural properties of these systems. Chapter 6 focuses on the interaction of these interfaces with other molecules[38] which are important not only from a fundamental perspective, but also in the context of the chemical recognition interest and possibly separations science interest. The results are consistent with fundamental laws governing adsorbate/substrate interactions whether describing chemisorbed alkanethiols/gold or physisorbed low molecular weight molecules onto an interface. It was found in these studies that the interactions of molecules at interfaces cannot be adequately described the same as interactions of bulk molecules.

1.1. Literature Cited

1. D. L. Allara, R. G. Nuzzo, *Langmuir*, **1985,** *1*, 45.

2. D. L. Allara, R. G. Nuzzo, *Langmuir*, **1985,** *1*, 52.

3. G. M. Whitesides, P. E. Laibinis *Langmuir*, **1990**, *6*, 87.

4. A. Ulman, *Introduction to Thin Organic Films: From Langmuir-Blodgett to Self-Assembly.* Academic Press: Boston. 1991.

5. S. H. Chen, C. W. Frank, *Langmuir*, **1989**, *5*, 978.

6. P. Fenter, P. Eisenberger, J. Li, N. Camillone III, S. Bernasek, G. Scoles, T. A. Ramanarayanan, K. S. Liang, *Langmuir*, **1991**, *7*, 2013.

7. L. H. Dubois, B. R. Zegarski, R. G. Nuzzo, *J. Am. Chem. Soc.*, **1990**, *112*, 570.

8. R. G. Nuzzo, L. H. Dubois, D. L. Allara, *J. Am. Chem. Soc.*, **1990**, *112*, 558

9. R. G. Nuzzo, E. M. Korenic, L. H. Dubois, *J. Chem. Phys.*, **1990**, *93*, 767.

10. C. E. D. Chidsey, D. N. Loiacono, *Langmuir*, **1990**, *6*, 682.

11. C. E. D. Chidsey, C. R. Bertozzi, T. M. Putvinski, A. M. Mujscu, *J. Am. Chem. Soc.*, **1990**, *112*, 4301.

12. C. D. Bain, E. B. Troughton, Y. T. Tao, J. Evall, G. M. Whitesides, R. G. Nuzzo, *J. Am. Chem. Soc.*, **1989**, *111*, 321.

13. C. D. Bain, J. Evall, G. M. Whitesides, *J. Am. Chem. Soc.*, **1989**, *111*, 7155.

14. E. B. Troughton, C. D. Bain, G. M. Whitesides, R. G. Nuzzo, D. L. Allara, M. D. Porter, *Langmuir*, **1988**, *4*, 365.

15. M. D. Porter, T. B. Bright, D. L. Allara, C. E. D. Chidsey, *J. Am. Chem. Soc.*, **1987**, *109*, 3559.

16. N. Camillone III, C. E. D. Chidsey, G.-Y. Liu, T. M. Putvinski, G. C. Scoles, J. Wang, *J. Chem. Phys.*, **1991**, *94*, 8493.

17. C. E. D. Chidsey, G.-Y. Liu, G. C. Scoles, J. Wang, *Langmuir*, **1990**, *6*, 1804.

18. S. R. Wasserman, G. M. Whitesides, I. M. Tidswell, B. M. Ocko, P. S. Pershan, J. D. Axe, *J. Am. Chem. Soc.*, **1989**, *111*, 5852.

19. A. N. Parikh, D. L. Allara, *J. Chem. Phys.*, **1992**, *96*, 927.

20. C. A. Widrig, C. A. Alves, M. D. Porter, *J. Am. Chem. Soc.*, **1991**, *113*, 2805.

21. G.-Y. Liu; M. B. Salmeron; *Langmuir*, **1994**, *10*, 367.

22. R. L. McCarley, Y.-T. Kim, A. J. Bard, *J. Phys. Chem.*, **1993**, *97*, 211.

23. R. L. McCarley, D. J. Dunaway, R. J. Willicut, *Langmuir*, **1993**, *9*, 2775.

24. L. Sun, L. J. Kepley, R. M. Crooks, *Langmuir*, **1992**, *8*, 2101

25. L. J. Kepley, R. M. Crooks, A. J. Ricco, *Anal. Chem.*, **1992**, *64*, 3191.

26. O. Chailapakul, R. M. Crooks, *Langmuir*, **1993**, *9*, 884.

27. O. Chailapakul, R. M. Crooks, *Langmuir*, **1995**, *11*, 1329.

28. K. D. Truong, P. A. Rowntree, submitted to *Langmuir*.

29. C. D. Bain, E. B. Troughton, Y. T. Tao, J. Evall, G. M. Whitesides, R. G. Nuzzo, *J. Am. Chem. Soc.*, **1989**, *111*, 321.

30. E. B. Troughton, C. B. Bain, G. M. Whitesides, R. G. Nuzzo, D. L. Allara, M. D. Porter, *Langmuir*, **1988**, *4*, 365.

31. J. B. Schlenoff, M. Li, H. Ly, *J. Am. Chem. Soc.*, **1995**, *117*, 12528.

32. L. Strong, G. M. Whitesides, *Langmuir*, **1988**, *4*, 546.

33. D. S. Karpovich, G. J. Blanchard, *Langmuir*, **1994**, *10*, 3315.

34. D. S. Karpovich, G. J. Blanchard, *J. Chem. Ed.*, **1995**, *72*, 466.

35. H. M. Schessler, D. S. Karpovich, G. J. Blanchard, *J. Am. Chem. Soc.*, in press.

36. D. S. Karpovich, G. J. Blanchard, *J. Phys. Chem.*, **1995**,*99*, 3951.

37. D. S. Karpovich, G. J. Blanchard, *Langmuir*, in press.

38. D. S. Karpovich, G. J. Blanchard, *Langmuir*, in review

Chapter 2

Direct Measurement of the Adsorption Kinetics of Alkanethiol Self-Assembled Monolayers on a Microcrystalline Gold Surface

Summary

We report measurements on the adsorption kinetics of alkanethiol monolayers onto a microcrystalline gold surface. Our data indicate that the formation of this monolayer is rapid and is described by the Langmuir adsorption isotherm. The concentration dependence of the monolayer formation rate indicates that there exists an equilibrium for the adsorption/desorption process. We determine from these measurements ΔG_{ads} = - 5.5 kcal/mol for 1-$C_{18}H_{37}SH$ in *n*-hexane and cyclohexane adsorbing onto gold and ΔG_{ads} = - 4.4 kcal/mol for 1-$C_8H_{17}SH$ in *n*-hexane adsorbing onto gold.

2.1. Introduction

The study of organic interfacial monolayer systems has attracted a great deal of research attention over the past decade because of the potential utility of these interfaces in materials science and chemical separation applications. Initial work on the structural and chemical properties of interfacial organic monolayers supported on amorphous substrates required statistical treatment to understand the role of their intrinsic heterogeneity. Recent chemical advances in the formation of single molecular layers on highly ordered metal[1-4] and dielectric[5-12] surfaces has allowed the structure of these assemblies to be examined more directly by removing structural variability induced by the surface. Much of the recent work on self-assembling organic monolayers at metal surfaces has focused on the alkanethiol/gold system, where alkanethiols adsorb spontaneously onto the metal surface to form a highly ordered array.[13-25] A variety of tools have been applied in studies of these self-assembled monolayers to elucidate their molecular-scale structural properties. FTIR spectroscopy has been used most commonly for the examination of molecular ordering in these films, and these results have shown that the interface is composed of densely packed, virtually all-*trans* aliphatic chains that are tilted at ~30° with respect to the surface normal.[15] Ellipsometric and contact angle measurements have indicated that these films are uniform over macroscopic distances (several μm), and recent atomic scale microscopy has demonstrated the existence of highly regular structure on molecular length scales.[26-29] Based on this large body of information, the alkanethiol/gold system has come to be viewed as largely immobile, once formed.

McCarley's recent scanning probe microscopy work has called into question the extent to which these monolayers are "fixed" in place subsequent to adsorption.[29] The island structures formed by the alkanethiol monolayers on an evaporated gold substrate exhibited macroscopic shape changes over periods as short as minutes, and the McCarley group has concluded that these shape changes are associated with mobile defects in the gold surface and that the Au-S bond is labile.[29] This finding indicates that, either the formation of the alkanethiol monolayer has a substantial effect on the mobility of the surface gold atoms, or that the overlayer itself exhibits structural mobility.

Virtually all examinations of the alkanethiol/gold monolayer system have been performed on monolayers that were formed prior to examination, and little effort has been spent on understanding the elementary steps in the formation of the monolayers. We have chosen to examine the formation of these monolayers gravimetrically. We have measured the rate at which these monolayers form in real time by monitoring the change in mass of a quartz crystal microbalance made with evaporated gold electrodes. These data show that the alkanethiol/gold system exhibits a measurable equilibrium between adsorbed thiol and the free species. From our data we have determined that the free energy of adsorption of the alkanethiol on gold is ~ -5 kcal/mol, and this value depends slightly on the aliphatic chain length of the alkanethiol adsorbate. We therefore expect that, at any given time, a significant fraction of surface active gold sites will be exposed and thus macroscopic changes in the appearance of the surface are likely to occur. Our findings also imply that the rate of electron transfer across these monolayers is mediated by the equilibrium dynamics of the interface.

2.2. Experimental

Kinetic measurements: We used a quartz crystal microbalance (QCM) to study the adsorption kinetics of alkanethiols onto gold. A quartz crystal microbalance with a resonance frequency of ~6 MHz is sensitive to mass changes as small as several nanograms.[30] The electrodes of the QCM we use are vapor deposited gold that posses a polycrystalline, predominantly (111), surface. There are several factors in addition to the mass loading of the QCM that affect its oscillation frequency. The resonance frequency of the QCM depends on mass loading according to the Sauerbrey equation.[31] This relationship holds well for gas phase measurements, but *in situ* solution phase measurements using the QCM are, in many cases, only semi-quantitative due to capacitive and colligative effects arising from the presence of the solvent and the adlayer(s). Our primary focus in this work lies in determining the rate of mass change associated with the formation of the alkanethiol monolayer, and we do not attempt to extract absolute mass change information from our data.

The QCM was suspended in solution with isolated electrical connections for both gold electrodes using a modified spring clip. *AT*-cut quartz crystal microbalances (6 MHz resonance frequency) with vapor deposited gold electrodes were obtained from McCoy Electronics (part number 78-18-4). These QCM devices were sufficiently robust to avoid breakage from the spring clip pressure required to ensure reliable electrical contact. The QCM was connected to a 6 MHz oscillator circuit (Maxtek part number 124200-4). A frequency counter (Phillips model PM 6673) was used to monitor the QCM oscillation frequency. This frequency counter has 1 Hz resolution with a gate time of 280 ms. The analog output of this frequency counter was sent to a computer for data

processing and storage. For all adsorption rate measurements the data were acquired at a rate of ten readings per second to ensure adequate sampling of the kinetic response. All electrical connections were made using shielded coaxial cables to minimize QCM frequency instability arising from electrical interference.

The resonant frequency of a QCM is strongly temperature dependent. To minimize QCM frequency drift associated with thermal fluctuations, the temperature of the solution and the QCM were controlled to within ± 0.05 K. Measurements were performed in a 150 mL jacketed beaker connected to a flowing liquid temperature controller (Neslab model RTE-110) set to 293.0 K. Total solution volume in the jacketed beaker was 100.0 mL for each measurement. Stirring was accomplished with a magnetic stirrer and a Teflon® coated stir bar. The stirring speed was set to be as fast as possible without introducing fluctuations to the QCM baseline frequency.

Glassware was cleaned using a chromic acid solution, rinsed with distilled water and subsequently the solvent of interest prior to each measurement. The QCMs were cleaned with piranha solution (1:3 H_2O_2 (30%)/H_2SO_4) for 5 minutes, rinsed with deionized water and dried in a stream of high purity N_2. The cleaned QCMs were then rinsed with tetrahydrofuran to remove any residual water, rinsed in the solvent to be used in the experiment (*n*-hexane or cyclohexane) and used immediately thereafter. Prolonged exposure to piranha solution damaged the QCM electrodes, and this damage was manifested by an increase in frequency fluctuations for the baseline readings. A new crystal was used approximately every third run, as determined by the stability of the baseline frequency. Individual monolayer adsorption measurements began with pure solvent in the temperature controlled vessel to establish a stable QCM baseline

oscillation frequency. An aliquot of stock thiol solution was then introduced by syringe. The stock solutions were of high enough thiol concentration to allow small injection volumes, minimizing mechanical disruption of the reaction vessel contents. For 10^{-4} **M** thiol final concentration, 99.0 mL of solvent was introduced to the jacketed beaker and, after thermal equilibration, with stirring, data were collected for 10 seconds to establish a QCM baseline frequency. Injection of 1.0 mL stock 10^{-2} **M** alkanethiol yielded a 10^{-4} **M** final concentration in the reaction vessel. The stock solutions were maintained at the same temperature as the solvent in the reaction vessel to avoid thermal disruptions from injection.

External Reflection FTIR measurements: We obtained infrared spectra of the adsorbed films via external reflection infrared spectroscopy using a Nicolet 520 Fourier transform infrared spectrometer. The spectrometer was equipped with a cooled MCT detector. The external reflection sample mount and optics used were obtained from Harrick Scientific Corp. and the polarization of the IR light was controlled using a Cambridge Physical Sciences broad band IR polarizer. The light was *p*-polarized and was incident at 75° with respect to the surface normal of the QCM. Achieving an 86.5° incidence angle to maximize the signal was not possible because of the geometric constraints imposed by the QCM electrode dimensions. Spectral resolution was 2 cm^{-1} for the scans we report here.

Chemicals. The alkanethiols 1-octadecanethiol and 1-octanethiol were purchased from Aldrich Chemical Co. and were used as received. These thiols were tested by gas chromatography and mass spectrometry to determine the presence of the corresponding dialkyl disulfide, and none was detected. The solvents *n*-hexane,

cyclohexane, and tetrahydrofuran were purchased from Baxter (Burdick and Jackson, UV spec. grade) and were used without further purification.

2.3. Results and Discussion

Despite extensive investigation of equilibrated alkanethiol monolayers, there is little fundamental information on the kinetics or energetics of their formation. Methods used commonly for the examination of alkanethiol-gold monolayers, such as external reflection infrared spectroscopy, contact angle measurement and optical ellipsometry, are sensitive to structural properties on a length scale many times longer than the aliphatic chains that comprise the monolayer, but, more importantly, these methods have been used to measure the response of an equilibrated chemical system. In the work we report here, we determine the rate of mass change of the alkanethiol-gold interface resulting from adsorption of alkanethiol from solution onto gold. This kinetic response, arising from systems that are initially far from equilibrium, provides fundamental information on the initial steps of the alkanethiol monolayer self-assembly process.

To provide a frame of reference, we recap briefly what is known about alkanethiol monolayers. Diffraction and scanning microscopic measurements have shown that these systems form a hexagonal close packed monolayer structure on Au(111) surfaces,[23,27,32,33] with infrared measurements showing that the all-*trans* aliphatic chains of the alkanethiol are oriented at ~30° with respect to the gold surface normal, and are rotated ~55° with respect to the plane formed by the surface normal and the orientation vector of the chain.[15] These monolayers are packed densely, with an interchain spacing of ~5Å, established by He diffraction measurements and corroborated by STM data.[23,26,32] While these monolayers were thought to be comparatively rigid

until recently, McCarley's STM measurements have provided compelling evidence for structural mobility within these monolayers.[29] In addition, several recent studies of electron transfer across these monolayers have suggested that the rate of transfer is mediated by the density of defect sites. The data that we present in this paper provide an explanation for these recent observations, and demonstrate that the apparently labile nature of these monolayers is a natural consequence of the strength of the bond responsible for the initial formation of the monolayer.

We have examined the formation kinetics for the alkanethiol-gold monolayer from two different solvents and for two different alkanethiol aliphatic chain lengths. 1-octadecanethiol was adsorbed onto the QCM electrodes from both *n*-hexane and cyclohexane and 1-octanethiol was adsorbed from *n*-hexane. For each of these chemical systems, data were collected over an alkanethiol concentration range large enough to establish the region in which the Langmuir isotherm predictions hold. Raw data (QCM resonant frequency vs. time after thiol introduction) for the adsorption of 1-octadecanethiol from a 10^{-4} **M** solution in *n*-hexane are shown in Figure 2.1. It is immediately apparent from these data that a chemical equilibrium is achieved within a very short time (<1 minute) following thiol introduction. Further, the rate at which this equilibrium is achieved depends on the concentration of the thiol (Figure 2.2), and it is information from this concentration dependence that yields the free energy of adsorption for these systems.

The adsorption reaction we detect is believed to be[34]

$$Au(s) + RS - H(solv.) \Leftrightarrow RS - Au(s) + \frac{1}{2}H_2(solv.) \qquad 2.i$$

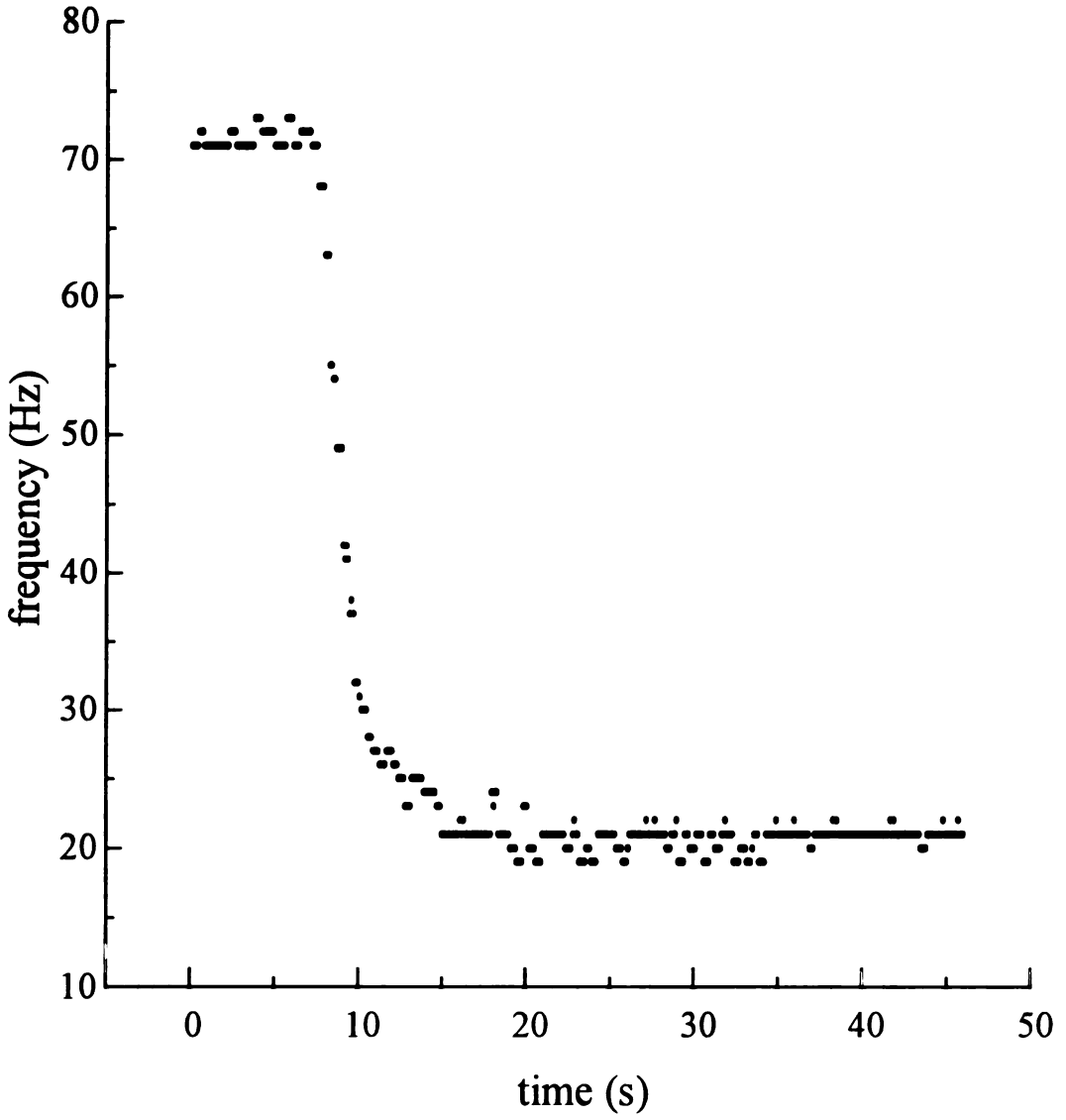

Figure 2.1. Representative raw data of QCM oscillation frequency vs. time subsequent to thiol injection.

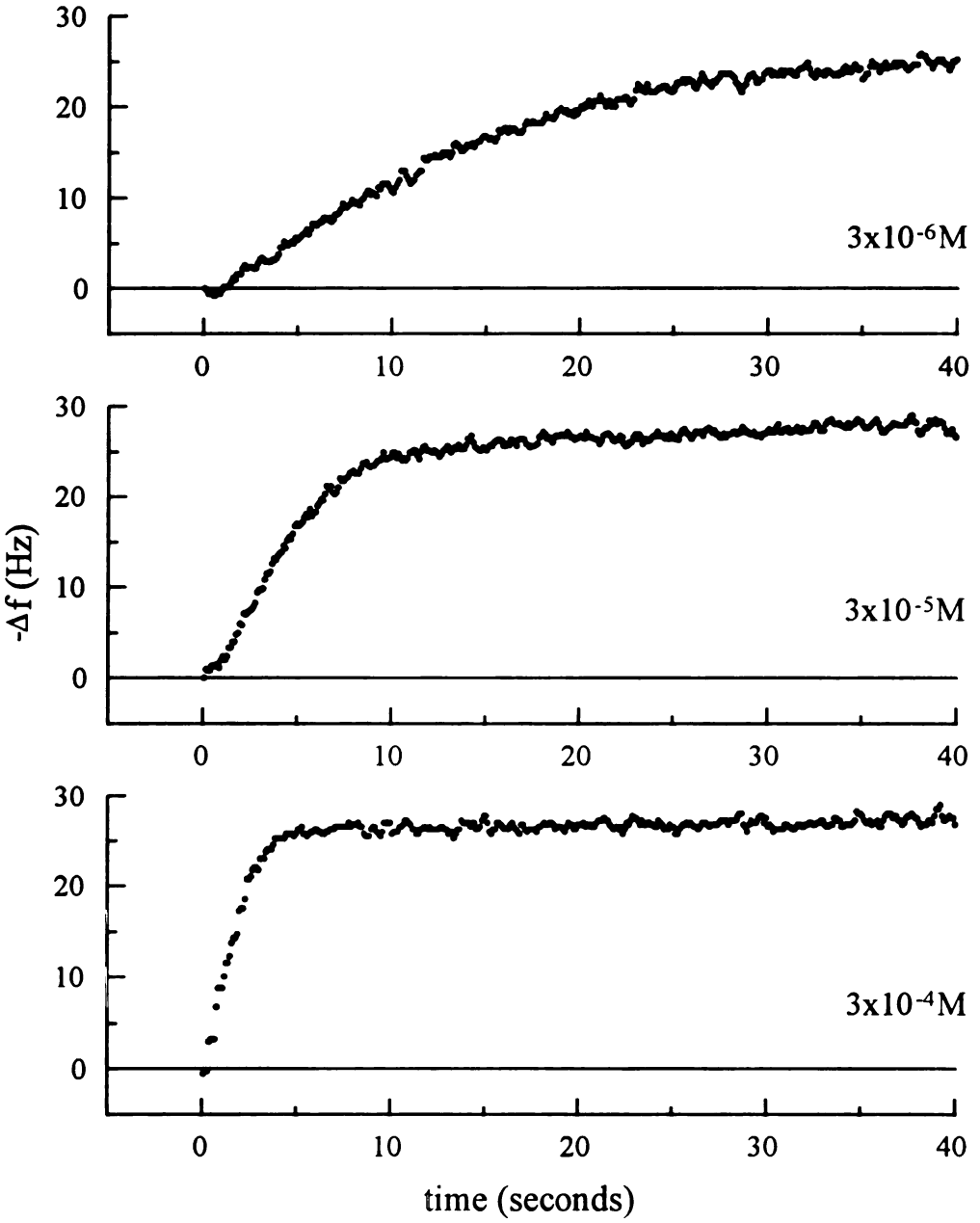

Figure 2.2. Thiol concentration dependence of QCM frequency change for 1-octadecanethiol in *n*-hexane. The top panel is data for a $3x10^{-6}$ **M** final thiol concentration, the center panel is for a $3x10^{-5}$ **M** final thiol concentration and the bottom panel is for a $3x10^{-4}$ **M** thiol concentration.

This reaction proceeds at a gold surface where the thiols react with the metal to form a gold thiol monolayer (Au-SR) and hydrogen. Our experimental data show that the Langmuir isotherm can be used to describe the kinetic response of this reaction over a substantial concentration range (*vide infra)*. The Langmuir isotherm is based on the assumptions that adsorption is limited to one monolayer, all surface sites are equivalent, and adsorption to one site is independent of the occupancy condition of the adjacent sites. The first assumption is clearly valid based on the chemical identity of the adsorbate. An equivalent expression of the second assumption is that the surface is defect-free. Clearly this assumption is not physically realistic. While there are a variety of defects at the gold surface associated with grain boundaries, step edges, adatoms and vacancies, the resultant modulation of surface site energies is apparently small enough that the Langmuir approximation holds. The physical and chemical bases for the third assumption are also open to significant question. The adsorbate alkyl chains interact with each other, but this interaction is likely only significant for nearly complete surface coverage because of the inherently short range nature of dispersive forces. In addition, it is likely that the time scale over which these interchain interactions proceed is significantly longer than the time scale associated with the formation of the gold-thiol bond (*vide infra)*. We note also that the Langmuir isotherm was derived initially for physisorption, not chemisorption, but the bond strength of the alkanethiol-gold bond is apparently small enough that this condition is not violated seriously (*vide infra*).

The effects of exposing the QCM electrodes to liquids have been studied by Thompson's group using network analysis as well as conventional series frequency measurements[.[35,36]] Network analysis involves measurement by standard circuit analysis

of four impedances in an equivalent circuit. These impedances are the static capacitance C_0, the motional resistance R_m, the motional inductance L_m, and the motional capacitance C_m. The static capacitance describes the QCM response at frequencies far from the resonant frequency where it is a simple parallel-plate capacitor. The motional resistance is related to the liquid density and viscosity such that R_m increases with increasing viscosity and density. The motional inductance increases with the increase in plate thickness associated with external mass loading. The motional capacitance represents the elasticity of the QCM. Ideally, the above parameters, except the motional inductance, will remain constant for over the time course of our measurements.

Given the motional resistance, and the measured frequency shift (also called the series frequency Δf_s), the individual components of the frequency shift can be estimated.[35,36]

$$\Delta f_s = \Delta f_d + \Delta f_m + \Delta f_a + \Delta f_x \qquad [2.0]$$

Where Δf_d is the portion of the frequency shift related to viscous damping, Δf_m is caused by adsorbed mass, Δf_a surface stress, and Δf_x is caused by energy dissipation by non-shear couplings. We need to consider how the frequency shifts we report are affected by each of these components.

According to Thompson's experiments on a QCM in air with both bare gold and thiol-modified gold surfaces, the viscoelastic properties of the QCM did not change with adsorption and thus the motional capacitance and Δf_d did not change with the presence of the thiol monolayer.[35,36] In other words, the thiol monolayer can be considered a rigid film for purposes of the QCM measurements. In a comparison of the thiol modified QCM and the bare gold QCM, Thompson noted that upon immersion into polar solvents

such as water, the frequency shifted more for the bare gold QCM than for the thiol-modified QCM. This was attributed with the interfacial properties exhibited with water at the hydrophilic and hydrophobic surfaces which would affect Δf_m and Δf_x.

Thompson's work also involved a study of the effects of roughness of the QCM's surface on its behavior in liquids.[35,36] He found that frequency shifts of polished surfaces upon immersion into liquids were less than those of unpolished surfaces in the same liquid. Electron microscopy showed that the polished and unpolished surfaces differed greatly in roughness, with the rough, unpolished surfaces possessing a higher number of adsorptive sites. The variability in surface roughness between individual QCM's introduces uncertainty in the number of active gold sites available for thiol adsorption. There is also a mechanical stress on our QCMs due to the spring clip used to hold the QCM. Although Δf_a would vary from one measurement to the next, this variation should not cause a frequency shift (Δf_s) error since Δf_a would remain constant through a single measurement. Changes in mechanical stress caused by the spring clip are the result of variability in the positioning of the spring clip, which would affect the amount of exposed gold surface available for the reaction.

The frequency changes we report for the formation of alkanethiol/gold monolayers are not simply due to the mass uptake of the surface. As a consequence of the adsorption, the interfacial monolayer is changing from hydrophilic to hydrophobic. The energy of interaction of the surface with solvent, which does affect the frequency, is therefore changing throughout the measurement in addition to the mass of the QCM. For our measurements, the frequency shift (Δf_s) is affected by changing Δf_m and Δf_x (the adsorbed mass and the energy dissipation by nonshear coupling) during a single

measurement. The net result of this complex process is that the frequency shifts from our measurements are not representative of only the mass changes, and thus extraction of fractional coverage information from these data is problematic at best. The time dependence of this response is however, a direct result of the formation of the monolayer, which affects both the mass uptake and changing surface/solvent interactions. Our time domain measurements are sensitive to the kinetics of formation of the monolayer. The run-to-run variation in Δf_s for our experiments results from variable gold surface roughness of the QCMs (which affect Δf_m and Δf_x) and variability in positioning the spring clip onto the QCM resulting in variability in the area of the exposed gold.

We have a limited gauge of the roughness of the gold surface at the atomic scale,[37] and while this information is important, it is not critical to our experiment for the reasons we have discussed above. We discuss this point in more detail in Chaper 6, where surface roughness is important to the interpretation of the data. The coverage of the QCM electrode surface is expressed as a unitless quantity θ, the fraction of available sites that have reacted, or equivalently, the fraction of a monolayer ($0 \leq \theta \leq 1$). The Langmuir isotherm dictates that the rate of surface reaction is given by

$$\frac{d\theta}{dt} = k_a(1-\theta)C - k_d\theta \qquad [2.1]$$

where θ is the fraction of surface covered, $(1-\theta)$ is the fraction of surface exposed, C is the alkanethiol concentration and k_a and k_d are the association and dissociation constants, respectively. Integration of Eq. 2.1 yields the time course of the monolayer formation

$$\theta(t) = \frac{C}{C + k_d/k_a}\left[1 - \exp\left(-(k_a C + k_d)t\right)\right] \qquad [2.2]$$

This result can be simplified by the substitutions $k_{obs} = k_a C + k_d$ and $K' = C/(C+(k_d/k_a))$, giving

$$\theta(t) = K'\left[1 - \exp\left(-k_{obs}t\right)\right] \qquad [2.3]$$

Notice from the raw data, shown in Figure 2.2, that the maximum initial *rate* of monolayer formation is not reached immediately upon injection. Depending on the volume and concentration of thiol aliquot injected, it may take up to several seconds to achieve the maximum adsorption rate because of limitations inherent to mixing of the solvent and the thiol aliquot. We have determined that the aliquot mixing time is substantially shorter than the monolayer formation time by measurement of the mixing time using a colored dye solution. The time required for thorough mixing is related to both the concentration and the volume of the injected aliquot; as either of these quantities decreases, the mixing time increases correspondingly. The onset of the maximum initial rate is caused by the concentration gradient introduced by mixing. We account for this mixing effect by modifying the variable "t" in Eq. 2.3 to "t-t_0" where t_0 is the time required to achieve a homogeneous solution.

$$\theta(t - t_0) = K'\left[1 - \exp\left(-k_{obs}(t - t_0)\right)\right] \qquad [2.4]$$

Fitting the portion of the curve from the onset of the maximum rate through a significant portion of equilibrium yields t_0, the predicted time of injection if mixing were instantaneous, or equivalently, the time required for the thiol reactant to achieve a homogeneous distribution in the reaction vessel.

The raw data were fit to Eq. 2.4, and the agreement between fit and data is shown for a representative scan in Figure 2.3. The results of these fits are presented in Table 2.1. For the purpose of fitting the data, k_{obs} is independent of K' because the absolute frequency changes vary from one run to the next due to the sensitive impedance matching conditions required by the electronics and the variation of the gold surface morphology from one QCM to another. Because θ is unitless, the absolute mass change is not important to the determination of kinetic quantities k_a and k_d. The QCM oscillation frequency in solution prior to thiol introduction represents a baseline and plotting the (negative) QCM frequency change vs. time subsequent to thiol introduction yields data of the for $z\theta(t)$ vs. t where z is an arbitrary scaling factor.

Fitting the experimental data to Eq. 2.4 gives k_{obs}. Since $k_{obs} = k_aC+k_d$, a plot of k_{obs} vs. C for a series of thiol concentrations gives a line with a slope of k_a and an intercept of k_d, as shown in Figure 2.4. The values of k_a and k_d obtained from these plots are presented in Table 2.2. The uncertainty in the values of k_a and k_d we obtain is significant, but the data show unambiguously that desorption plays an important role in the formation of the alkanethiol monolayers, *i.e.* $k_d > 0$. This is an important finding in and of itself, because the existence of a non-zero k_d for alkanethiol-gold self assembled monolayers demonstrates that these are equilibrium systems, and therefore at any given instant in time, some fraction of the adsorbate sites on the surface are unoccupied.

The data we present in Table 2.2 allow the determination of the equilibrium constant, K_{eq}, for the monolayer system

$$K_{eq} = \frac{k_a}{k_d} \qquad [2.5]$$

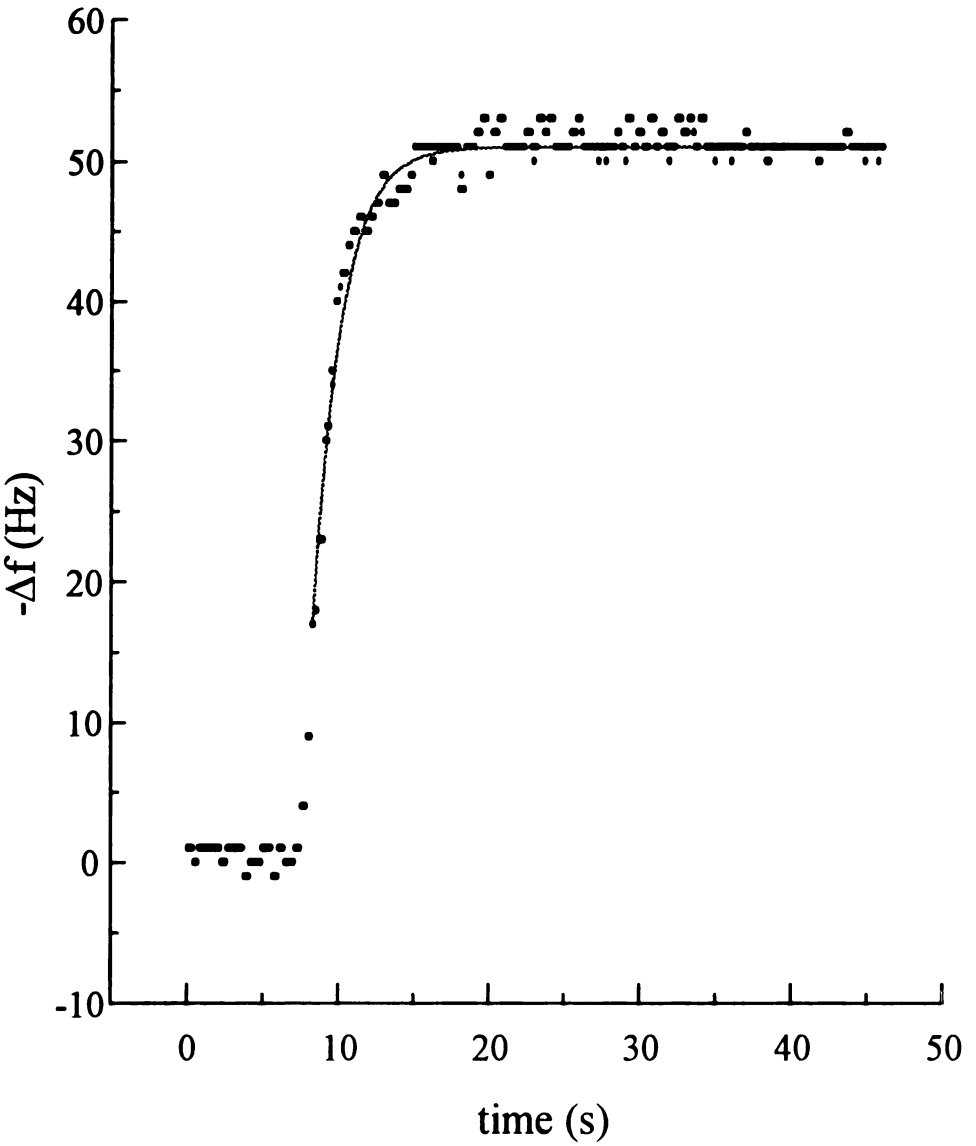

Figure 2.3. Fit of Langmuir adsorption isotherm (Eq. 2.4) to experimental data.

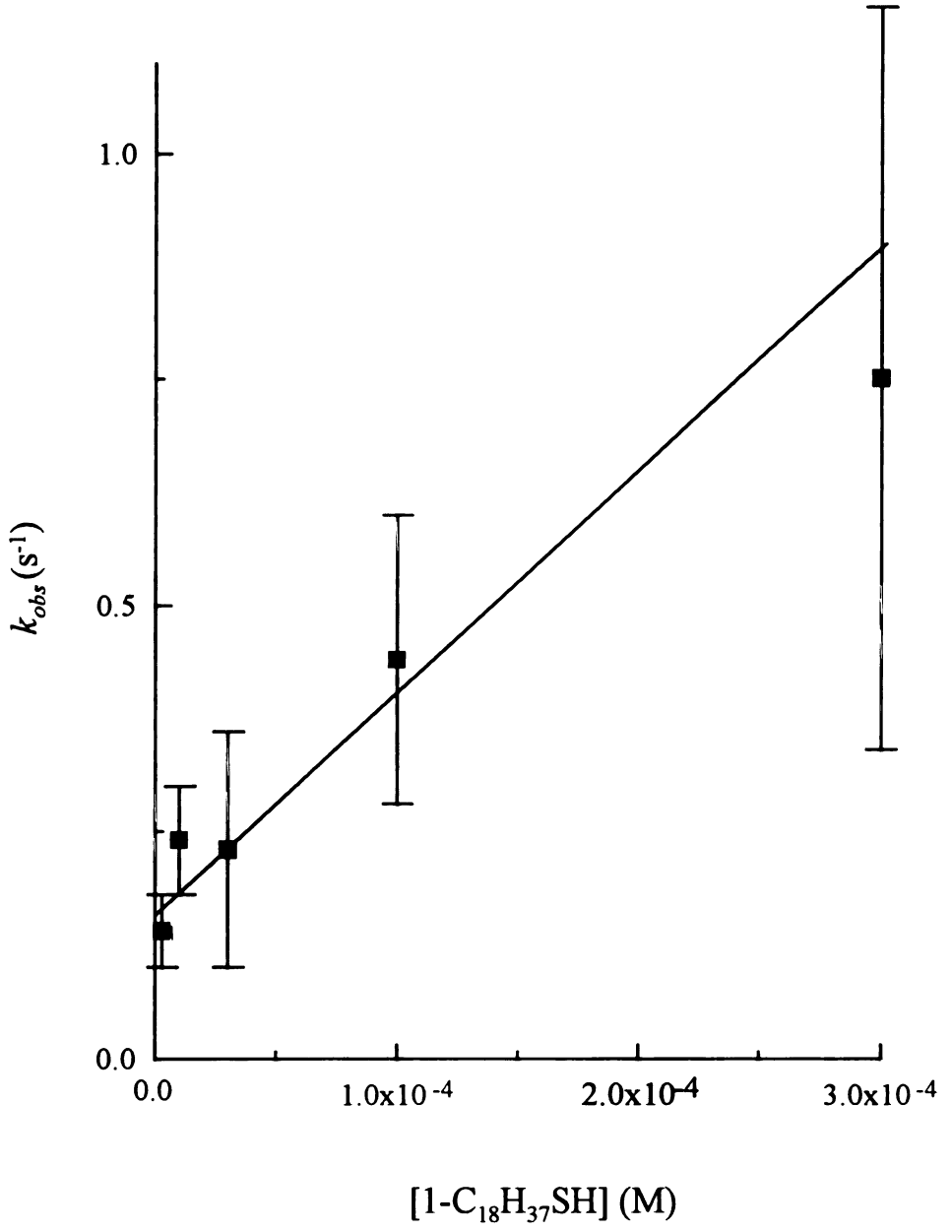

Figure 2.4. Concentration dependence of k_{obs} for 1-octadecanethiol in *n*-hexane. The best fit line through the data has a slope of k_a and an intercept of k_d. See Table 2.2 for results of the fits to the data.

Table 2.1. k_{obs} values determined from raw data as a function of thiol concentration.

adsorbate/solvent	thiol concentration (M)	k_{obs} ± 95% C.I. (s^{-2})
1-octadecanethiol/cyclohexane	$1x10^{-5}$	0.06 ± 0.02
	$3x10^{-5}$	0.23 ± 0.07
	$1x10^{-4}$	0.51 ± 0.16
	$3x10^{-4}$	0.58 ± 0.43
1-octadecanethiol/*n*-hexane	$1x10^{-6}$	0.06 ± 0.04
	$3x10^{-6}$	0.14 ± 0.04
	$1x10^{-5}$	0.24 ± 0.06
	$3x10^{-5}$	0.23 ± 0.13
	$1x10^{-4}$	0.44 ± 0.16
	$3x10^{-4}$	0.75 ± 0.41
1-octanethiol/*n*-hexane	$1x10^{-5}$	0.17 ± 0.03
	$3x10^{-5}$	0.44 ± 0.06
	$1x10^{-4}$	0.52 ± 0.11
	$3x10^{-4}$	0.70 ± 0.23
	$1x10^{-3}$	1.20 ± 0.34
	$3x10^{-3}$	0.90 ± 0.34

Table 2.2. k_a and k_d determined from concentration dependence of k_{obs}.

adsorbate/solvent	k_a ($M^{-1}s^{-1}$) ± 95% C.I.	k_d (s^{-1}) ± 95% C.I.
1-octadecanethiol/cyclohexane	2059 ± 1394	0.19 ± 0.09
1-octadecanethiol/*n*-hexane	2440 ± 1074	0.16 ± 0.03
1-octanethiol/*n*-hexane	811 ± 334	0.42 ± 0.06

We can obtain two important physical quantities from K_{eq}. The steady state fractional coverage of the gold surface, $\theta(\infty)$, is given by

$$\theta(\infty) = \frac{C}{C + 1/K_{eq}} \qquad [2.6]$$

We show in Table 2.3 the fractional coverage values calculated for the 1-octadecanethiol-gold system using the experimental concentrations and equilibrium constant. The $\theta(\infty)$ values approach unity only at comparatively high thiol concentrations. The free energy of adsorption of the monolayer is also found directly from the equilibrium constant data.

$$\Delta G_{ads} = -RT \cdot \ln K_{eq} \qquad [2.7]$$

We show in Table 2.4 the free energies and equilibrium constants we have determined. Our data provide direct proof that the alkanethiol-gold system is an equilibrium system. Recent atomic microscopy studies have shown that regions of the monolayers exhibit structural mobility[29] and this finding is explained by the fact that the monolayer system is an equilibrium system.

Limits of applicability for Langmuir behavior. We observe a negative deviation from linearity for the relationship between k_{obs} and C for both high and low thiol concentrations. We discuss below how the observed deviations do *not* indicate that these systems are ill-described by the Langmuir adsorption model, but, rather, demonstrate the limits intrinsic to this treatment of a complex equilibrium process.

The first deviation we consider is for low thiol concentrations. At low thiol concentration the perturbation introduced to the system by the thiol is small. In other words, for low thiol concentrations, the system remains in close proximity to equilibrium

Table 2.3. Fractional surface coverage as a function of thiol concentration, calculated using Eq. 2.6, for the 1-octadecanethiol/*n*-hexane system. The uncertainty is determined by uncertainty in k_a and k_d.

thiol concentration (M)	$\theta(\infty)$
$3x10^{-6}$	0.04 ± 0.02
$1x10^{-5}$	0.13 ± 0.07
$3x10^{-5}$	0.31 ± 0.16
$1x10^{-4}$	0.60 ± 0.34
$3x10^{-4}$	0.82 ± 0.51

Table 2.4. K_{eq} and ΔG_{ads} determined from the experimental data.

adsorbate/solvent	*Keq* (M^{-1})	ΔG_{ads} (kcal/mol)
1-octadecanethiol/*n*-hexane	15250 ± 7300	-5.6 ± 0.2
1-octadecanethiol/cyclohexane	10850 ± 8950	-5.5 ± 0.4
1-octanethiol/*n*-hexane	1930 ± 840	-4.4 ± 0.2

and the expected mass change for such conditions lies beneath our limit of detection ($\theta << 1$). At equilibrium, the net rate of reaction is zero, although there remain non-zero adsorption and desorption rates for the thiol.

$$\frac{d\theta}{dt} = 0 = k_a(1-\theta)C - k_d\theta$$

$$k_a(1-\theta)C = k_d\theta \qquad [2.8]$$

For small C, θ approaches zero, and the equilibrium rate of monolayer formation becomes very close to the initial rate of monolayer formation (k_a C). The perturbation from equilibrium introduced into the system by a low concentration of thiol is negligibly small, and the difference between the initial rate and the equilibrium monolayer formation rate tends to zero before C=0. We define the quantity Δ to describe the displacement from equilibrium for low thiol concentration. The quantity Δ is the difference between initial rate of adsorption and the equilibrium rate of adsorption.

$$\Delta = k_aC - k_a(1-\theta)C = \frac{(k_aC)^2}{(k_aC + k_d)} \qquad [2.9]$$

A plot of Δ vs. C yields a line with a slope >> 1, indicating that Δ becomes negligibly small as C$\rightarrow$0 (Figure 2.5). Our data are explained by this prediction, and we expect a negative deviation from Langmuir behavior at low thiol concentrations.

For high thiol concentrations we also observe a negative deviation from Langmuir isotherm predictions. At high thiol concentration the initial rate of adsorption approaches zeroth order behavior, *i.e.* the initial rate of adsorption becomes concentration independent for high thiol concentrations (Figure 2.6). This change in behavior is indicative of the mechanism of monolayer formation. It is important to note

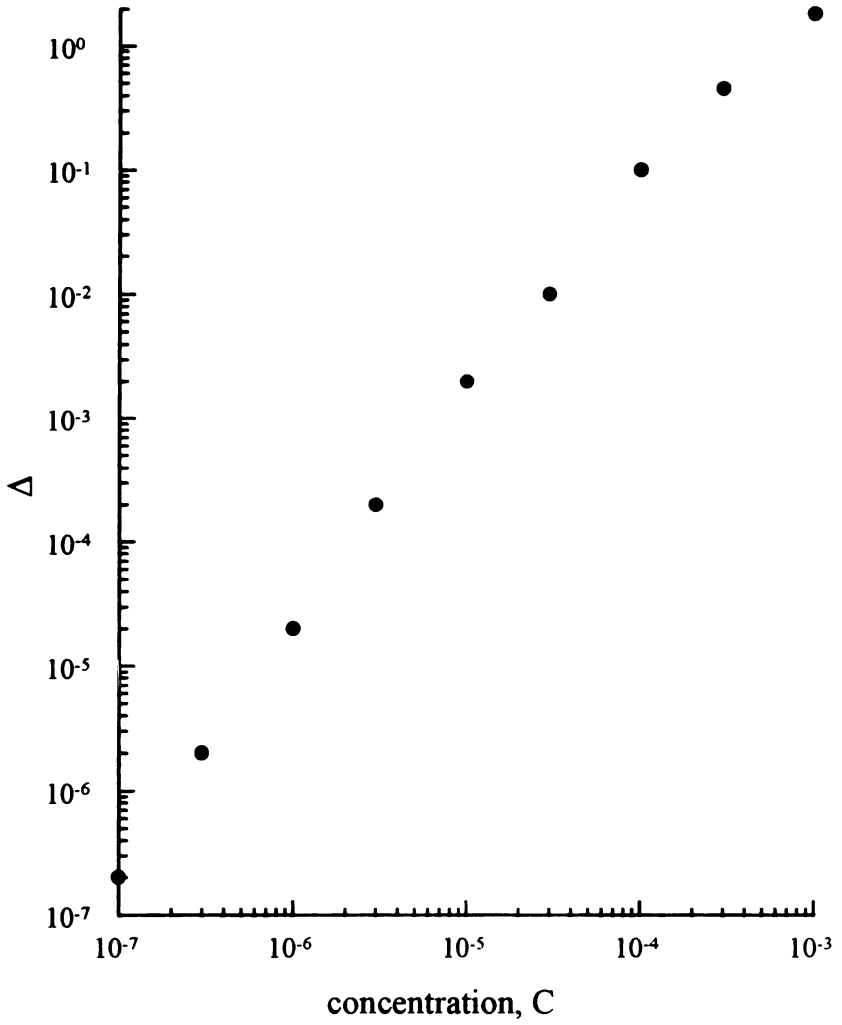

Figure 2.5. Concentration dependence of Δ for $k_a = 2000\ \mathbf{M}^{-1}\mathrm{s}^{-1}$ and $k_d = 0.2\ \mathrm{s}^{-1}$.

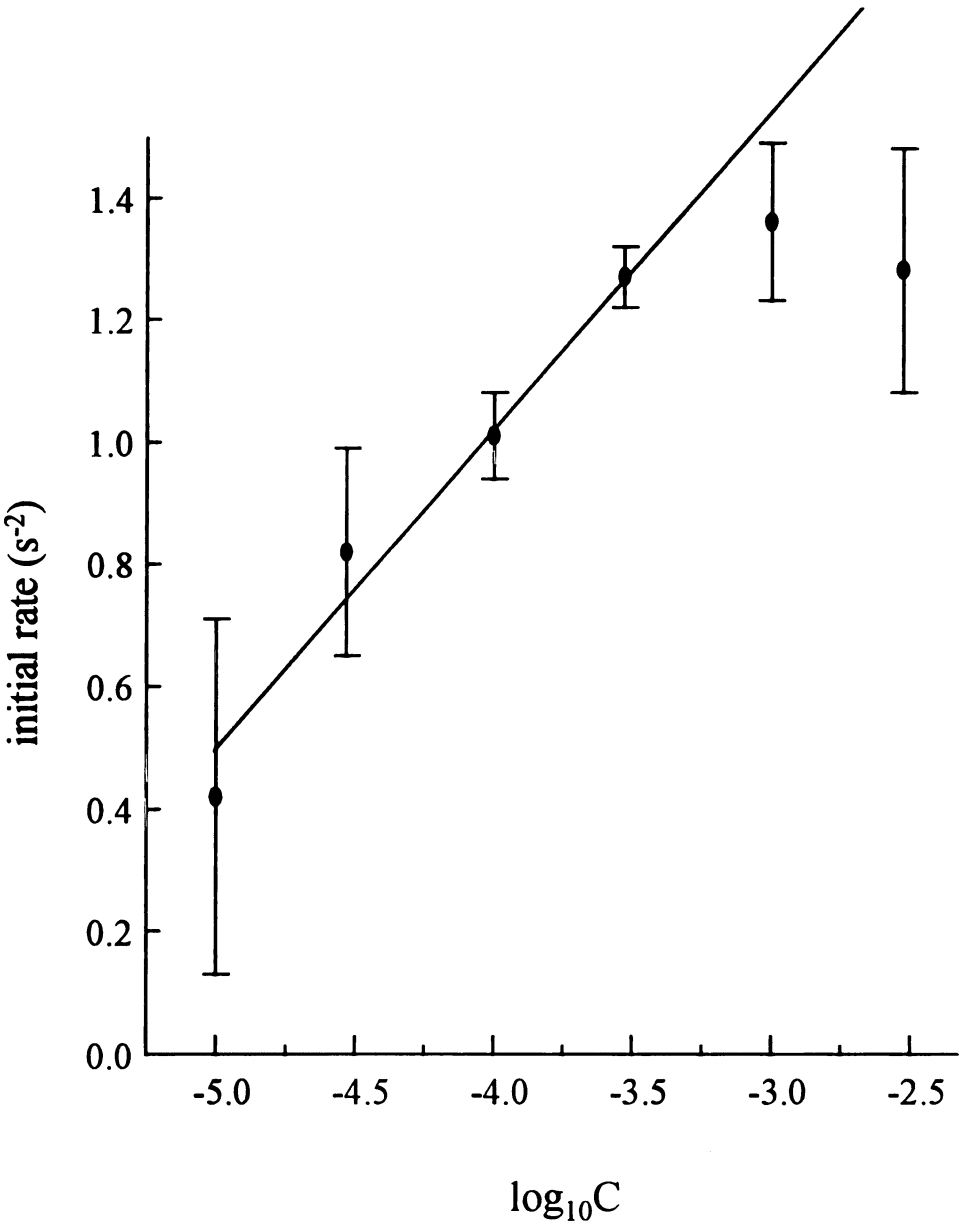

Figure 2.6. Concentration dependence for initial rate of monolayer formation for 1-octanethiol adsorbed from *n*-hexane. Note the high concentration region where the rate becomes concentration independent.

that the initial rates in the zeroth order regime are not the same for each system studied (see Table 2.5), suggesting that the onset of pseudo zeroth order behavior is not a stoichiometric effect. If stoichiometry were limiting, then the initial rates of adsorption would be independent of thiol and/or solvent identity. If an intermediate state plays a role in the adsorption reaction, then we would expect a solvent and alkanethiol dependence, as is seen. The solvent-dependence of the initial rates in the zeroth order regime implies that the rate of monolayer formation is limited by the time required to form some intermediate state. Our data do not shed light on the structure of the intermediate state, but does suggest its presence.

Comparison to electrochemical data. An important question relating to these monolayer assemblies is the actual identity of the adsorbing and desorbing species. Specifically, is the labile hydrogen from the thiol eliminated as a proton or as neutral hydrogen? Recent electrochemical work by the Porter group indicates that neutral hydrogen is the product of this reaction, or H_2O_2 if oxygen participates in the reaction.[34,38] Using data from their work, we can estimate ΔG_{ads} for the adsorption of alkanethiols onto gold for both possible chemical reactions. Porter *et. al.* measured the potential corresponding to the desorption of alkanethiols from gold.

$$RS-Au+1e^{-} \rightarrow RS^{-}+Au \qquad [2.ii]$$

The potential reported was -1.25 V vs. saturated Ag/AgCl, or -1.05 V vs. SHE for 10^{-2} M thiol in 0.5 **M** ethanolic KOH, and the variation of this potential with aliphatic chain length is small.[38] For adsorption to occur, the thiol must dissociate.

$$RSH \Leftrightarrow RS^{-}+H^{+} \qquad [2.iii]$$

Table 2.5. Limiting initial rates of monolayer formation for high thiol concentration.

adsorbate/solvent	initial rate (s^{-2}) ± 95% C.I.
1-octadecanethiol/*n*-hexane	31 ± 12
1-octadecanethiol/cyclohexane	12 ± 4
1-octanethiol/*n*-hexane	19 ± 9

There is little information in the literature on the pK_a of alkanethiols. Based on the limited information available, pK_a values in the range of 9 to 12 are expected, depending on the solvent.[39] For pK_a values of 9 and 12, we calculate the potential for thiol dissociation to be -0.53 V and -0.71 V, respectively, vs. SHE. The third reaction we must consider is the reduction of protons to hydrogen.

$$2H^+(solv.) + 2e^- \Leftrightarrow H_2(g) \qquad [2.iv]$$

We can estimate the half cell potential for this reaction by taking into account the proton concentration contributed from thiol dissociation and the partial pressure of atmospheric hydrogen in the air-saturated solution. For pK_a values of 9 and 12 we calculate half cell potentials of -0.23V and -0.31V, respectively, vs. SHE. From the above estimates we *approximate* the free energies for alkanethiol-gold adsorption for conditions of either the generation of a proton or of hydrogen. For the generation of a proton,

$$RSH(solv.) + Au(s) \Leftrightarrow RS - Au(s) + H^+(solv.) + 1e^- \qquad [2.v]$$

we calculate a potential of +0.43V vs. SHE, corresponding to a ΔG_{ads} = -9.9 kcal/mol. If instead, as indicated by the Porter group's data,[34,38] the formation of the gold thiol monolayer produces neutral hydrogen (scheme 2.i), we calculate a potential of +0.16V vs. SHE, giving ΔG_{ads} = -3.7 kcal/mol. In addition to the ambiguity of the locations of the excess electron and proton generated in scheme 2.v, the calculated ΔG_{ads} for scheme 2.i is closer to the experimentally determined values we report here. We caution that the extent to which a comparison can be made between our data and the above estimate is limited because the experimental conditions and sources for the electrochemical and equilibrium data vary for parameters used in the approximation. Nonetheless, the

agreement between our data and the estimate is quite good, and provides further support, albeit only qualitative, for the monolayer formation proceeding according to scheme i and not scheme 2.ii. We return to a broader discussion of this point in Chapter 3.

Infrared spectra: External reflection infrared spectroscopy has been used extensively to study macroscopic ordering in alkanethiol self-assembled monolayers. The spectral positions of the methylene stretching modes for the alkanethiol monolayers can be compared to those for *n*-alkanes which differ between liquid and crystalline environments. FTIR studies of self assembled monolayers have shown that the alkyl chains exist in densely packed environments, where a high degree of crystallinity was assumed to be necessary to achieve the packing density. The band position(s) of these vibrational modes have been reported to evolve in time subsequent to monolayer formation, and this evolution time has been shown to be on the order of hours to days.[18] The fact that we see chemical equilibration within one minute suggests that the equilibrium achieved amongst the aliphatic chains can be largely separated from the formation of the alkanethiol monolayer.[40] In order to ensure the correspondence between our self-assembled monolayer systems and those studied earlier, we have examined the spectral evolution of the CH stretching region of the IR spectra of our films.

We show in Figures 2.7 the spectra for 1-octadecanethiol monolayers on the QCM surface. The IR response of the 1-octanethiol monolayers was below our detection limit. The 1-octadecanethiol monolayers were formed by adsorption from a $3x10^{-4}$ **M** solution of *n*-hexane. Formation of the monolayer measured with the FTIR was

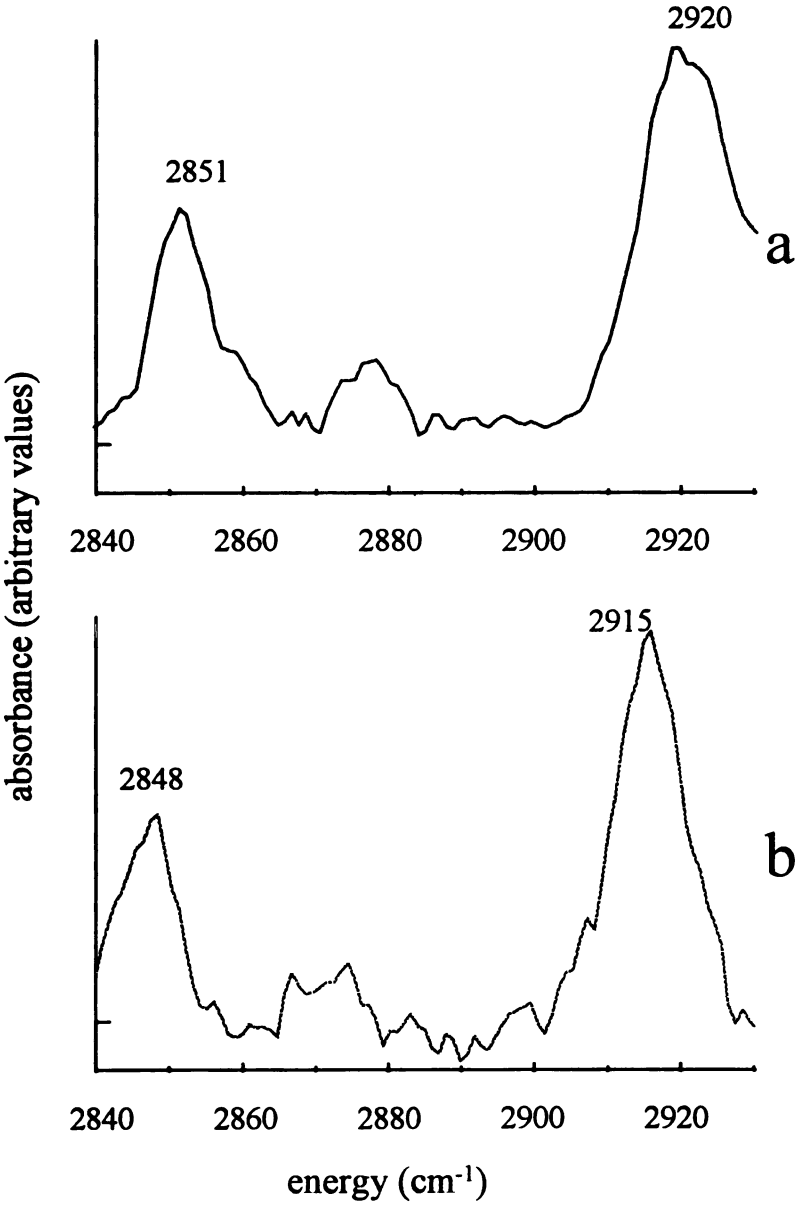

Figure 2.7. FTIR spectra of a 1-octadecanethiol/gold monolayer formed on the QCM surface, taken with 2 cm^{-1} resolution. (a) Spectrum recorded immediately after adsorption. (b) Spectrum recorded two weeks after adsorption.

determined to be gravimetrically complete based on the time invariance of the QCM response. The spectrum shown in Figure 2.7a was taken for a monolayer adsorbed immediately prior to the IR measurement. The symmetric and asymmetric methylene stretching modes occurred at 2851 and 2920 cm^{-1}, respectively. The spectrum of the same monolayer, stored in inert atmosphere for two weeks, is presented in Figure 2.7b. In this spectrum the symmetric and asymmetric methylene stretching modes appear at 2848 and 2915 cm^{-1}, respectively. Because the spectral resolution used in these measurements was 2 cm^{-1}, the red shifts we report are significant and indicate an approach to a more densely packed, and possibly crystalline, environment for the adsorbed alkanethiol chains. We note that the results for a monolayer that was aged for 24 hours were identical to those we report in Figure 2.7b.

Implications of the ΔG_{ads} data. The magnitude of ΔG_{ads} that we have measured for alkanethiol/gold systems is important because it provides insight into the chemical processes relevant to the formation of this interface. We consider that there are two significant interactions that contribute to the formation of the observed monolayers.

The first interaction is that of the thiol moiety with the gold surface to form a gold-thiol bond. The second interaction is the intermolecular attraction between adjacent aliphatic chains that must also contribute to the stability of the system. We consider the expected contributions from each of these interactions individually.

The first fundamental question to be addressed is the energy associated with bond formation for gold/thiol systems. We are not aware of detailed thermodynamic measurements on this chemical system, but note that Bockris has reported a free energy of formation for butanethiol on mercury of - 4.9 kcal/mol.[41] The similarity of this value

to the ΔG_{ads} we measure indicates that the dominant contribution to the formation of this thiol-metal bond is determined by the creation of the thiol species. The strength of interaction between aliphatic chains must also be considered. Obtaining an estimate of this interaction energy is difficult, but we approximate this interaction through the viscous flow energy of the corresponding liquid *n*-alkanes. The comparison we make is between a three dimensional liquid and a nominally two dimensional interface. Such a comparison is directly relevant to the system under consideration because adsorption and desorption at the interface must involve adsorbate molecular translation into and out of the plane of the interface. The "viscosity" exhibited by a given liquid can be considered as an activated process, and thus the temperature dependence will obey Arrhenius behavior.

$$\eta = A\exp\left(E_{vis}/RT\right) \qquad [2.10]$$

The interaction energy, E_{vis}, is an energy of interaction between molecules and, while this energy may be expected to be slightly different for a two dimensional interface than for a three dimensional bulk liquid, we do expect this difference to be comparatively small, *i.e.* within a factor of about two of the interaction energy within the monolayer. Measurement of the viscous flow energy for a given solvent requires knowledge of the temperature dependence of the solvent bulk viscosity, and the pre-exponential factor A is strongly solvent-dependent. The viscous flow energy for a given liquid is typically 1/3 to 1/4 of the latent heat of vaporization for the liquid.[42] Indeed, the qualitative reason for the relationship of E_{vis} to ΔH_v is not surprising, since the heat of vaporization is a measure of the energy required to overcome the collective attractive forces within the

system, and those same attractive forces are responsible for viscous flow in the liquid. For *n*-octane and *n*-octadecane we estimate the viscous flow energies to be 3 and 6 kcal/mol, respectively. This energy is essentially the same, within the uncertainty of the estimate, to that of the measured ΔG_{ads}.

There are two possible explanations for the similarities of these two quantities. The first is that we are, in fact, measuring the net energy of adsorption of the gold-thiol system, which is dominated by interchain interactions amongst the aliphatic chains of the alkanethiols. This explanation is not likely because, if true, it would imply that the attractive inter-chain forces would lead to the spontaneous formation of alkanethiol molecular assemblies in solution, and we do not observe this experimentally. The second possibility is that the quantity we measure gravimetrically is largely unaffected by these interchain interactions because the thiols that contribute to the observed equilibrium are not involved in the formation of the "bulk" monolayer, and thus exhibit a ΔG_{ads} characteristic of only the thiol-gold bond. Such a condition could occur at interfaces between domains on the surfaces where an edge of a monolayer is at least partially exposed to the solvent overlayer. In addition, the time scales on which the interchain forces operate must necessarily be longer than that for the gold-thiol bond formation because of the large number of possible conformers of the alkyl chains and the large amplitude motions required for the chains to achieve a predominantly all-*trans* conformation. We expect that it is not possible to separate the relative contributions to the observed ΔG_{ads} cleanly, and there is a contribution to the observed data from both interchain interactions and the gold-thiol bond. Based on our estimates of the interchain

interaction energy, we believe that at least some diminution of this interaction is required to measure a free energy of adsorption that is as small as we observe.

It is important to note that we measure the total free energy of the adsorption process, and have not separated the entropic and enthalpic contributions. Previous measurements of the heat of desorption for alkanethiol monolayers has provided a value of ~28 kcal/mol.[43] While it might be tempting to use this value for ΔH_{des} and infer the entropic contribution to the adsorption, this is not possible without knowing the heat of solution of the alkanethiol in the solvents we use here. For our measurements we determine the adsorption from solution, and for the ΔH_{des} determination, desorption is from the surface into vacuum. Thus the heat of solution for the alkanethiol is required in order to determine the entropic contribution to the formation of these monolayers. We will present in Chapter 3 a family of measurements that yield ΔS_{ads} and ΔS_{ads} information directly.

2.4. Conclusions

We have presented kinetic measurements of the formation of alkanethiol monolayers on microcrystalline gold. The adsorption behavior of these systems follows the predictions of the Langmuir isotherm over a limited concentration range, and the deviations observed from the Langmuir prediction are expected based on limits inherent to the assumptions of the Langmuir isotherm. Our data demonstrate that the alkanethiol-gold system is in equilibrium with free gold sites and alkanethiol moieties. From our data we derive $\Delta G_{ads} = -5.5 \pm 0.4$ kcal/mol for *n*-$C_{18}H_{37}SH$ adsorption onto gold, and $\Delta G_{ads} = -4.4 \pm 0.2$ kcal/mol for *n*-$C_8H_{17}SH$ adsorption onto gold. These values are virtually the same as our estimates for the aliphatic interchain interaction energies, indicating that the equilibrium behavior we observe proceeds predominantly at the edges of monolayer islands and/or at step edges and defect sites. The infrared data demonstrate that the mass equilibrium for alkanethiol monolayers is achieved within about one minute, but the structural equilibration of the aliphatic chains proceeds over a much longer time scale.

2.5. Literature Cited

1. D. L. Allara; R. G. Nuzzo; *Langmuir*, **1985**, *1*, 45.

2. D. L. Allara; R. G. Nuzzo; *Langmuir*, **1985**, *1*, 52.

3. A. H. M. Sondag; M. C. Raas; *J. Chem. Phys.*, **1989**, *91*, 4926.

4. L. K. Chau; M. D. Porter; *Chem. Phys. Lett.*, **1990**, *167*, 198.

5. H. Lee; L. J. Kepley; H. G. Hong; T. E. Mallouk; *J. Am. Chem. Soc.*, **1988**, *110*, 618.

6. H. Lee; L. J. Kepley; H. G. Hong; S. Akhter; T. E. Mallouk; *J. Phys. Chem.*, **1988**, *92*, 2597.

7. G. Cao; T. E. Mallouk; *J. Solid State Chem.*, **1991,** *94*, 59.

8. S. Akhter, H. Lee, T. E. Mallouk; J. M. White; H. G. Hong; *J. Vac. Sci. Tech. A*, **1989,** *7*, 1608.

9. H. G. Hong; T. E. Mallouk; *Langmuir*, **1991,** *7*, 2362.

10. G. Cao; L. K. Rabenberg; C. M. Nunn; T. E. Mallouk; *Chem. Mater.*, **1991,** *3*, 149.

11. L. J. Kepley, D. D. Sackett; C. M. Bell; T. E. Mallouk; *Thin Solid Films*, **1992,** *208*, 132.

12. H. G. Hong; D. D. Sackett; T. E. Mallouk; *Chem. Mater.*, **1991,** *3*, 521.

13. L. H. Dubois; B. R. Zegarski; R. G. Nuzzo; *J. Am. Chem. Soc.*, **1990,** *112*, 570.

14. R. G. Nuzzo; L. H. Dubois; D. L. Allara; *J. Am. Chem. Soc.*, **1990,** *112*, 558.

15. R. G. Nuzzo; E. M. Korenic; L. H. Dubois; *J. Chem. Phys.*, **1990,** *93*, 767.

16. C. E. D. Chidsey; D. N. Loiacono; *Langmuir*, **1990,** *6*, 682.

17. C. E. D. Chidsey; C. R. Bertozzi; T. M. Putvinski; A. M. Mujsce; *J. Am. Chem. Soc.*, **1990,** *112*, 4301.

18. C. D. Bain; E. B. Troughton; Y. T. Tao; J. Evall; G. M. Whitesides; R. G. Nuzzo; *J. Am. Chem. Soc.*, **1989,** *111*, 321.

19. C. D. Bain; J. Evall; G. M. Whitesides; *J. Am. Chem. Soc.*, **1989,** *111*, 7155.

20. E. B. Troughton; C. D. Bain; G. M. Whitesides; R. G. Nuzzo; D. L. Allara; M. D. Porter; *Langmuir*, **1988,** *4*, 365.

21. M. D. Porter; T. B. Bright; D. L. Allara; C. E. D. Chidsey; *J. Am. Chem. Soc.*, **1987,** *109*, 3559.

22. G. M. Whitesides; P. E. Laibinis; *Langmuir*, **1990,** *6*, 87.

23. N. Camillone III; C. E. D. Chidsey; G.-Y. Liu; T. M. Putvinski; G. C. Scoles; J. Wang; *J. Chem. Phys.*, **1991,** *94*, 8493.

24. C. E. D. Chidsey; G.-Y. Liu; G. C. Scoles; J. Wang; *Langmuir*, **1990,** *6*, 1804.

25. S. R. Wasserman; G. M. Whitesides; I. M. Tidswell; B. M. Ocko; P. S. Pershan; J. D. Axe; *J. Am. Chem. Soc.*, **1989**, *111*, 5852.

26. C. A. Widrig; C. A. Alves; M. D. Porter; *J. Am. Chem. Soc.*, **1991**, *113*, 2805.

27. G.-Y. Liu; M. B. Salmeron; *Langmuir*, **1994,** *10*, 367.

28. R. L. McCarley; Y.-T. Kim; A. J. Bard; *J. Phys. Chem.*, **1993,** *97*, 211.

29. R. L. McCarley; D. J. Dunaway; R. J. Willicut; *Langmuir*, **1993, *9***, 2775.

30. G. G. Guilbault; *Methods and Phenomena 7: Applications of Piezoelectric Quartz Crystal Microbalances*, Elsevier Science Publishing Co., New York, **1984**. p. 252.

31. G. Z. Sauerbrey, *Z. Phys.*, **1959,** *155*, 206.

32. L. Strong; G. M. Whitesides; *Langmuir*, **1988,** *4*, 546.

33. C. E. D. Chidsey; G.-Y. Liu; P. Rowntree; G. Scoles; *J. Chem. Phys.*, **1989,** *91*, 4421.

34. C. A. Widrig; C. Chung; M. D. Porter; *J. Electroanal. Chem.*, **1991,** *310*, 335.

35. M. Yang; M. Thompson; *Langmuir*, **1993,** *9*, 802.

36. M. Yang, M. Thompson; *Langmuir*, **1993,** *9*, 1990.

37. J. B. Schlenoff, M. Li, H. Ly, *J. Am. Chem. Soc.*, **1995**, *117*, 12528.

38. D. E. Weishaar; B. D. Lamp; M. D. Porter; *J. Am. Chem. Soc.*, **1992, *114***, 5860.

39. Shigeru Oae; *Organic Sulfur Chemistry: Structure and Mechanism*, CRC Press, **1991**.

40. G. Hahner; Ch. Woll; M. Buck; M. Grunze; *Langmuir*, **1993,** *9*, 1955.

41. E. Blomgren; J. O'M. Bockris; C. Jesch; *J. Phys. Chem.*, **1961,** *65*, 2000.

42. W. J. Moore, *Physical Chemistry*, 3rd Edition, Prentice-Hall, Englewood Cliffs, NJ, **1963**, p. 724.

43. R. G. Nuzzo; B. R. Zegarski; L. H. Dubois; *J. Am. Chem. Soc.*, **1987,** *109*, 733.

Chapter 3

Quantitating the Balance Between Enthalpic and Entropic Forces in Alkanethiol/Gold Monolayer Self-Assembly

Summary

We have studied the temperature and adsorbate concentration dependence of alkanethiol/gold monolayer formation *in-situ* and in real time using a quartz crystal microbalance to monitor the rate of reaction. The temperature dependence of the experimental rate constants, for a given concentration, demonstrates that the formation of these monolayers is not diffusion rate limited for the conditions we report. Our data are modeled accurately by the Langmuir adsorption isotherm and, using this model, we have determined the adsorption and desorption rate constants for monolayer self assembly. We have extracted from these data the thermodynamic quantities ΔG_{ads}, ΔH_{ads} and ΔS_{ads} for monolayer formation. For 1-octadecanethiol adsorption from *n*-hexane onto gold, ΔG_{ads} is temperature dependent and is *ca.* -5.5 kcal/mol, ΔH_{ads} = -20 ± 1 kcal/mol and ΔS_{ads} = -48 ± 1 cal/mol-K. These data have direct bearing on the broader field of interface chemistry because they underscore the dominant role that entropy plays in determining the course of chemical reactions at interfaces and the robustness of the resulting molecular assembly. We discuss the implications of these data on the stability of the monolayers and the limits that these values place on the extent of experimental control available over their formation.

3.1. Introduction

The self-assembly of alkanethiol monolayers onto gold has been studied extensively[1-47] due to the potential applications of these interfaces to important technologies such as chemical sensing, micro-device patterning and surface lubrication.[48-53] The extensive literature that exists on these systems is aimed largely at understanding the steady state properties of the monolayers once they have formed, and from these studies has emerged a reasonably consistent picture. For long chain *n*-alkanethiols ($\geq C_{10}H_{21}SH$),[9] the aliphatic chains are densely packed with a 5Å inter-chain spacing on Au(111), once formed and annealed.[54,55] These chains are in a predominantly all-*trans* conformation, and the thiol head groups exist in a $(\sqrt{3}x\sqrt{3})R30°$ configuration on the hexagonal close-packed Au(111) surface.[3,9] Recently, it has become increasingly clear that these monolayers are highly dynamic,[17,18,56,57] with desorption and structural rearrangement playing an important role in determining the evolution of the macroscopic properties of the interfaces. Despite this significant level of understanding, there remain several substantial open questions in this field relating to the mechanism of monolayer formation and the extent to which surface defects mediate the dynamics of the monolayers, once they have formed.

The prospect of using self-assembled monolayers for patterning and chemical sensing applications requires that monolayers possessing functionalities more complex than available with simple aliphatic thiols be synthesized.[4,5,27,43,50,58-60] The details of the interaction between the thiol head group and the gold surface remain, to some extent, uncertain and in addition, it has been demonstrated that the "tail group" can alter the organization of the formed monolayer if the organic tail contains chemically active or

bulky termini. Thus there is a competition between different regions of the monolayer to determine the macroscopic organization of the system. In order to understand the balance that exists between the thiol head group interactions with the metal surface and organic tail group interactions with adjacent adsorbates, there needs to be a better understanding of the initial self-assembly process, and that is the focus of this work.

We have reported in Chapter 2 on a method to monitor, *in-situ*, the adsorption of alkanethiols onto gold using a quartz crystal microbalance (QCM) fabricated with evaporated gold electrodes that are predominantly Au(111).[18,61] We were able to monitor the mass change of the QCM resulting from the adsorption of alkanethiols onto the gold electrodes with sub-second time resolution, allowing access to direct information on the formation of the monolayer. Earlier studies of alkanethiol/gold monolayer formation, performed *ex situ* with techniques such as external reflection FT-IR,[62] optical ellipsometry,[6,8] radio isotope labeling[63] and liquid contact angle measurements,[6,8] were limited to time resolution on the order of minutes to hours. Our *in situ* data demonstrate a kinetic response fully consistent with that predicted by the Langmuir adsorption isotherm[64-66] and, by modeling the experimental adsorption data using this isotherm, we were able to determine the free energy of adsorption for the monolayer. The values we obtained for ΔG_{ads} at 293 K were -5.6 ± 0.4 kcal/mol for 1-octadecanethiol adsorption onto gold from *n*-hexane, -5.5 ± 0.2 kcal/mol for formation of 1-octadecanethiol/gold from cyclohexane, and -4.4 ± 0.2 kcal/mol for formation of 1-octanethiol/gold from *n*-hexane.[18] These modest free energies, on the order of the hydrogen bond strength characteristic of liquid alcohols,[67] demonstrated that these systems are highly labile, a finding at odds with the then-prevailing thought that, once

formed, the monolayers exhibited few dynamics. Studies of the mobility of alkanethiol/gold monolayers by the McCarley and Tarlov groups using scanning probe microscopy have revealed the presence of mobile defect sites, providing a different indication of the labile nature of these monolayers.[17,56] In that work, it was shown that the rate at which these defects migrated across the surface was independent of alkanethiol chain length, suggesting that the thiol head group plays the dominant role in mediating the adsorption and desorption steps,[17] and that the first layer of gold atoms were apparently involved in the monolayer rearrangement directly.[56] The relatively small free energies of adsorption we obtained in our earlier work indicated that alkanethiols are not bound to the surface strongly, but it was not clear, based on a single quantity (ΔG_{ads}) whether the labile nature of these films was a consequence of chemically weak interactions between the adsorbate and the surface or the counter-balance of two significant but opposing forces, specifically the enthalpy and entropy of adsorption. The answer to this question was indicated by earlier work on the thermal desorption of a monolayer of alkanethiols from gold. Nuzzo and coworkers desorbed a dimethyl disulfide monolayer from gold thermally, recovering a heat of desorption (ΔH_{des}) of 28 kcal/mol.[68] The implied heat of adsorption, ΔH_{ads} = -28 kcal/mol was determined in the absence of solvent and using a different adsorbate and, while leading, the utility of this value for comparison with our experimental data on ΔG_{ads} is limited due to the unknown solvent-thiol contribution to our data. In order to determine the enthalpic and entropic contributions to the small ΔG_{ads} we measure for adsorption from solution, we have measured these quantities directly through the temperature dependence of k_a and k_d, the adsorption and desorption rate constants for monolayer assembly. Our data indicate that

the formation of these monolayers is spontaneous by ~-5.5 kcal/mol at room temperature because of the offsetting effects of large enthalpic and entropic forces. In this chapter, we focus on 1-octadecanethiol/gold monolayer formation from *n*-hexane. We measure the temperature dependence of the equilibrium constant K_{eq} to determine the enthalpy of adsorption, ΔH_{ads}. From $\Delta G_{ads}(T)$ and ΔH_{ads} we determine the entropy of adsorption, ΔS_{ads}. These thermodynamic quantities underscore the high degree of molecular organization characteristic of self-assembled monolayers and serve to place limits on the ultimate structural robustness and chemical "tunability" attainable with a thiol/gold monolayer assembly approach.

3.2. Experimental

Kinetic measurements: We have reported previously on the microbalance apparatus used to measure monolayer adsorption kinetics in chapter 2[18] and recap only the essential details here. The QCM was suspended in solution with isolated electrical connections for both gold electrodes using a modified spring clip. AT-cut quartz crystal microbalances (6 MHz resonance frequency) with vapor deposited gold electrodes were obtained from McCoy Electronics (part number 78-18-4). The QCM was connected to a ~6 MHz oscillator tank circuit (Maxtek part number 124200-4) and a frequency counter (Phillips model PM 6673) was used to monitor the QCM oscillation frequency. This frequency counter has 1 Hz resolution with a gate time of 280 ms. The analog output of the frequency counter was routed to a computer for acquisition, A/D conversion and storage. For all adsorption rate measurements, the data were acquired at ten readings per second to ensure adequate sampling of the QCM kinetic response. Electrical

connections between components were made using shielded coaxial cables to minimize QCM frequency instability arising from electrical interference.

QCMs with a resonance frequency of ~ 6 MHz are sensitive to mass changes as small as a few nanograms. Several factors, in addition to the mass loading of the device surfaces, can affect its oscillation frequency. The resonance frequency of the QCM is related to mass loading according to the Sauerbrey equation.[69] This relationship holds quantitatively for gas phase measurements, but *in situ* solution phase measurements using the QCM are, in many cases, only semi-quantitative due to the complex dielectric response of the solvent and the presence of the adlayer(s). The basis for complications associated with QCM mass measurement in liquids is discussed in detail elsewhere,[70,71] and is not directly relevant to the focus of this work. Our primary objective here is to determine the rate of mass change associated with the formation of the alkanethiol monolayer. We do not attempt to extract absolute mass change information from our data and thus many of the complications associated with the operation of a QCM in solution for quantitative applications do not play a role in our measurements.

In addition to the several material factors that contribute to the experimental response of the QCM, the resonant frequency of these devices depends sensitively on temperature. To minimize QCM frequency drift associated with thermal fluctuations, the temperature of the solution and QCM was controlled to within ± 0.05 K for a given set point. Measurements were performed in a 150 mL jacketed beaker connected to a flowing liquid temperature controller (Neslab model RTE-110). The temperature was varied from 288 K to 303 K in increments of 5 K. Total solution volume in the jacketed beaker was 100.0 mL for each measurement. Stirring was accomplished with a magnetic

stirrer and a Teflon® coated stir bar. The stirring speed was set to be as fast as possible without introducing fluctuations to the QCM baseline frequency.

The jacketed beakers and other glassware used for the measurements were cleaned using the same methods reported in Chapter 2. The cleaned QCMs were then rinsed with THF to remove any residual water, then with *n*-hexane and used immediately thereafter. Individual monolayer adsorption measurements began with pure solvent in the temperature controlled vessel to establish a stable QCM baseline oscillation frequency. An aliquot of stock thiol solution was then introduced by syringe. The stock solutions were maintained at the same temperature as the solvent in the reaction vessel to avoid thermal disruptions resulting from injection.

Conductivity measurements. The conductivity of suspensions of gold dust in ethanol were measured before and after the addition of 1-octadecanethiol using a conductivity meter and cell (Cole-Parmer model 19100-00).

Chemicals. 1-Octadecanethiol was purchased from Aldrich Chemical Co. and used as received. The thiol was tested by gas chromatography and mass spectrometry to determine the presence of the corresponding dioctadecyldisulfide, and none was detected. The solvent *n*-hexane was purchased from Baxter (Burdick and Jackson) and used without further purification. For conductivity measurements, 1 - 3 μm gold dust was purchased from Aldrich Chemical Co. and used as received. For the conductivity measurements, anhydrous ethanol solvent was used.

3.3. Results and Discussion

The adsorption and desorption reactions. Before presenting our experimental data on the thermodynamics of monolayer formation, it is important to have a clear

understanding of the chemical reaction to which these data apply. While the initial reactants are known and the product monolayer is comparatively well characterized, the structural identities of monolayer constituents that desorb from the gold surface remains open to speculation and is awaiting direct experimental verification of their identity. Specifically, there are two points of uncertainty that exist in the literature. These are the fate of the thiol hydrogen and its role in desorption, and the competition between thiol desorption and disulfide desorption. We consider below the current understanding of these reactions, the possible desorption products and the likely reaction scheme for our experimental conditions.

The initial adsorption reaction can, in principle, proceed either by ionic dissociation of the thiol or by formation of H·,

$$RSH + Au \longrightarrow RSAu^- + H^+ \qquad [3.i]$$

$$RSH + Au \longrightarrow RSAu + H\bullet \qquad [3.ii]$$

and based on available electrochemical evidence as presented in Chapter 2[18,19,24] as well as conductometric data,[72] reaction 3.*ii* is favored significantly over reaction 3.*i*. This portion of the monolayer formation reaction is comparatively well understood, save for the fate of H· at the gold surface. The role of H· is different in the two most likely desorption reactions,

$$2RSH_{(solv.)} + 2Au_{(s)} \underset{k_{-1}}{\overset{k_1}{\rightleftharpoons}} 2RSAu_{(s)} + H_2 \qquad [3.iii]$$

$$2RSAu_{(s)} \underset{k_{-2}}{\overset{k_2}{\rightleftharpoons}} RSSR_{(solv.)} + 2Au \qquad [3.iv]$$

We consider first the enthalpic contributions to the reactions 3.*iii* and 3.*iv* to estimate the course of the desorption, whether it is predominantly via k_{-1} or k_2. Given the starting materials, $RSH_{(solv.)}$ and $Au_{(s)}$, the forward reaction, with rate constant k_1, is the starting point. In order to estimate the heat of reaction, we need first to understand the fate of H·. There is literature precedent for absorption of H· into thin gold films,[73] and such an absorption would be in competition with formation of H_2 from 2 H·. For the reaction $2H\cdot \rightarrow H_2$, ΔH = -104 kcal/mol,[74] and for $H\cdot + Au_{(s)} \rightarrow H\cdot Au_{(s)}$, $\Delta H \cong$ -2 kcal/mol.[73] The formation of molecular hydrogen will be favored over dissolution of H· into the gold matrix, although this is not necessarily the case for all metals, such as Pd or Pt. We must also consider the possibility that H_2 is stored as H_2O_2 if O_2 is available to the reaction at the time of monolayer formation. The enthalpy of formation of H_2O_2 from H_2 and O_2 is ~ - 45 kcal/mol, and the dissociation reaction of H_2O_2 to form $H\cdot + HO_2\cdot$ yields -40 kcal/mol.[74] Thus the presence of O_2 at the surface has some effect on the availability of H· to the desorption but the energies are modest and the desorption to the thiol will still proceed because of the limited amount of O_2 available at the gold reaction site.

For the formation of the monolayer, where the bond dissociation energy for the RS-H bond is taken to be ~ 87 kcal/mol,[20] the RS-Au bond dissociation energy is ~ 40 kcal/mol[1] and $2\ H\cdot \rightarrow H_2$ dominates over gold matrix absorption of H·, the calculated heat of this reaction is -5 kcal/mol. The heat of the reverse reaction, denoted by the rate constant k_{-1} in scheme 3.*iii*, is 5 kcal/mol, if all of the reactants are available. We compare the desorptive reaction yielding starting materials to the formation of the

disulfide, according to the reaction denoted by rate constant k_2 in scheme 3.*iv*. The reaction to form RSSR involves the breakage of two RS-Au bonds (40 kcal/mol each) and the formation of a RS-SR disulfide bond, (~74 kcal/mol for disulfide bond cleavage[20]), yielding a net heat for the k_2 desorptive process of +6 kcal/mol. Note that this latter reaction does not require hydrogen to proceed, where the reaction to form thiol from the adsorbed monolayer does require a source of H_2. Based on enthalpic arguments alone, and given the presence of H_2 from the initial monolayer formation, we would predict that both desorption reactions will contribute to the monolayer dynamics.

The enthalpic contributions to the formation and dynamics of these monolayers do not provide a complete picture, however. In addition to enthalpic contributions to the reaction, there are also entropic considerations that are non-negligible (*vide infra*). As we detail below, our data indicate a large negative entropy associated with the formation of the monolayer. In other words, there is a significant increase in the order of the system in going from a clean metal surface and solvated thiols to an organized two-dimensional array of gold-thiol adsorbed species. There is a significant entropic driving force for the desorption of the monolayer, and the expected entropic contributions for the two processes presented in schemes 3.*iii* and 3.*iv* need to be compared. We measure experimentally that $\Delta S_{des} > 0$, and argue that, on stoichiometric grounds, $\Delta S_{des}^{RSH} \sim 2\Delta S_{des}^{RSSR}$. Given that the enthalpic contributions to each desorption reaction are essentially identical, to within the uncertainty of the values used in these estimates, the difference in the free energy of desorption for the two processes will be determined by the entropic term,

$$\Delta G_{des}^{2RSH} - \Delta G_{des}^{RSSR} = -T\Delta S_{des}^{RSSR} \qquad [3.1]$$

Eq. 3.1 indicates that the energetic barrier for desorption of the monolayer back to thiol is smaller than that for desorption of a disulfide by an amount $\sim T\Delta S_{des}^{RSSR}$. For our experimental conditions, which we describe below, we estimate that desorption back to the thiol is favored over disulfide desorption by ~ 6 - 12 kcal/mol near 300 K.

As noted above, the dominance of desorption to yield the thiol requires the availability of H_2 and/or H·, and if these species are not available, then desorption to form disulfides in solution would dominate the reaction pathway. Given the presence of H_2 in the system by the formation of the monolayer, the solubility of H· in gold, and the presence of air, we believe that the dominant reaction for our experiments is

$$RSH_{(solv.)} + Au_{(s)} \underset{k_d}{\overset{k_a}{\rightleftharpoons}} RSAu_{(s)} + 1/2H_{2(solv.)} \qquad [3.v]$$

where k_a and k_d are the adsorption and desorption rate constants for monolayer formation. There are several conditions for which this could not be the dominant desorption pathway, such as when disulfides[68] or thioethers[20] are used in forming the monolayer. Under these conditions, where H_2 is not available as a product of the initial adsorption reaction, we expect that desorption of disulfides will be the primary reaction pathway. With the probable chemical reaction pathway determined for our measurements, we consider next the form and interpretation of the QCM kinetic data.

Experimental data and reaction kinetics. The monolayer formation experiments yield information about the assembly of alkanethiol/gold monolayers based on *in-situ*, real-time data (Chapter 2, Figure 2.1). Noticeable is the short time it takes to achieve a steady state condition (seconds). Early studies reported that monolayers required

formation times of hours to days.[6,8,62] However, these *ex-situ* studies were done using techniques that measured properties resulting from monolayer formation such as ellipsometric thickness, IR peak position or solvent contact angle.[6,8,62] It has since been found that the monolayer properties mentioned above are the result of ordering brought about by the structural annealing of the monolayer aliphatic chains. More recent studies have shown that there are two distinct processes associated with monolayer formation. The first process is adsorption of thiol head group to the gold surface and the second is structural annealing of the adsorbate aliphatic chains. There is some very recent and compelling evidence for cooperative interactions between head and tail groups in the formation of monolayers by UHV vapor phase adsorption.[57] Adsorption from solution, however, will be mediated by the solvent interactions with the thiol tail group and the cooperative formation of highly organized islands of alkanethiols on gold for low fractional coverages from solution remains to be demonstrated. We consider for solution phase processes that the adsorption and annealing processes can be treated separately to good approximation based on the significant body of experimental data indicating their widely differing timescales.[6,8,18,62] An important factor in the acquisition of the raw data is the temporal resolution of the measurement. We designed our experiment so that we would have sufficient data for determination of the kinetic rate constants. The frequency counter we used had a gate time of 280 ms (~ 4 readings/second), and the computer data collection program acquired 10 readings/second. Oversampling in this manner ensures that the frequency counter time resolution is limiting for these experiments.

We next consider the interpretation of our raw kinetic QCM responses. We have provided a detailed explanation of the data processing and modeling in Chapter 2,[18] and

include only the essential aspects of this treatment here. The adsorption experiments were performed in solutions with concentrations ranging from $3x10^{-6}$ M to $3x10^{-4}$ M 1-octadecanethiol in *n*-hexane. The adsorption kinetics exhibit a concentration dependence with the rates increasing in proportion to thiol solution concentration. Within the concentration range used here, we model our Δf vs. time data using the Langmuir adsorption isotherm,[64-66]

$$\frac{d\theta}{dt} = k_a(1-\theta)C - k_d\theta \qquad [3.2]$$

where θ is the fraction of available sites, and the quantities k_a and k_d are the adsorption and desorption rate constants, respectively. As noted previously, there are several assumptions implicit in the use of the Langmuir adsorption isotherm for describing the formation and desorption of these monolayers. Based on our previous measurement of $\Delta G_{ads} \sim -5.5$ kcal/mol for these monolayers,[18] the assumption of non-interacting adjacent adsorption sites is not violated seriously. In addition, the identity of the monolayer constituents precludes multilayer formation, at least in the concentration range used here. The Langmuir adsorption isotherm provides a framework for data interpretation that is consistent with our knowledge of this system. Integration of Eq. 3.2 yields the time dependence of monolayer formation, indicating exponential growth of the layer in time,

$$\theta(t) = \frac{C}{C + k_d/k_a}\left[1 - \exp\left(-k_aC + k_d\right)t\right] \qquad [3.3]$$

We measure, for a given thiol concentration and temperature, a build-up of the monolayer in time that is fit best by a single rate constant, $k_{obs} = k_aC + k_d$. We also

substitute k'=C/(C+[k_d/k_a]) into Eq. 3.3 because we are not attempting to quantitate the mass adsorbed. The term k' corresponds to the steady state fractional coverage of the monolayer, $\theta(\infty)$. To account for finite introduction time of the thiol into the reaction vessel, we incorporate a temporal offset (t_0) in our fitting equation. The simplified form of Eq. 3.3 used to fit the data is

$$\theta(t-t_0) = k'\left[1-\exp\left(-k_{obs}\left(t-t_0\right)\right)\right] \qquad [3.4]$$

See Chapter 2, Figure 2.3 for an example of the fit of Eq. 3.4 to the experimental data. Note that, as discussed above, we are not attempting to extract adsorbed mass information because of the complications associated with solution phase measurements. We have determined the concentration and temperature dependence of k_{obs} (Table 3.1). For a given temperature, the dependence of k_{obs} on thiol concentration (Figure 3.1) provides information on the adsorption and desorption rate constants k_a and k_d (Table 3.2). These data can be used to calculate the equilibrium constant K_{eq} and thus the Gibbs free energy of adsorption, ΔG_{ads}, for the adsorption reaction 3.*v*,

$$K_{eq} = \frac{k_a}{k_d}$$
$$\Delta G_{ads} = -RT\ln K_{eq} \qquad [3.5]$$

By performing our experiments at specific temperatures in the range of 288 K to 303 K, we have measured the temperature dependence of K_{eq} and ΔG_{ads} which we present in Table 3.3 and Figures 3.2. The data exhibit a substantial decrease in K_{eq} with increasing temperature; ΔG_{ads} becomes less negative with increasing temperature. Since a negative

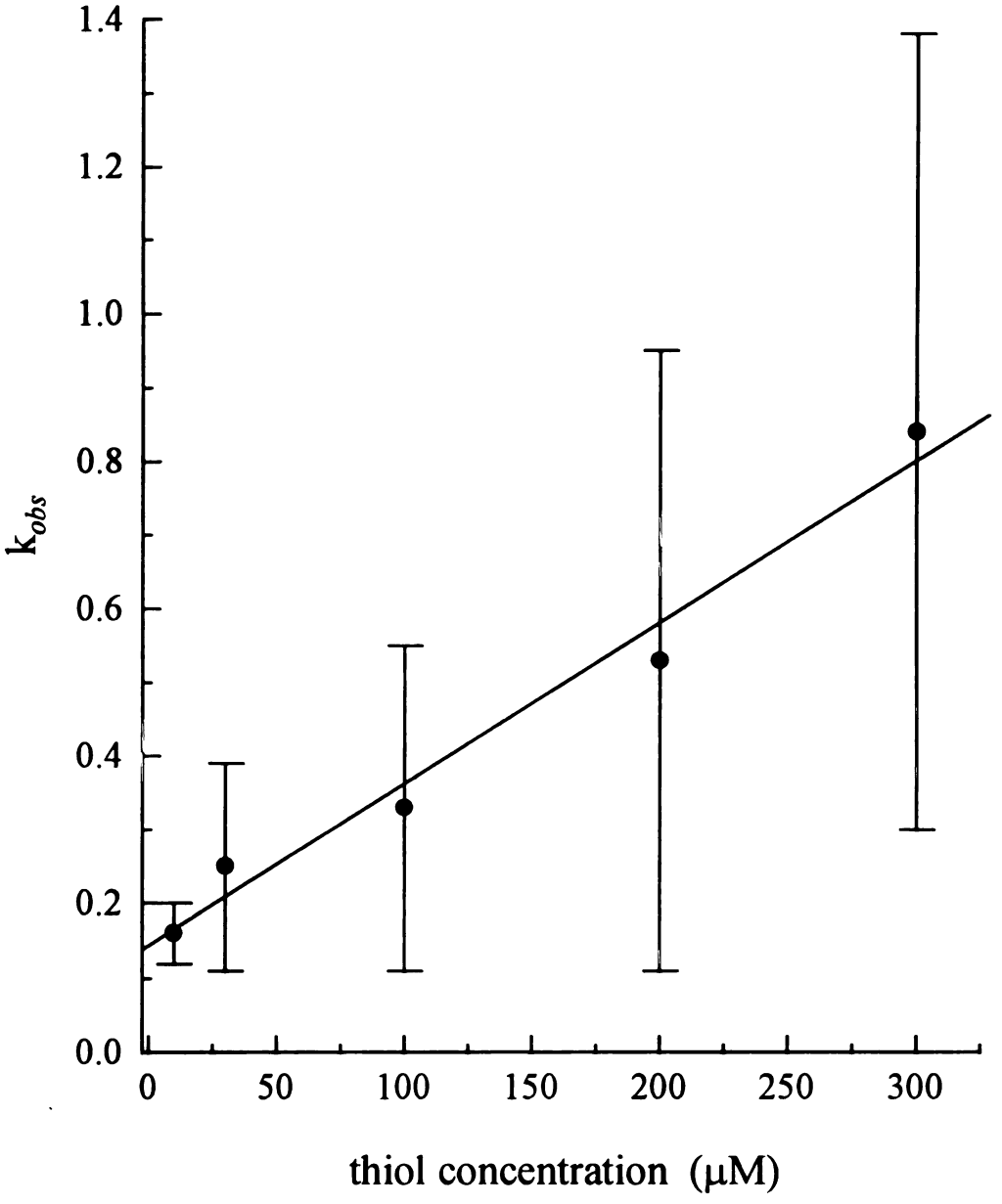

Figure 3.1. Concentration dependence of k_{obs} at 293 K. From these data we obtain best fit values of $k_a = 2278 \pm 92\ M^{-1}\ s^{-1}$ and $k_d = 0.08 \pm 0.02\ s^{-1}$

Table 3.1: k_{obs} values determined from raw data as a function of thiol concentration.

Temperature (K)	thiol concentration (M)	$k_{obs} \pm 95\%$ C.I. (s^{-1})
288	1×10^{-5}	0.17 ± 0.09
	3×10^{-5}	0.28 ± 0.10
	1×10^{-4}	0.96 ± 0.84
	2×10^{-4}	1.44 ± 0.86
293	1×10^{-5}	0.11 ± 0.04
	3×10^{-5}	0.15 ± 0.11
	2×10^{-4}	0.51 ± 0.35
	3×10^{-4}	0.78 ± 0.46
298	1×10^{-5}	0.16 ± 0.04
	3×10^{-5}	0.25 ± 0.14
	1×10^{-4}	0.33 ± 0.22
	2×10^{-4}	0.53 ± 0.42
	3×10^{-4}	0.84 ± 0.54
303	1×10^{-5}	0.21 ± 0.08
	3×10^{-5}	0.40 ± 0.13
	1×10^{-4}	0.43 ± 0.20
	2×10^{-4}	0.71 ± 0.33

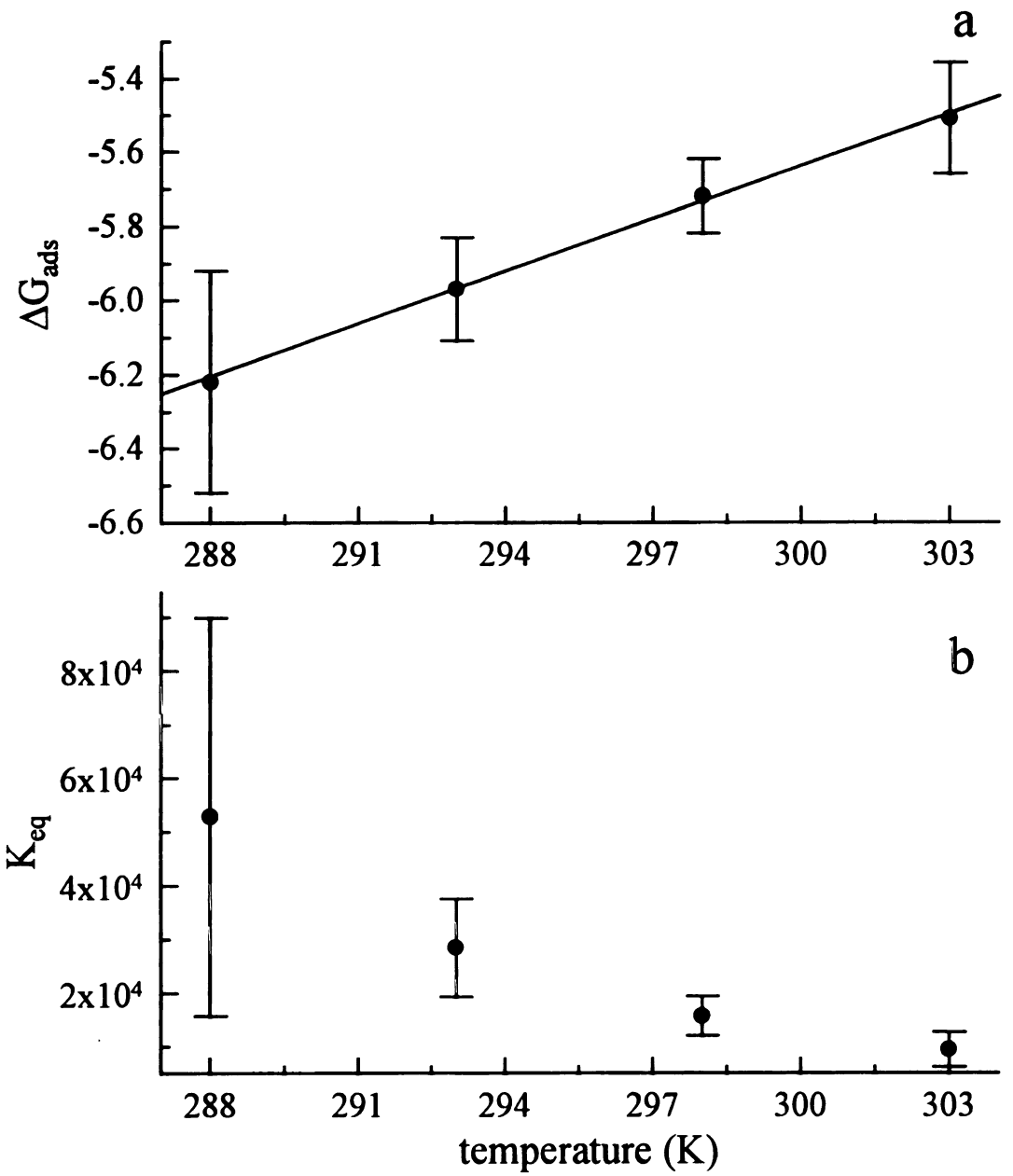

Figure 3.2. Temperature dependence of (a) ΔG_{ads} and (b) K_{eq}. The regressed line shown in (a) yields a slope of $-\Delta S_{ads}$ = 48 ±1 cal/mol-K and an intercept of ΔH_{ads} = -19.9 ± 0.4 kcal/mol.

Table 3.2: Adsorption and desorption rate constants (k_a and k_d) from fits of Eq. 3.4 and $k_{obs} = k_a C + k_d$ to the experimental data.

Temperature (K)	$k_a \pm$ 95% C.I. ($M^{-1}s^{-1}$)	$k_d \pm$ 95% C.I. (s^{-1})
288	6871 ± 803	0.13 ± 0.09
293	2278 ± 92	0.08 ± 0.02
298	2201 ± 198	0.14 ± 0.03
303	2278 ± 537	0.24 ± 0.06

Table 3.3: Temperature Dependence of the Equilibrium Constant (K_{eq}) and the Gibbs Free Energy of Adsorption (ΔG_{ads}).

Temperature (K)	$K_{eq} \pm$ 95% C.I.	$\Delta G_{ads} \pm$ 95% C.I. (kcal/mol)
288	52854 ± 37100	-6.22 ± 0.30
293	28475 ± 9134	-5.97 ± 0.14
298	15721 ± 3653	-5.72 ± 0.10
303	9492 ± 3262	-5.51 ± 0.15

ΔG_{ads} indicates a spontaneous condition, the trend to less spontaneous ΔG_{ads} with increasing temperature indicates that the adsorption process we measure is exothermic. The temperature dependence of K_{eq} allows the calculation of the enthalpy of adsorption, ΔH_{ads}, using the van't Hoff equation,[66]

$$\frac{-\Delta H_{ads}}{R} = \frac{\ln K_{eq}}{T^{-1}} \qquad [3.6]$$

We show in Figure 3.3 the linear dependence of $ln\ K_{eq}$ on T^{-1} giving a slope of $-\Delta H_{ads}/R$. We obtain ΔH_{ads} = -20 ± 1 kcal/mol for the adsorption of 1-octadecanethiol/gold monolayers from *n*-hexane. From the $\Delta G_{ads}(T)$ and ΔH_{ads}, we obtain the entropy of adsorption,

$$\Delta G_{ads} = \Delta H_{ads} - T\Delta S_{ads} \qquad [3.7]$$

The dependence of ΔG_{ads} on T is shown in Figure 3.2a. We find from a regression of these data that ΔS_{ads} = -48 ± 1 cal/mol K and, as a comparison to the van't Hoff determination of ΔH_{ads}, we obtain ΔH_{ads} = -19.9 ± 0.4 kcal/mol. This alternate route to ΔH_{ads} serves as a useful self-consistency check on our results.

We note that, because the alkanethiol/gold system is an equilibrium system, the fractional coverage of the Au surface depends on the concentration of the thiol solution, and over the concentration range studied here the fraction of the surface, $\theta \sim 0.1$ (RSH = $1x10^{-5}$M) to $\theta \sim 1$ (RSH = $3x10^{-4}$M).[18] This concentration dependent surface coverage is expressed in the prefactor of Eq. 3.3 and is an expected result based on the predictions of the Langmuir adsorption isotherm. The phenomenon under examination in this work is the initial formation of the gold-thiol bond, which is expected to proceed more rapidly than rearrangement and annealing steps in the formation of the monolayer. The

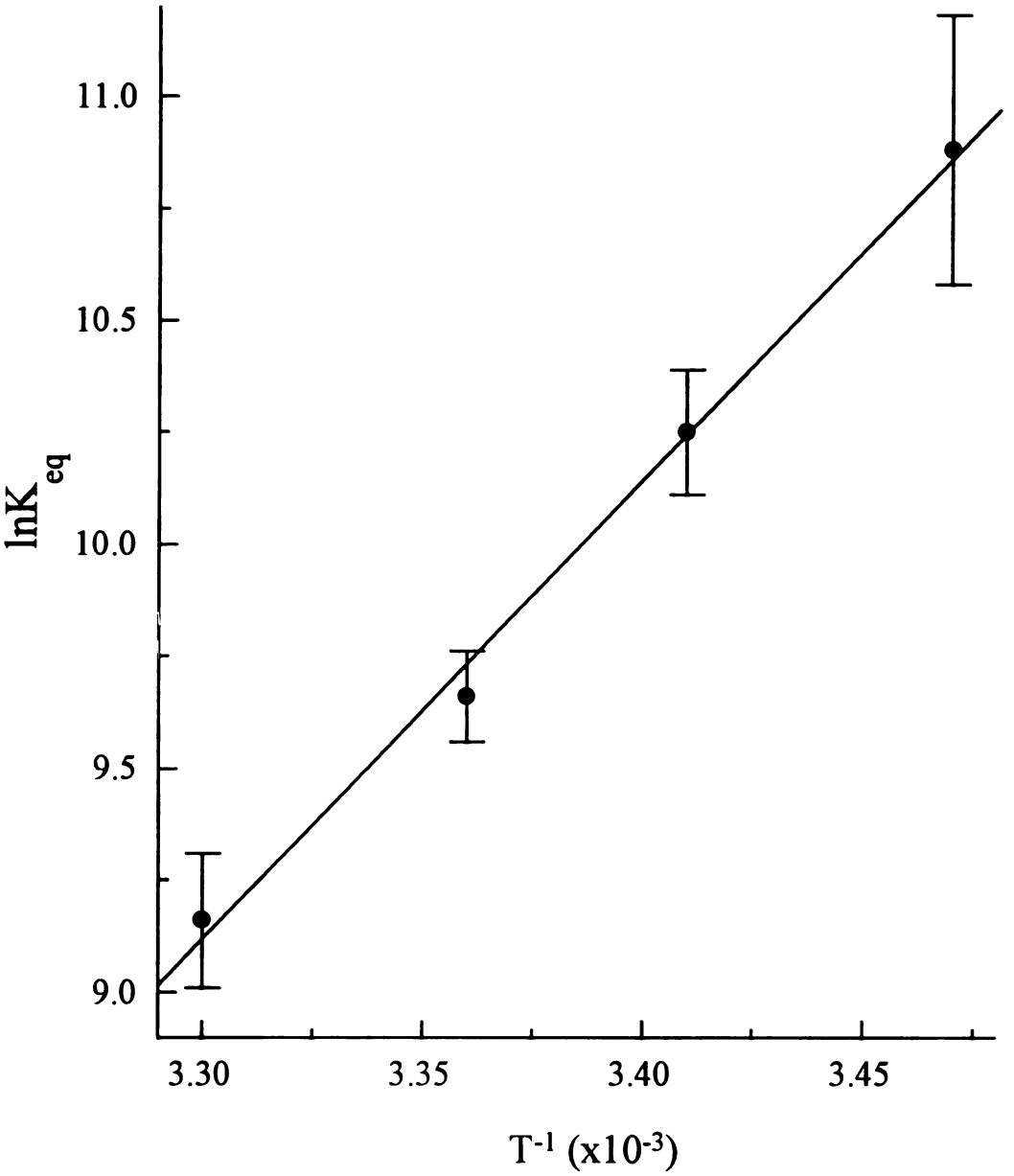

Figure 3.3. Van't Hoff plot of *ln* K_{eq} vs. T^{-1}. From these data, we determined ΔH_{ads} = -20 ± 1 kcal/mol.

thermodynamic results on alkanethiol adsorption to gold are interesting in and of themselves and are consistent with the other, limited thermodynamic data that exist for these systems. We consider next the implications and chemical information content of these results.

Before discussing the chemical implications of these data, we need to consider whether or not the adsorption process is diffusion limited. Indeed, if the reaction under consideration is diffusion limited, then a Langmuir treatment of our data is inappropriate. We presume as a starting point that both adsorption and desorption occur, and this *ansatz* is supported by both McCarley's[17] and Poirier's[56] atomic microscopy data. Recently, the Schlenoff group has suggested that the adsorption reaction is diffusion rate limited[63] based on initial rate data that we had reported previously.[18] The temperature dependence of the observed rate constant for a fixed thiol concentration (Figure 3.4) demonstrate clearly that the adsorption reaction is not diffusion rate limited. Our basis for this statement is that a diffusion rate limited reaction should possess a rate constant that depends linearly on temperature,[65] and the data presented in Figure 3.5 are independent of T, to within the uncertainty of the measurement. We note that the data presented in Figure 3.4 are rate constants extracted directly from raw data and do not depend on the use of the Langmuir isotherm. Regardless of the isotherm under consideration, our data demonstrate that the adsorption of alkanethiols onto gold are not diffusion limited for these conditions.

There are two processes intrinsic to the formation of self-assembled monolayers, and they proceed on significantly different time scales. These processes are the initial adsorption of the thiol head group to the gold surface, which occurs within seconds of

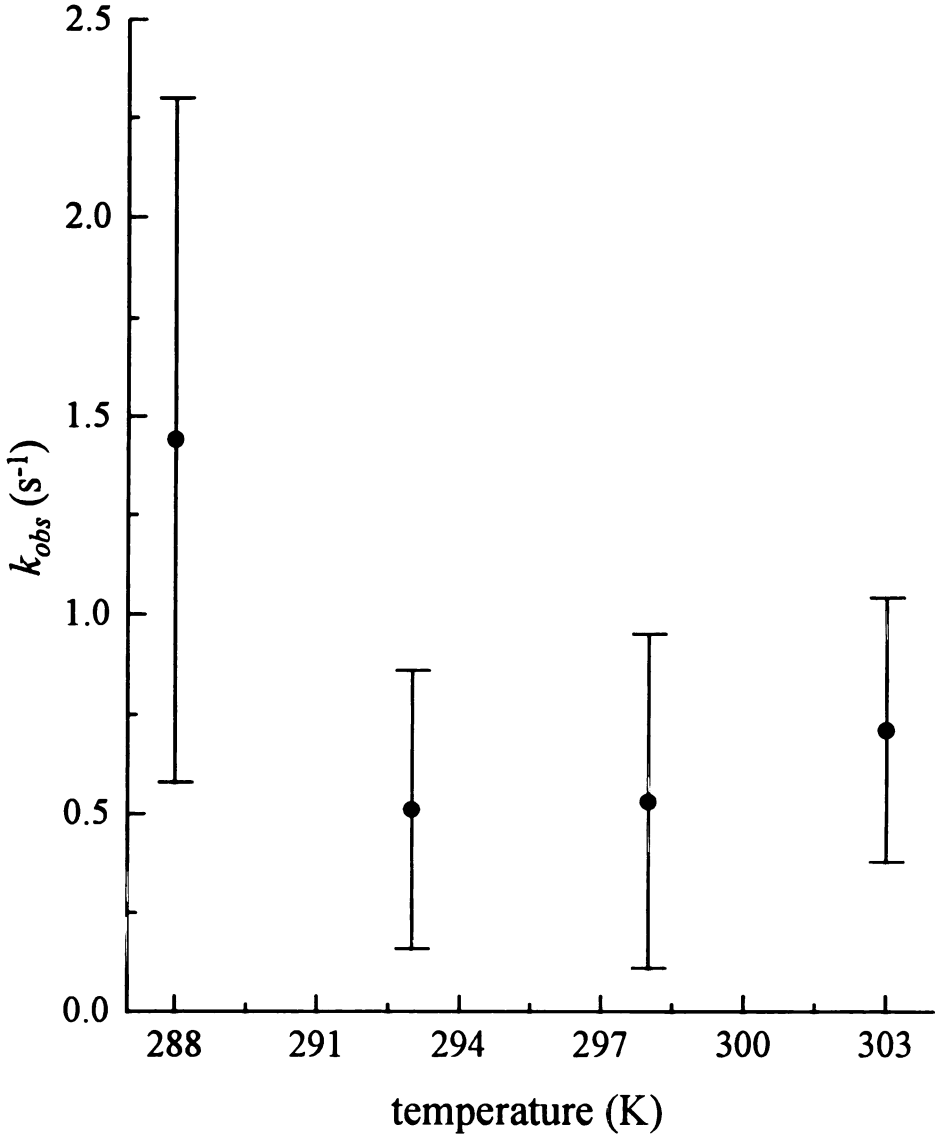

Figure 3.4. Temperature dependence of the observed rate constants, k_{obs}. These data are essentially temperature independent, to within the uncertainty of the measurements. No linear dependence of k_{obs} on T is detectable from these data.

exposure and, subsequent to head group adsorption, the aliphatic chains anneal from an initially statistical distribution of conformers to a predominantly all-*trans* conformation over a period of hours to days. Our QCM-based kinetic studies yield information about thiol head group adsorption. Accordingly, we consider the processes of initial adsorption and aliphatic annealing separately and assume that they are significantly decoupled.

For 1-octadecanethiol/gold monolayer formation from *n*-hexane, $\Delta G_{ads} \cong -5.5$ kcal/mol depending on the temperature. The magnitude of ΔG_{ads} for the 1-octadecanethiol/gold monolayer is the same as that of a liquid alcohol hydrogen bond; the result of a close balance between the enthalpy and entropy of adsorption, both of which are significant for this reaction. The enthalpy of adsorption, ΔH_{ads}, was found to be -20 ± 1 kcal/mol. We note that this value does not correspond closely with the calculated quantities discussed above for the formation and desorption of the monolayer. We understand the differences between calculation and experiment based on our use of standard enthalpies in the calculations and the significant difference between our experimental conditions, which include solvation effects, and standard conditions. We can compare our experimental value of ΔH_{ads} to the ΔH for desorption of a monolayer of 28 kcal/mol for desorption into air obtained by Nuzzo and coworkers.[68] Our data contain both solvation and adsorption information and their data are a direct measure of (reversible) desorption. The difference between their data and ours indicates the enthalpy of solvation, $\Delta H_{solv} \sim -8$ kcal/mol for 1-octadecanethiol in *n*-hexane because their data represent, almost exclusively, the gold-sulfur interaction. The enthalpy of solvation is both solvent and thiol dependent and thus -8 kcal/mol is a useful, but only

qualitative, estimate for other systems. The adsorption enthalpy we measure, ΔH_{ads} (-20 kcal/mol), consists of the balance between the solvation enthalpy ΔH_{solv} (-8 kcal/mol) and the monolayer formation enthalpy ΔH_{ml} (-28 kcal/mol).

$$\Delta H_{ads} = \Delta H_{ml} - \Delta H_{solv} \qquad [3.8]$$

The quantity ΔH_{ml} is dominated by Au-S bond formation and any energy associated with displacement of solvent from the gold surface during the formation of the monolayer. We expect that ΔH_{ml} will be largely independent of thiol chain length because the dominant process on these comparatively short time scales is the interaction between the thiol head group and the metal surface. We note that one potential solvent-dependent contribution to ΔH_{ml} may be associated with the polarity of the transition state in the formation of the gold-thiol bond and the extent to which the solvent stabilizes or destabilizes that state,[40] but this effect is likely to be modest because of steric constraints in the formation of the monolayer and the presence of the metal interface.

The entropy of adsorption, ΔS_{ads} = -48 ± 1 cal/mol-K. This quantity is approximately four times larger than a typical ΔS_{fus} for a liquid-to-solid phase transition.[74] For the same reason that ΔH_{ml} is largely thiol independent, we expect the entropy of adsorption, ΔS_{ads}, to be substantially independent of thiol aliphatic chain length. This large entropic term is dominated by the change in system order associated with alkanethiols oriented randomly in solution going to produce a highly organized, two-dimensional crystalline array of thiol head groups on gold.

Given the predicted thiol independence of ΔH_{ml} and ΔS_{ads}, it is important to review our previous experiments indicating solvent and thiol dependent monolayer

formation. We account for the thiol dependence of ΔG_{ads} we observed for monolayer formation from *n*-hexane based on different solvation enthalpies for the two thiols. For the adsorption of 1-$C_{18}H_{37}SH$, ΔG_{ads} = -5.6 ± 0.2 kcal/mol at 293 K and for 1-$C_8H_{17}SH$ monolayer formation, ΔG_{ads} = -4.4 ± 0.2 kcal/mol at the same temperature.[18] As discussed above, we believe that the enthalpy of monolayer formation, ΔH_{ml}, is constant for all thiols at -28 kcal/mol. The solvation enthalpy ΔH_{solv} is, of course, solvent dependent. We calculate ΔH_{solv} = -8 kcal/mol for 1-octadecanethiol in *n*-hexane and ΔH_{solv} = -9 kcal/mol for 1-octanethiol in *n*-hexane. Invoking the thiol independence of ΔS_{ads} yields ΔH_{ads} = -19 kcal/mol for the 1-octanethiol/gold monolayer. For alkanethiol monolayer formation on gold, the enthalpy of solvation, ΔH_{solv}, is the primary quantity under the influence of experimental control, and attempts to enhance the robustness of alkanethiol monolayers will ultimately be limited by the extent to which ΔH_{solv} can be adjusted.

3.4. Conclusions

We have measured the thermodynamics of 1-octadecanethiol/gold monolayer formation from *n*-hexane solution. Our data indicate that the comparatively small free energy of adsorption for this system is the result of a close balance between the enthalpic driving force for the reaction and an entropic penalty associated with the high degree of organization that accompanies self-assembly. For our experimental conditions, the dominant chemical reaction is the reversible adsorption of the alkanethiol, and the temperature dependence of the QCM kinetic response demonstrates that the reaction, for our conditions, is not diffusion rate limited. These data point collectively to the fact that

there are limits to the robustness of alkanethiol/gold monolayers and that the ability to adjust the formation properties of this system is limited primarily by the solubility of the alkanethiol in the solvent from which the adsorption takes place. Because the formation of the thiol-gold bond is fast compared to the structural annealing of the organic tail group, these data may be of some utility in predicting the formation properties of other thiol/gold assemblies in the limit that steric contributions from the organic tail groups do not preclude significant monolayer formation.

3.5. Literature Cited

1. R. G. Nuzzo, L. H. Dubois, D. L. Allara, *J. Am. Chem. Soc.*, **1990**, *112*, 558.

2. L. H. Dubois, B. R. Zegarski, R. G. Nuzzo, *J. Am. Chem. Soc.*, **1990**, *112*, 570.

3. R. G. Nuzzo, E. M. Korenic, L. H. Dubois, *J. Chem. Phys.*, **1990**, *93*, 767.

4. C. E. D. Chidsey, D. N. Loiacono, *Langmuir*, **1990**, *6*, 682.

5. C. E. D. Chidsey, C. R. Bertozzi, T. M. Putvinski, A. M. Muscje, *J. Am. Chem. Soc.*, **1990**, *112*, 4301.

6. C. D. Bain, E. B. Troughton, Y. T. Tao, J. Evall, G. M. Whitesides, R. G. Nuzzo, *J. Am. Chem. Soc.*, **1989**, *111*, 321.

7. C. D. Bain, G. M. Whitesides, *J. Am. Chem. Soc.*, **1989**, *111*, 7155.

8. E. B. Troughton, C. D. Bain, G. M. Whitesides, R. G. Nuzzo, D. L. Allara, M. D. Porter, *Langmuir*, **1988**, *4*, 365.

9. M. D. Porter, T. B. Bright, D. L. Allara, C. E. D. Chidsey, *J. Am. Chem. Soc.*, **1987**, *109*, 3559.

10. G. M. Whitesides, P. E. Laibinis, *Langmuir*, **1990**, *6*, 87.

11. N. Camillone III, C. E. D. Chidsey, G. Y. Liu, T. M. Putvinski, G. C. Scoles, J. Wang, *J. Chem. Phys.*, **1991**, *94*, 8493.

12. C. E. D. Chidsey, G.-Y. Liu, J. Wang, *Langmuir*, **1990**, *6*, 1804.

13. S. R. Wasserman, G. M. Whitesides, I. M. Tidswell, B. M. Ocko, P. S. Pershan, J. D. Axe, *J. Am. Chem. Soc.*, **1989**, *111*, 5852.

14. C. A. Widrig, C. A. Alves, M. D. Porter, *J. Am. Chem. Soc.*, **1991**, *113*, 2805.

15. G.-Y. Liu, M. B. Salmeron, *Langmuir*, **1994**, *10*, 367.

16. R. L. McCarley, Y.-T. Kim, A. J. Bard, *J. Phys. Chem.*, **1993**, *97*, 211.

17. R. L. McCarley, D. J. Dunnaway, R. J. Willicut, *Langmuir*, **1993**, *9*, 2775.

18. D. S. Karpovich, G. J. Blanchard, *Langmuir*, **1994**, *10*, 3315.

19. C. A. Widrig, C. Chung, M. D. Porter, *J. Electroanal. Chem.*, **1991**, *310*, 335.

20. C.-J. Zhong, M. D. Porter, *J. Am. Chem. Soc.*, **1994**, *116*, 11616.

21. D. E. Weishaar, M. M. Walczak, M. D. Porter, *Langmuir*, **1993**, *9*, 323.

22. C. A. Alves, E. L. Smith, M. D. Porter, *J. Am. Chem. Soc.*, **1992**, *114*, 1222.

23. C.-J. Zhong, M. D. Porter, *Anal. Chem.*, **1995**, *67*, 709A.

24. D. E. Weishaar, B. D. Lamp, M. D. Porter, *J. Am. Chem. Soc.*, **1992**, *114*, 5860.

25. E. L. Smith, C. A. Alves, J. W. Anderegg, M. D. Porter, L. M. Siperko, *Langmuir*, **1992**, *8*, 2707.

26. E. L. Smith, M. D. Porter, *J. Phys. Chem.*, **1993**, *97*, 8032.

27. M. O. Wolf, M. A. Fox, *Langmuir*, **1996**, *12*, 955.

28. J. M. Tour, L. Jones II, D. L. Pearson, J. J. S. Lamba, T. P. Burgin, G. M. Whitesides, D. L. Allara, A. N. Parikh, S. V. Atre, *J. Am. Chem. Soc.*, **1995**, *117*, 9529.

29. N. Lewis, M. Tarlov, *J. Am. Chem. Soc.*, **1995**, *117*, 9574.

30. R. J. Willicut, R. L. McCarley, *Langmuir*, **1995**, *11*, 296.

31. K. Sinniah, J. Cheng, S. Terrataz, J. E. Reutt-Robey, C. J. Miller, *J. Phys. Chem.*, **1995**, *99*, 14500.

32. R. L. Garrell, J. E. Chadwick, D. L. Severance, N. A. McDonald, D. C. Miles, *J. Am. Chem. Soc.*, **1995**, *117*, 11563.

33. J.-PBucher, L. Santesson, K. Kern, *Langmuir*, **1994**, *10*, 979.

34. E. Delamarche, B. Michel, H. Kang, Ch. Gerber,; *Langmuir*, **1994**, *10*, 4103.

35. S.-C. Chang, I. Chao, Y.-T. Tao, *J. Am. Chem. Soc.*, **1994**, *116*, 6792.

36. P. Fenter, A. Eberhardt, P. Eisenberger, *Science*, **1994**, *266*, 1216.

37. N. Camillone, III, P. Eisenberger, T. Y. B. Leung, P. Schwartz, G. Scoles, G. E. Poirier, M. J. Tarlov, *J. Chem. Phys.*, **1994**, *101*, 11031.

38. M. R. Anderson, M. Gatin, *Langmuir*, **1994**, *10*, 1638.

39. H. A. Biebuyck, C. D. Bain, G. M. Whitesides, *Langmuir*, **1994**, *10*, 1825.

40. H. Sellers, A. Ulman, Y. Shnidman, J. E. Eilers, *J. Am. Chem. Soc.*, **1993**, *115*, 9389.

41. Y.-T. Kim, R. L. McCarley, A. J. Bard, *Langmuir*, **1993**, *9*, 743.

42. S. E. Creager, L. A. Hockett, G. K. Rowe, *Langmuir*, **1992**, *8*, 854.

43. D. M. Collard, M. A. Fox, *Langmuir*, **1991**, *7*, 1192.

44. P. Krysinski, R. V. Chamberlain, M. M. Majda, *Langmuir*, **1994**, *10*, 4286.

45. O. Chailapakul, L. Sun, C. Xu, R. M. Crooks, *J. Am. Chem. Soc.*, **1993**, *115*, 12459.

46. L. Sun, R. M. Crooks, A. J. Ricco, *Langmuir*, **1993**, *9*, 1775.

47. R. C. Thomas, J. E. Houston, T. A. Michalske, R. M. Crooks, *Science*, **1993**, *259*, 1883.

48. C. D. Bain, G. M. Whitesides, *Science*, **1988**, *240*, 62.

49. J. L. Wilbur, H. A. Biebuyck, J. C. MacDonald, G. M. Whitesides, *Langmuir*, **1995**, *11*, 825.

50. R. A. Drawhorn, N. L. Abbott, *J. Phys. Chem.*, **1995**, *99*, 16511.

51. Y. Xia, X.-M. Zhao, E. Kim, G. M. Whitesides, *Chem. Mater.*, **1995**, *7*, 2332.

52. J. F. Ford, T. M. Vickers, C. K. Mann, J. B. Schlenoff, *Langmuir*, **1992**, *12*, 1944.

53. E. Kim, G. M. Whitesides, L. K. Lee, S. P. Smith, M. Prentiss, *Adv. Mater.*, **1996**, *8*, 139.

54. N. Camillone III, C. E. D. Chidsey, G.-Y Liu, G. Scoles, *J. Chem. Phys.*, **1993**, *98*, 4234.

55. L. Strong, G. M. Whitesides, *Langmuir*, **1988**, *4*, 546.

56. G. E. Poirier, M. J. Tarlov, *J. Phys. Chem.*, **1995**, *99*, 10966.

57. G. E. Poirier, E. D. Pylant, *Science*, **1996**, *272*, 1145.

58. T. M. Nahir, R. A. Clark, E. F. Bowden, *Anal. Chem.*, **1994**, *66*, 2595.

59. I. Taniguchi, K. Toyosawa, H. Yamaguchi, K. Yasukouchi, *J. Electroanal. Chem.*, **1982**, *140*, 187.

60. T. Sagara, K. Niwa, A. Sone, C. Hinnen, K. Niki, *Langmuir*, **1990**, *6*, 254.

61. D. S. Karpovich, G. J. Blanchard, *J. Chem. Ed.*, **1995**, *72*, 466.

62. K. D. Truong, P. A. Rowntree, submitted to *Langmuir*.

63. J. B. Schlenoff, M. Li, H. Ly, *J. Am. Chem. Soc.*, **1995**, *117*, 12528.

64. S. H. Chen, C. W. Frank, *Langmuir*, **1989**, *5*, 978.

65. K. J. Laidler, *Chemical Kinetics, 3rd Ed.*, Harper Collins, New York, **1987**, pp. 231-232.

66. P. W. Atkins, *Physical Chemistry, 4th Ed.*, Freeman, New York, **1990**, pp. 885-887.

67. G. J. Blanchard, *J. Phys. Chem.*, **1988**, *92*, 6303.

68. R. G. Nuzzo, B. R. Zegarski, L. H. Dubois, *J. Am. Chem. Soc.*, **1987**, *109*, 733.

69. G. Z. Sauerbrey, *Z. Phys.*, **1959**, *155*, 206.

70. M. Yang, M. Thompson, *Langmuir*, **1993**, *9*, 802.

71. M. Yang, M. Thompson, *Langmuir*, **1993**, *9*, 1990.

72. We measured the conductivity of a suspension of 1-3 μm gold in anhydrous ethanol during the addition of ethanolic 1-octadecanethiol. We detected no change in the conductivity of the solution as a result of RSH/Au interaction (< 0.01 μ-mho). If the dissociation of H^+ from RS^- were complete, for our experimental conditions we would expect the change in $[H^+] = 4.6x10^{-6}$ M. The corresponding change in conductivity of a $4.6x10^{-6}$ M ethanolic HCl solution relative to neat ethanol was measured to be 0.47 μ-mho.

73. L. Stobinski, R. Dus, *Appl. Surf. Sci.*, **1992**, *62*, 77.

74. *CRC Handbook of Chemistry and Physics, 71st Ed.*, Lide, D. R., Ed.; CRC Press, Boca Raton, FL, 1990.

Chapter 4

Relating the Polarity-Dependent Fluorescence Response of Pyrene to Vibronic Coupling. Achieving a Fundamental Understanding of the *py* Polarity Scale

Summary

We have investigated the fluorescence response of pyrene, a widely used polycyclic aromatic hydrocarbon probe molecule, in a series of solvents that span the empirical "*py*" polarity scale. The relative band intensities in the pyrene fluorescence response are determined by the extent of vibronic coupling between the weakly allowed first excited singlet state and the strongly allowed second excited singlet state. The solvent-dependence of vibronic coupling in pyrene can be inferred from steady state fluorescence measurements in conjunction with fluorescence lifetime and quantum yield measurements. These data, taken collectively, point to the presence of vibronic coupling in pyrene arising from two different mechanisms. The solvent "polarity" sensed by the pyrene molecule is related to dipole-induced dipole interactions between the solvent and pyrene vibrational modes of b_{3g} symmetry which span the nuclear coordinates of the two excited electronic states.

4.1. Introduction

Understanding the bulk characteristics of solutions and more highly organized systems from the perspective of individual molecules is a subject central to the study of chemistry. Intermolecular interactions ultimately determine the bulk properties of a chemical system, and a variety of factors need to be considered in establishing this relationship. Among these factors are molecular structure and conformation, electrostatic, dipolar and multipolar interactions, and short range dispersive interactions. The "polarity" of the environment immediately surrounding a molecule often determines basic properties such as solubility or optical response and, as such, the determination of "polarity" on a molecular length scale has received a great deal of experimental attention. One of the most common methods used in the determination of local polar character is the measurement of some portion of the optical response of a molecule that is sensitive to a particular property of the local medium. For example, solvatochromic molecules are a class of molecules that exhibit absorption and/or emission spectral shifts that depend on the dielectric and dipolar properties of their local environment. Pyrene and other selected polycyclic aromatic hydrocarbons (PAH) are used extensively for probing local polarity.[1-10] While these PAHs do not exhibit spectral frequency shifts similar to solvatochromic molecules, they do exhibit a variation in the ratio of emission band intensities that has been correlated with the "polarity" of the PAH immediate environment. The empirical "*py*" scale of solvent polarity has been established based on the emission response of pyrene and has been catalogued for a wide variety of experimental conditions, ranging from bulk liquids[2,3] to interfacial monolayers.[11-17]

While the *py* polarity scale has enjoyed wide use, there is no general understanding of the molecular processes responsible for the correlation between emission band intensity ratios and solvent "polarity".[4-9] Part of the difficulty in elucidating the mechanism(s) underlying this correlation lies in the ill-defined nature of the "polarity" to which the PAH emission features respond. The other significant question that has limited the utility of this interesting photophysical effect is that there is not presently a model that can predict, from the linear response, whether a given PAH will exhibit this effect or not. Many PAHs have been tested and only a limited number have exhibited behavior similar to that of pyrene.[4-9] The linear optical response of pyrene has been investigated extensively, in part because of the importance of vibronic coupling in determining the emission and absorption responses of this molecule.[18-29] Despite the significant understanding of pyrene's linear response, a firm connection between that body of information and the empirical "*py*" scale has not been made. We assert that there is a direct connection between these two bodies of knowledge and it is the purpose of this work to make that connection. We propose a mechanistic explanation for the empirical "*py*" scale based on what is known about vibronic coupling in pyrene and several experimental measurements of basic photophysical properties, such as spontaneous emission frequency dependence, radiative quantum yield and radiative decay rate constant. These data, taken collectively, can be used to demonstrate a direct correlation between vibronic coupling exhibited by pyrene and the empirical *py* solvent polarity scale. In this paper, following a brief description of the experimental techniques we have applied to this problem, we detail the relationships between fundamental quantities such as radiative decay rate constants, fluorescence quantum yield and

emission band intensities and then provide experimental data that demonstrate the correlation between the empirically measured solvent "polarity" and vibronic coupling in pyrene. We include a discussion of the molecular-scale processes that determine the pyrene steady state fluorescence response and how the linear absorption response of other PAHs can be used to predict the presence or absence of a solvent polarity-dependent emission response.

4.2. Experimental

Chemicals: Pyrene was obtained from Aldrich at 99% purity and was purified by recrystallizing twice from methanol, followed by vacuum sublimation at 130°C.[30] Solvents (Burdick and Jackson Brand high purity grade) were purchased from Baxter Diagnostics Inc., and were used as received. Prior to lifetime and quantum yield measurements, all pyrene solutions were subjected to several (at least three) freeze/pump/thaw cycles to remove oxygen.

Steady state absorption and emission spectra: Emission spectra were recorded on a Hitachi F-4500 fluorimeter. Excitation was at 334 nm with the excitation slits set for a 10 nm bandpass. Emission slit width was set to a 2.5 nm bandpass. Absorption spectra were taken on a Hitachi U-4000 UV-Vis absorption spectrometer.

Fluorescence quantum yield measurements: The fluorescence quantum yield of pyrene was measured in several solvents by means of comparison of the integrated emission intensities in those solvents to the intensity measured for a solution of pyrene in cyclohexane, where the fluorescence quantum yield has been determined before.[31] The equation used to determine the fluorescence quantum yield is[26]

$$\frac{\phi_{fl}^{x}}{\phi_{fl}^{r}} = \left(\frac{n_x^2}{n_r^2}\right)\left(\frac{D_x}{D_r}\right)\left(\frac{A_r}{A_x}\right) \qquad [4.1]$$

The designators *x* and *r* indicate sample and reference, respectively, and ϕ_{fl} is the fluorescence quantum yield. The term (n_x^2/n_r^2) is a correction factor for the refractive index of the solvent and the terms D_i are the integrated intensities under the corrected emission spectra. A_i is the absorbance of the solutions, a quantity used to correct for concentration variation between samples. The absorbances and integrated intensities were available from our steady state absorption and emission spectra, taken from deoxygenated solutions. It is well known that the fluorescence spectrum of pyrene is quenched effectively by oxygen dissolved in solution. The mechanism of this quenching is typically taken to be collisional. Our data show that ϕ_{fl} and τ_{fl} depend sensitively on the presence of oxygen, but the I/III band intensity ratio is not sensitive to the presence of oxygen. This finding is important in its own right because the I/III band intensity ratio is the most commonly reported solvent polarity-dependent quantity.

Fluorescence lifetime measurements: The time-correlated single photon counting spectrometer (Figure 4.1) we used to measure the fluorescence lifetimes of pyrene in different solvents has been described in detail before.[32] All pyrene solutions (~10^{-5} M) were excited at 332 nm, and fluorescence was collected at 390 nm using a 10 nm FWHM detection bandwidth. Fluorescence was collected over all polarization angles to ensure the absence of a contribution from rotational diffusion dynamics to the observed data, although the rotational diffusion time of pyrene in any of the solvents examined is negligible compared to its fluorescence lifetime. Typical instrument response time is ~25-50 ps FWHM and the measured fluorescence lifetimes are several

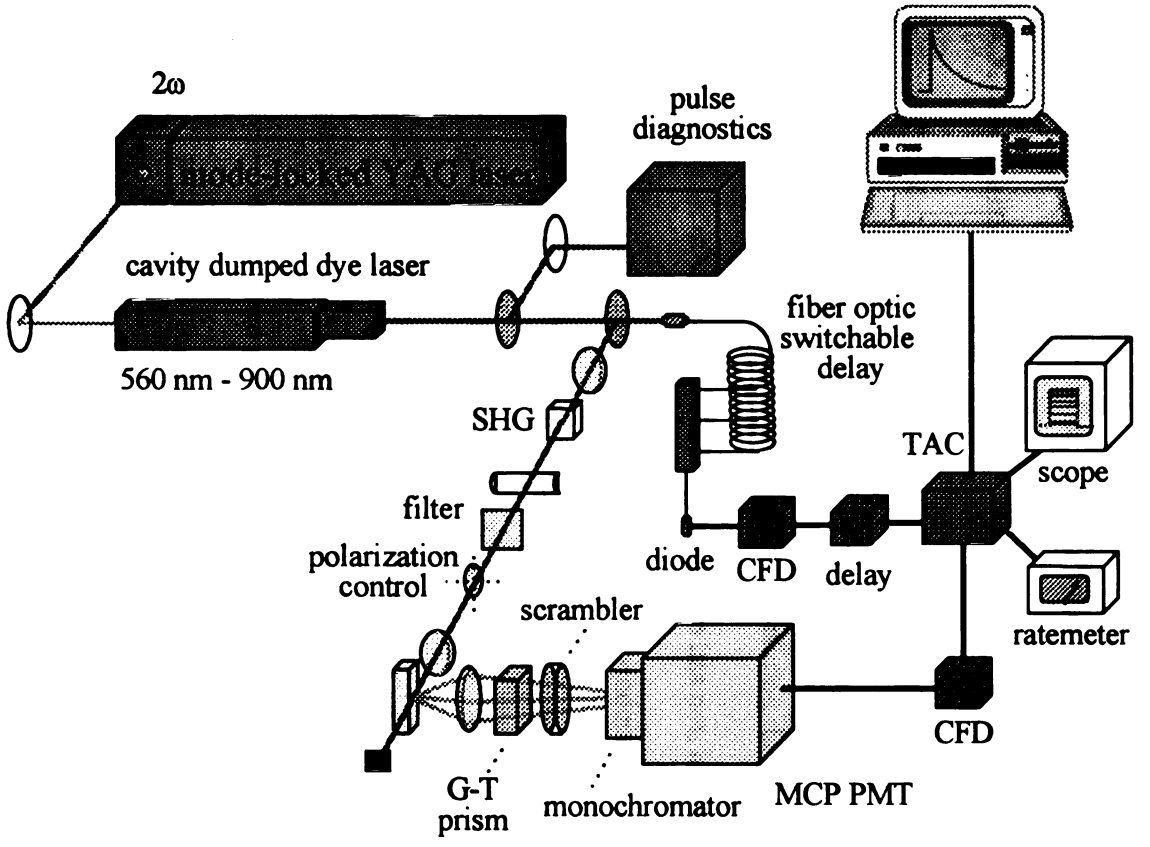

Figure 4.1. Time correlated single photon counting spectrometer used for fluorescence lifetime measurements.

hundreds of nanoseconds. A typical lifetime scan, together with the instrument response function is shown in Figure 4.2. We found the measured lifetimes to be very sensitive to the presence of oxygen. For example, we measure the fluorescence lifetime of pyrene in deoxygenated cyclohexane to be τ_{fl} = 382 ns, and in air-saturated cyclohexane we measure τ_{fl} = 20 ns. Reintroduction of O_2 into a deoxygenated solutions occurs very rapidly (seconds to minutes) after exposure to air.

4.3. Results and Discussion

Previous work on the emission response of pyrene has established the empirical relationship between solvent polarity and the pyrene spontaneous emission band ratios.[2-4] In addition, there have been other reports measuring the radiative rate constant(s) of pyrene in series of solvents.[23,26] The connection has not, however, been drawn directly between vibronic coupling and solvent polarity-dependent emission response. The correlations we report in this paper suggest that vibronic coupling can be used to explain the empirical *py* scale. The relationship between vibronic coupling and solvent polarity can explain why many polycyclic aromatic hydrocarbons do not exhibit a response similar to that seen for pyrene, and also offers insight into the mechanism by which solvent polarity is related to the empirical *py* scale.

In an effort to understand the solvent polarity-dependent emission response of pyrene, we have measured the steady state fluorescence spectrum, the fluorescence lifetime, and the fluorescence quantum yield in a range of solvents spanning the empirical *py* scale. Each of these quantities exhibits a solvent polarity dependence, but it is different for each measured property. As we discuss below, the spectroscopic origin

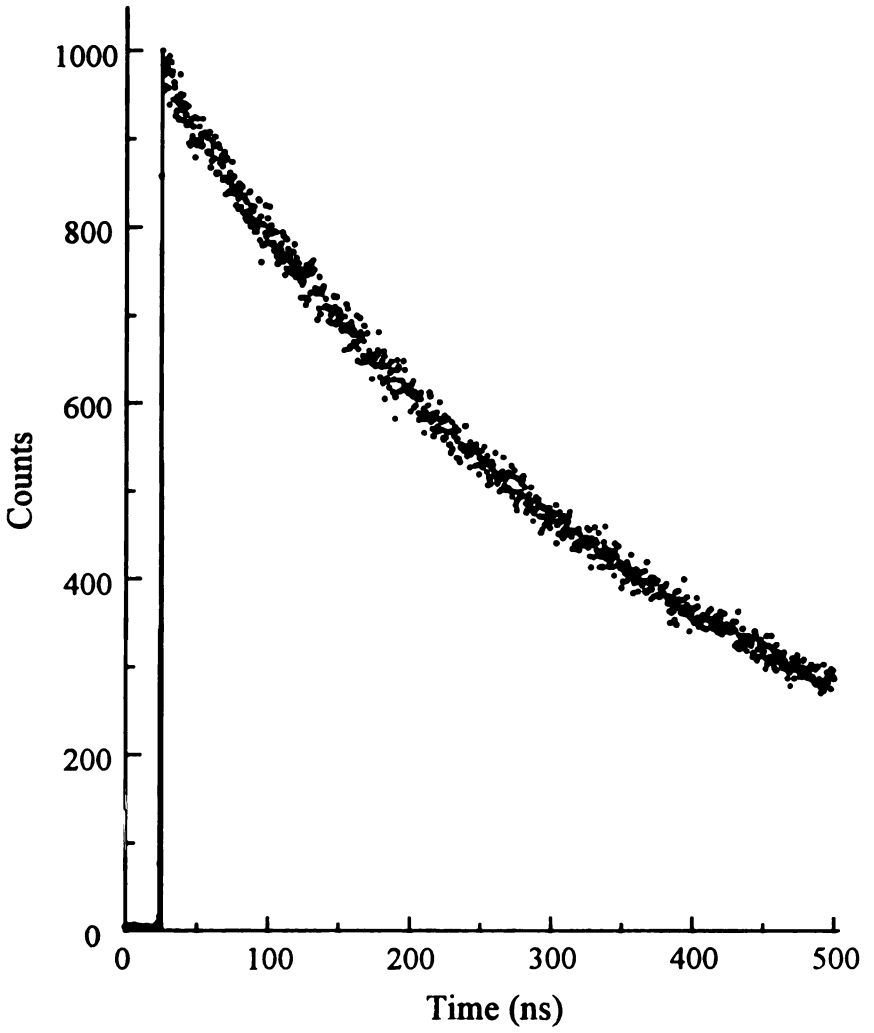

Figure 4.2. Fluorescence decay data for pyrene in cyclohexane showing both the instrument response function (solid line at $\tau \sim 30$ ns) and the spontaneous emission decay (dots).

responds to vibronic coupling perturbations arising only from Herzberg-Teller effects and the emissive response according to the difference between Herzberg-Teller and so-called Born-Oppenheimer vibronic coupling contributions. By separating these components in the observed responses, we can determine the relationship between solvent polarity and vibronic coupling.

The simplest model for predicting the relative intensities of electronic and vibronic transitions in a given molecule assumes that the electronic wavefunction varies slowly on the length scale of the nuclear motions associated with molecular vibrations.[33] In the Born-Oppenheimer approximation, the wavefunctions of the states involved in the transition of interest can be separated into their electronic and vibrational components.

$$\psi_{e,v}(q,Q) = \varphi_e(q,Q)\theta_v(Q) \qquad [4.2]$$

The electronic coordinate is designated q and the nuclear (vibrational) coordinate by Q. This treatment includes the dependence of the electronic wavefunction on nuclear coordinates but neglects the effect of electron motion on nuclear motion. If the dependence of φ_e on q is assumed weak, *i.e.* the electronic wavefunction varies slowly over the relevant nuclear coordinate, then the transition moment for a vibronic transition can be expressed as[33]

$$M_{ee',vv'} = \langle \theta_v | \langle \varphi_e | \sum_i e_i q_i | \varphi_{e'} \rangle | \theta_{v'} \rangle \approx R_{ee'} \langle \theta_v | \theta_{v'} \rangle \qquad [4.3]$$

where e and e' represent the two electronic states, and v and v' are vibrational states within the two electronic states. $R_{ee'}$ is the *average* electronic transition dipole moment for the $e \leftrightarrow e'$ transition. In this approximation, the vibrational overlap integral is a deterministic term in the intensity of a particular vibronic transition. While this level of

approximation is useful in describing the spectral response of a variety of molecules, the limitations of this approach are also realized in many other complex organic molecules. It is not always possible to separate the electronic and nuclear coordinates, and we need to consider the conditions under which these approximations are not valid. One of the consequences of the breakdown of these approximations is that "intensity borrowing", the exchange of oscillator strength between electronic states, is observed, resulting in the effective transition cross section of the weaker transition being enhanced by vibrationally mediated coupling to the neighboring electronic states.[33] It is typically held that the separation of electronic and nuclear coordinates, as described by Eq. 4.3, is the most limiting approximation and its failure leads to so-called Herzberg-Teller (HT) vibronic coupling. The second limitation is the breakdown of the adiabatic approximation, *i.e.* non-Born-Oppenheimer behavior, which is often termed "BO" vibronic coupling. Vibronic coupling arises from the dependence of the transition moment, $M_{ee'vv'}$, on nuclear positions (HT coupling) and on nuclear momenta (BO coupling). It is clearly artificial to completely separate these two mechanisms because both depend on nuclear motion, but in different ways. In limiting cases, however, where one mechanism dominates over the other, the two mechanisms exhibit different frequency dependencies.[19-21]

Prior work on the origins of vibronic coupling in complex organic molecules has shown that both types of coupling can, under certain circumstances, be significant. Experimentally, the presence of both HT and BO vibronic coupling have been inferred by the different isotope dependencies of individual absorption and emission bands and by asymmetry between absorption and emission spectra.[19,21] We focus here on the

emissive response of pyrene and how the absorption/emission asymmetry arising from vibronic coupling can be used to understand the solvent-dependence of the emission profile for pyrene and, by extension, other PAHs. Solvent-mediation of the efficiency of vibronic coupling gives rise to the observed solvent polarity dependent emission response of pyrene.

Although it is well recognized that vibronic coupling between many electronic manifolds can contribute to the linear response of molecules like pyrene,[19-22] it is typically assumed that the dominant vibronic coupling is between the excited states involved in the transitions. Vibrationally mediated coupling between the electronic manifolds can be expressed through a perturbation treatment, yielding expressions that contain both HT and BO contributions to vibronic coupling. For a molecule with electronic states 0, 1 and 2, where state 0 is the ground electronic state, the 0-1 transition is forbidden or weakly allowed and the 0-2 transition is more strongly allowed, the vibronically induced absorption from the ground electronic state to a vibronic level in the first excited state is described by[19]

$$M_{e=0,e'=1;v=0,v'=1} = -\sum_{v_{e=2}} \left\{ \left[1 + \frac{\hbar\omega_c}{\Delta E_0 + v_{e=2}\hbar\omega_v - \hbar\omega_c} \right] \times \left[\frac{\left\langle \theta_{e=2}^{v=v} \cdots \left| \langle \varphi_2 | \frac{\partial H_e}{\partial q_c} | \varphi_1 \rangle \right| \theta_{e=0}^{v=c} \right\rangle \left\langle \theta_{e=0}^{v=c} \left| q_c \right| \theta_{e=1}^{v=c} \right\rangle \left| \theta_{e=1}^{v=0} \right\rangle}{\Delta E_0 + v_{e=2}\hbar\omega_v} \right] \right\} \cdot R_{02} \left\langle \theta_{e=0}^{v=0} \middle| \theta_{e=2}^{v=v} \right\rangle$$

[4.4]

where the 0-2 transition is strongly allowed and therefore described adequately in the Condon approximation. Implicit in this treatment is the assumption that a vibrational mode spanning the appropriate coordinates of the two electronic states couples the two

electronic manifolds. The numerator of the second term in Eq. 4.4 describes the extent of coupling between the electronic states 1 and 2 due to the nuclear perturbation along the coupling coordinate q_c, the vibrational coupling for mode v_c between electronic states 0 and 1 and the extent of vibrational overlap between electronic manifolds 1 and 2. The first and third terms in Eq. 4.4 will not be affected significantly by solvent polarity while the magnitude of nuclear displacement along q_c will be sensitive to the dipolar and dielectric properties of the surrounding medium. The solvent polarity dependence of M arises from either a change in polarizability or dipole moment associated with a nuclear displacement along q_c. The vibrational states that act as final states in the linear emission response are Raman active modes, and because pyrene possesses a center of inversion, none of these modes will exhibit a change in dipole moment on population. Indeed, it is not critical that an induced dipole moment in pyrene span the entirety of q_c to interact with the solvent dipole. *Local* induced dipoles in pyrene that are canceled when vibrational motions are integrated over the entire molecular framework may play an important role in determining the strength of the solvent-solute interaction. In other words, the solvent-solute interaction need not be symmetric with respect to the pyrene nuclear framework. It makes intuitive sense that solvent-solute interactions need not coincide with the solute symmetry axes, especially when the relative sizes of pyrene and individual solvent molecules are compared.[34] Many solvent molecules are too small to span the entire length of the pyrene molecule. Our previous work on T_1 relaxation in perylene/*n*-alkane systems shows that local solvent structure, persisting over a length scale much shorter than the perylene molecule, plays an important part in determining the vibrational relaxation dynamics of that molecule.[35-37] We discuss below how the solvent

polarity dependence of M is manifested in the emission response of pyrene. The transition moment for the emission response (1-0) is given by[19]

$$M_{e=0,e'=1;v=1,v'=0} = -\sum_{v_{e=2}} \left\{ \left[1 - \frac{\hbar\omega_c}{\Delta E_0 + v_{e=2}\hbar\omega_v + \hbar\omega_c} \right] \times \left[\frac{\left\langle \theta_{e=2}^{v=v} \cdots \left| \langle \varphi_2 | \frac{\partial H_e}{\partial q_c} | \varphi_1 \rangle \left\langle \theta_{e=0}^{v=c} \middle| q_c \middle| \theta_{e=1}^{v=c} \right\rangle \right| \theta_{e=1}^{v=0} \right\rangle}{\Delta E_0 + v_{e=2}\hbar\omega_v} \right] \right\} \cdot R_{02} \left\langle \theta_{e=0}^{v=0} \middle| \theta_{e=2}^{v=v} \right\rangle \qquad [4.5]$$

While similar to Eq. 4.4, the transition moment for emission differs from that for absorption by two signs. One sign change is not obvious by inspection, and arises from the anti-hermitian nature of the terms $\langle\varphi_2|\partial H_e/\partial q_c|\varphi_1\rangle$ and $\langle\varphi_1|\partial H_e/\partial q_c|\varphi_2\rangle$[19,21] while the other sign change occurs for energetic reasons. In the case of absorption, the frequency difference between the mode v_c and the final state of the $0\rightarrow1$ transition is $2\hbar\omega$ more than that for the corresponding ($1\rightarrow0$) emission process. This intrinsic asymmetry in vibronic coupling for absorption and emission can also be considered in terms of the BO and HT contributions to the process. The vibronic coupling contributions are, in general, additive for absorption and subtractive for emission. This property of vibronic coupling is central to understanding the solvent polarity dependent fluorescence response of pyrene.

Individual features in the emission band of pyrene change according to the polarity of its local medium. This polarity dependence is expressed in terms of the "I/III" band ratio,[2,3] where the I band is the $S_1^{v=0} \rightarrow S_0^{v=0}$ (0-0) transition and III is an $S_1^{v=0} \rightarrow S_0^{v=1}$ transition. For the III band, the v=1 resonance is dominated by one (or more) ~1100 cm^{-1} b_{3g} Raman active vibrational mode(s).[38,39] Because the S_1 state in pyrene

($^1B_{2u}$) is y axis polarized and the S_2 state ($^1B_{1u}$) is z axis polarized, the vibrational coordinate, q_c, appropriate for coupling these two states must necessarily span both y and z axes.[26] For a molecule belonging to the D_{2h} point group, the dominant coupling mode is thus of b_{3g} symmetry. In order to understand the relationship between the I/III band intensity ratio and the solvent polarity dependence of M, we must consider the nature of the vibronic coupling that contributes to each transition. Experimental data presented by Hara and Ware[26] demonstrate that the 0-0 transition cross section of pyrene is correlated to solvent polarity, although they did not attempt to extract from these data a mechanistic explanation for the polarity-dependence of the I/III band intensity ratio. The strength of the 0-0 transition depends on vibronic coupling between states S_1 and S_2. While the coupling between S_2 and S_1 involves specific vibrational levels in each state, the second terms in Eqs. 4.4 and 4.5 couple the vibrational wavefunctions $\theta_{e=2}^{v=v}$ and $\theta_{e=1}^{v=0}$, and thus because the $\theta_{e=1}^{v=0}$ wavefunction is affected, the 0-0 transition moment will necessarily also be affected by vibronic coupling. For a two level system, such as the pyrene 0-0 transition, the cross section for the absorptive process must be equal to the cross section for the emissive process.[19] The vibronic coupling contribution to the absorption cross section of the 0-0 transition will scale as the sum of the HT and BO contributions and the vibronic coupling contribution to the emission intensity of the 0-0 transition will scale as the difference between the HT and BO contributions.[19-21] Since the cross sections for these two transitions are necessarily equal, as we have indicated in Figure 4.3, we are left with the conclusion that, for the 0-0 transition, the sum of the vibronic coupling contributions is equal to the difference between them, *i.e.* $(HT+BO)_{0\text{-}0} = (HT-BO)_{0\text{-}0}$. Thus, the vibronic coupling induced

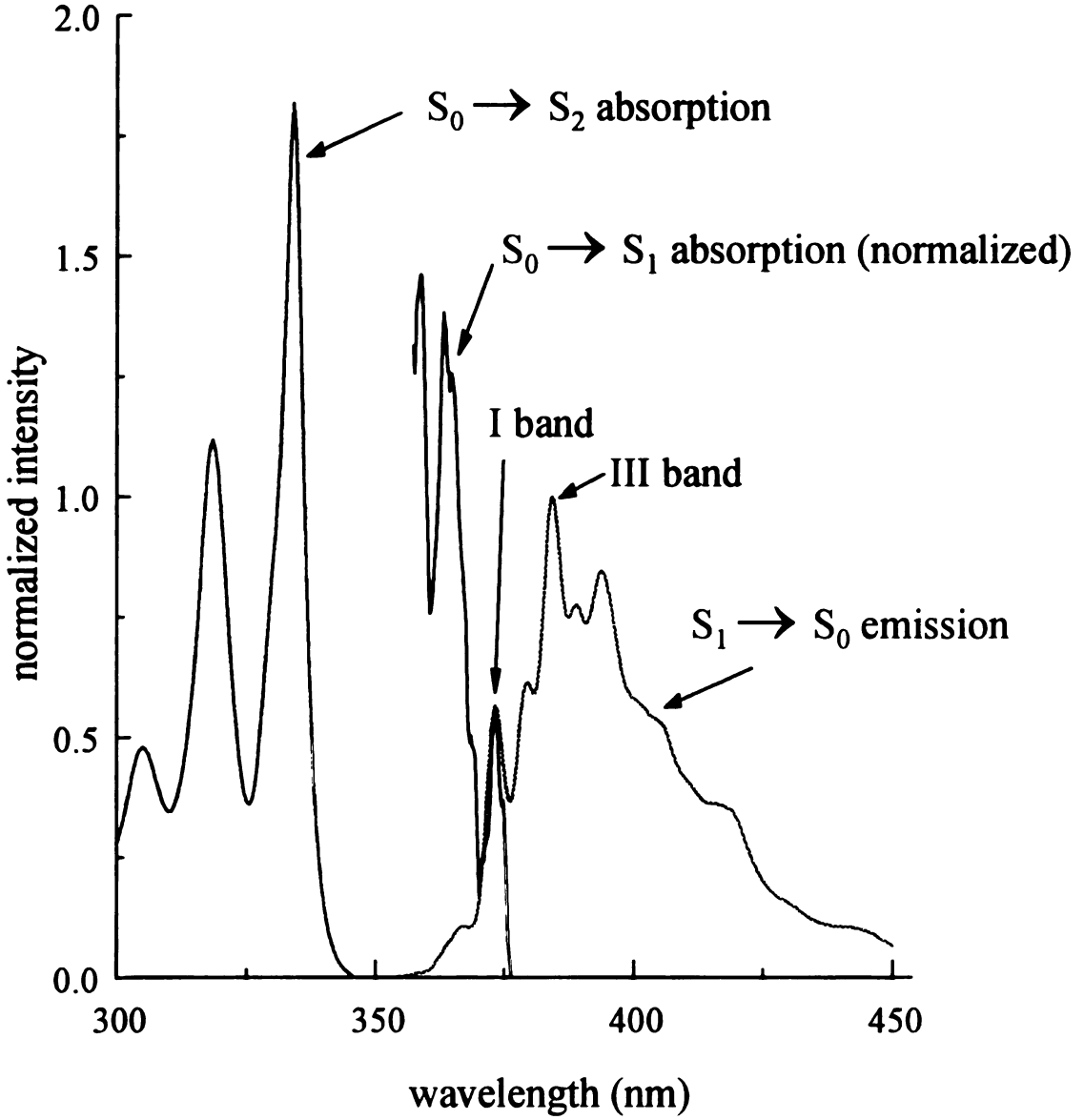

Figure 4.3. Absorption and spontaneous emission spectra of pyrene in cyclohexane. We report the $S_0 \rightarrow S_1$ absorption spectrum with the intensity of the 0-0 band normalized to the 0-0 emission transition.

intensity of the 0-0 transition is determined exclusively by HT coupling between electronic states S_2 and S_1. The III band is an ($S_1^{v=0} \rightarrow S_0^{v=1}$) transition and its intensity will scale with the difference between the HT and BO vibronic contributions. The ratio of the bands will scale with the magnitude of HT coupling divided by the difference between HT and BO contributions. As solvent polarity increases, the I/III band ratio should increase, as is observed experimentally.

To determine the validity of our assertion that vibronic coupling is the mechanism of the solvent polarity dependent emission response seen in pyrene, we must relate the quantities that we determine experimentally to the properties related directly to emission intensities for the I and III bands of pyrene. Measurement of the spontaneous emission spectra of pyrene in series of solvents does not, by itself, provide sufficient quantitative information for the determination of *absolute* fluorescence intensities for each band. Time domain measurements are more amenable to the determination of absolute spectroscopic quantities. We separate the fluorescence spectrum of pyrene into two portions; the 0-0 transition and all else. We can determine the fluorescence lifetime and the fluorescence quantum yield quantitatively, and can estimate the fractional contribution of the 0-0 transition to the total emission response. The spontaneous emission lifetime is related to the Einstein *A* coefficient,[33]

$$A_{S_1 \rightarrow S_0} = k_R = \frac{\phi_{fl}}{\tau_{fl}}$$
$$A_{S_1 \rightarrow S_0} = \sum_{v=0,n} A_{S_1(v=0) \rightarrow S_0(v=v)} = \sum_{v=0,n} A_{0v} \qquad [4.6]$$

where τ_{fl} is the measured fluorescence lifetime and ϕ_{fl} is the fluorescence quantum yield. We estimate the contribution of the total emission response arising from the 0-0

transition by peak fitting and integration. The intensity and transition cross section of the 0-0 transition are related to the fluorescence lifetime through the Einstein *A* coefficient.[33]

$$I_{em}^{0-0} = N_0 hc\nu_{0-0}A_{0-0}$$
$$\sigma_{0-0} = \frac{I_{em}^{0-0}}{8\pi hc^2\nu_{0-0}^3} \qquad [4.7]$$

Similarly, the intensity and transition cross section for the remainder of the emission band is related to the radiative rate constants,

$$\sigma_{0-0} \propto k_R^{0-0}$$
$$\sigma_{0-\nu} \propto k_R^{0-\nu} \qquad [4.8]$$

Measurement of the fluorescence quantum yield in conjunction with the fluorescence lifetime data provides a quantitative determination of k_R and k_{NR} ($=(1-\phi_{fl})/\tau_{fl}$). The solvent polarity-dependence of k_R^{0-0} and $k_R^{0-\nu}$ provide insight into the role that vibronic coupling plays in this process because the transition cross sections are related directly to the transition moments by[33]

$$\sigma_{a-b} = \frac{8\pi^3\nu_{a-b}N_a}{3hc}|M_{a-b}|^2 \qquad [4.9]$$

where *a* is the lower energy state in the transition and N_a is the population of that state.

We show in Figure 4.4a the relationship between the radiative rate constant and pyrene I/III band ratio. At best there is a weak correlation between these two quantities, and we endeavor to determine more precisely which contributions to the radiative decay rate depend on solvent polarity and which ones do not. We consider, as implied above, that there are essentially three excited state decay channels that are important to the

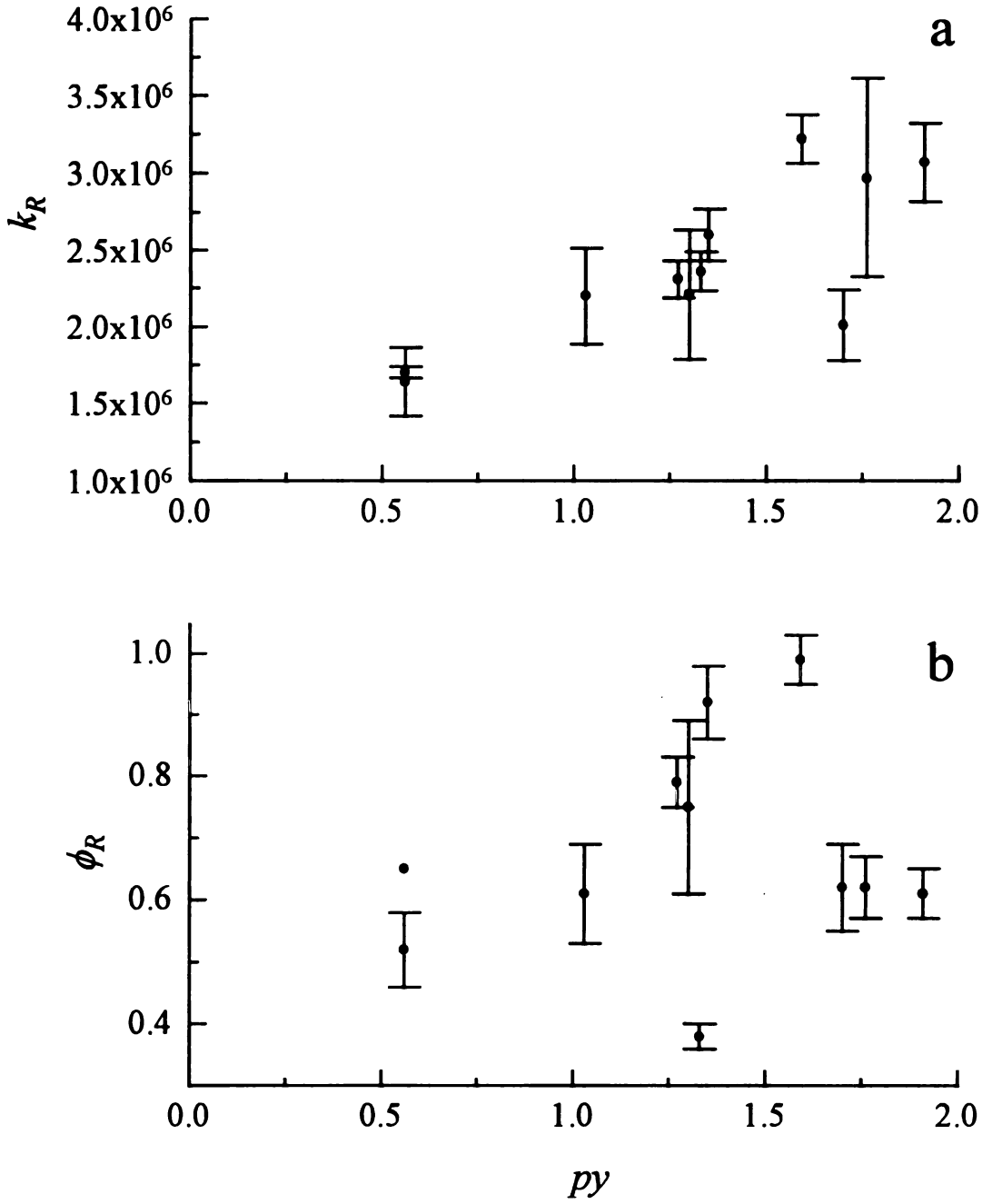

Figure 4.4: (a) Radiative transition rate constant, k_R, for pyrene in the solvents used in this work plotted versus empirical solvent polarity parameter, *py*. (b) Dependence of fluorescence quantum yield, ϕ_{fl}, on solvent polarity. Uncertainties reported in these figures are ± 1σ.

solvent polarity dependence of pyrene's emission; the radiative decay rate for the 0-0 transition, with associated rate constant k_R^{0-0}, the radiative decay rate for the balance of the emission spectrum, with rate constant k_R^{0-v}, and the non-radiative decay rate, with rate constant k_{NR}. Indeed, it is important to consider non-radiative processes because ϕ_{fl} ~ 0.65, and there is no discernible correlation between fluorescence quantum yield and the *py* scale (Figure 4.4b). We have determined k_R^{0-0} by multiplication of the total radiative rate constant by the fraction of the emission spectrum composed of the 0-0 band. This means for the determination of k_R^{0-0} is valid because the measured fluorescence lifetime is uniform across the entire emission profile, *i.e.* only one excited electronic state contributes to the observed steady state emission spectrum. We show in Figure 4.5 the correlation between k_R^{0-0} and the I/III band ratio (*py* scale). The relationship between k_R^{0-v} and the I/III band ratio is shown in Figure 4.6. While there is a direct correlation between k_R^{0-0} and *py*, k_R^{0-v} is only weakly solvent-dependent. The only other decay channel which could exhibit a solvent dependence is the non-radiative decay channel, and we show in Figure 4.7 the relationship between k_{NR} and *py*. While there are variations between solvents, it is clear that there is no systematic trend in the data. We note that the reported ϕ_{fl} for acetone appears to be anomalously large. The reason for this anomaly is that acetone absorbs light significantly at the excitation wavelengths used for the quantum yield measurements (334 nm ± 5 nm), making uncertain the amount of energy absorbed by pyrene. Such an effect gives rise to an apparently low quantum yield, and the value that we report is corrected according to a previously reported method.[26] We believe that this correction is limited in its accuracy because of the large

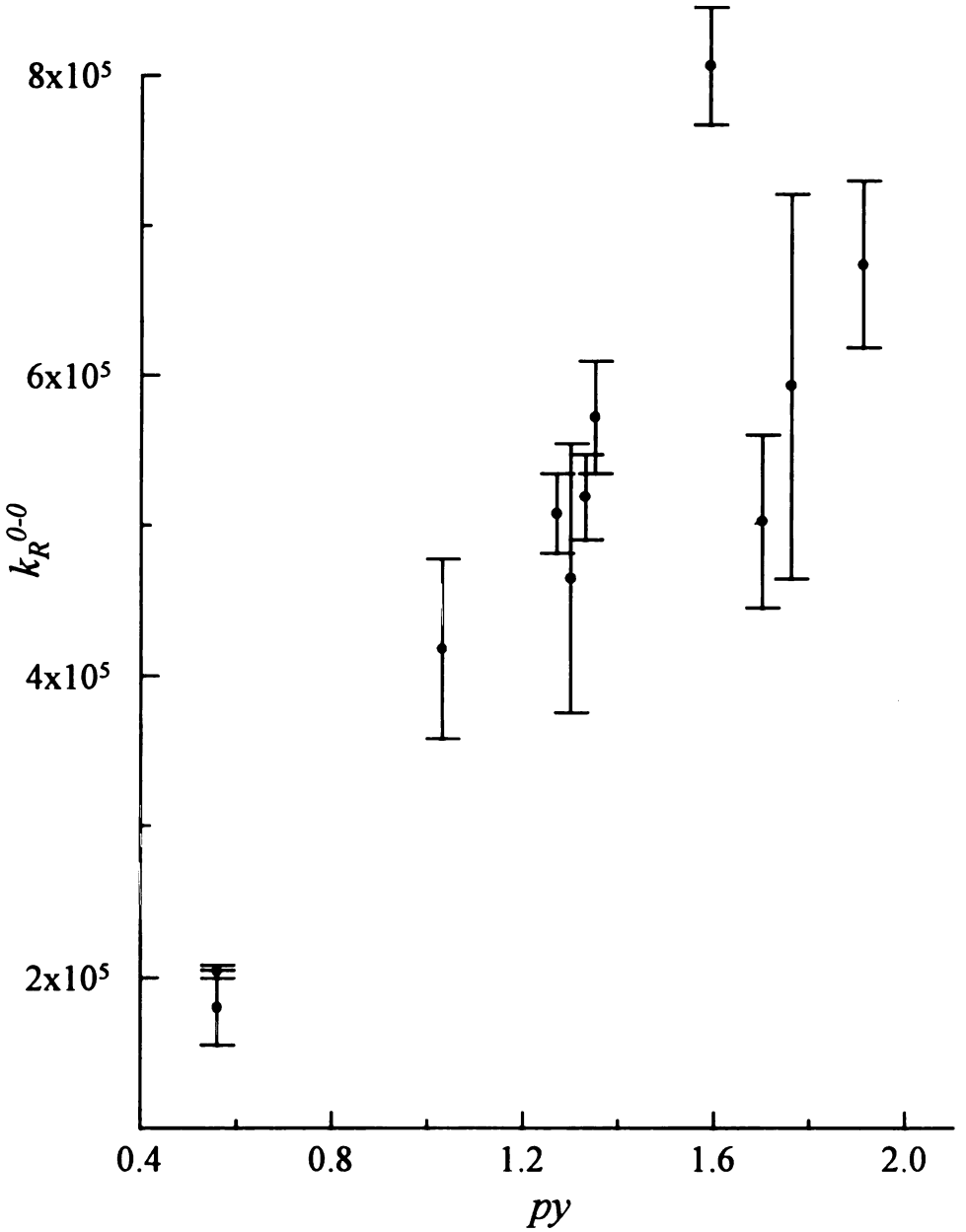

Figure 4.5. Radiative transition rate constant for the 0-0 transition of pyrene, plotted versus solvent *py* value. The reported uncertainties are ± 1σ.

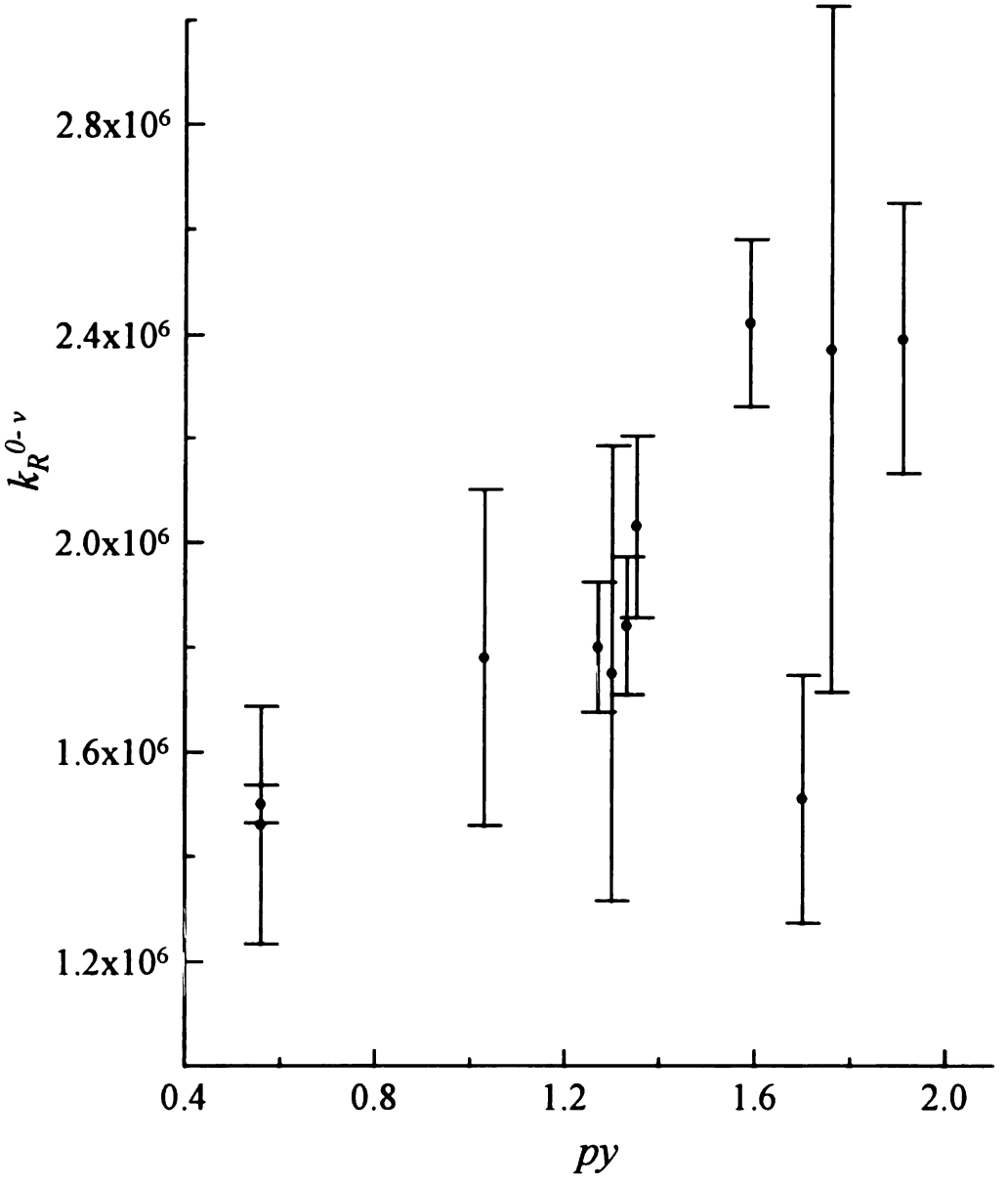

Figure 4.6. Radiative transition rate constant for the family of 0-v transitions that comprise the dominant portion of the pyrene emission band, plotted versus solvent *py* value. The reported uncertainties are ± 1σ.

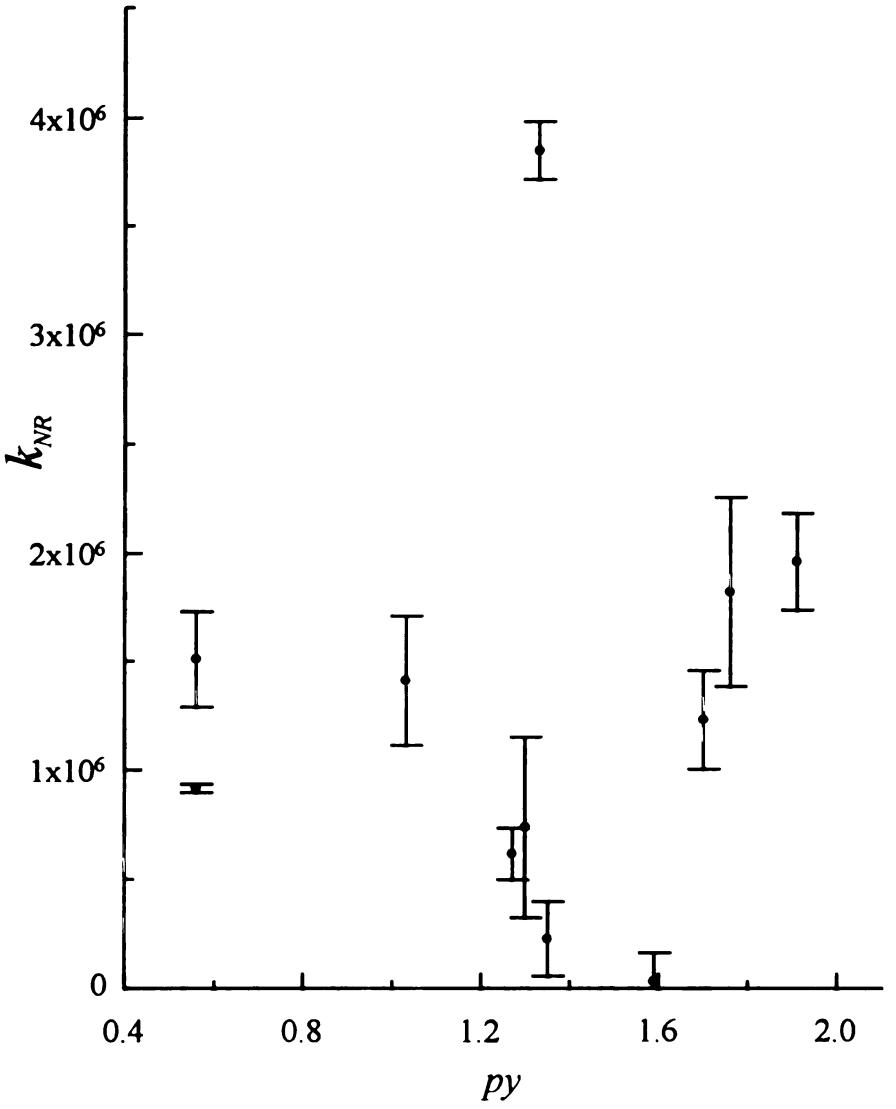

Figure 4.7. Nonradiative transition rate constant for the pyrene emission band, plotted versus solvent *py* value. The reported uncertainties are ± 1σ.

concentration difference between absorbing species and the unknown extent to which energy transfer proceeds in the dilute pyrene/acetone solution.

As detailed above, the cross section for the $S_1^{v=0} \leftrightarrow S_0^{v=0}$ transition is sensitive to vibronic coupling arising from deviations from the Condon approximation (HT coupling), while the $S_1^{v=0} \rightarrow S_0^{v=1}$ transition senses the difference between HT and BO vibronic coupling contributions. Because both of these contributions depend on nuclear motion, we expect that they will scale with one another in some manner, although the details of this relationship are not clear and must be considered in the context of the specific coupling vibrational mode and the dielectric and dipolar properties of the surrounding medium. We note two important results from our data. First, $k_R^{0\text{-}0}$ correlates with solvent polarity, indicating that HT contributions increase with solvent polarity, as expected. We note (Table 4.1 and Table 4.2) that the *py* scale and $k_R^{0\text{-}0}$ both scale with solvent dipole moment and not dielectric constant. The second significant result is that the portion of the spontaneous response that is related to the difference between HT and BO terms, $k_R^{0\text{-}v}$, depends on solvent polarity differently than $k_R^{0\text{-}0}$. The correlation between solvent polarity and $k_R^{0\text{-}v}$ is in qualitative agreement with theoretical predictions. In the classical treatment, the relationship between transition moments arising from HT and BO coupling is described by[21]

$$\left|\frac{M_{BO}}{M_{HT}}\right|_{S_0 \leftrightarrow S_1} = \frac{\hbar\omega_c}{\left|E_{S_2} - E_{S_1}\right|} \qquad [4.10]$$

for a coupling mode of frequency $\hbar\omega_c$ (1100 cm^{-1} for pyrene) and two non-degenerate electronic states. For pyrene, $|E_{S2} - E_{S1}| \sim 2700$ cm^{-1} and therefore the

Table 4.1. Properties of the optical response of pyrene as a function of solvent. Uncertainties are ± 1σ.

solvent	*py* value	τ_{fl} (ns)	ϕ_{fl}	k_R ($\times 10^{-6}$ s^{-1})	k_{NR} ($\times 10^{-6}$ s^{-1})	$\sigma_{0\text{-}0}/\sigma_{tot}$	$k_R^{0\text{-}0}$ ($\times 10^{-6}$ s^{-1})
cyclohexane	0.56±0.01	382±8	0.65	1.70±0.04	0.92±0.02	0.12	0.204±0.004
n-hexane	0.56±0.01	318±24	0.52±0.06	1.64±0.23	1.51±0.22	0.11	0.180±0.025
toluene	1.03±0.01	277±16	0.61±0.08	2.20±0.32	1.41±0.30	0.19	0.418±0.060
tetrahydrofuran	1.27±0.02	342±4	0.79±0.04	2.31±0.12	0.61±0.12	0.22	0.508±0.026
methanol	1.30±0.01	339±16	0.75±0.14	2.21±0.43	0.74±0.42	0.21	0.465±0.090
methylene chloride	1.33±0.02	161±2	0.38±0.02	2.36±0.13	3.85±0.13	0.22	0.519±0.028
ethyl acetate	1.35±0.02	354±2	0.92±0.06	2.60±0.17	0.23±0.17	0.22	0.572±0.037
acetone	1.59±0.01	307±8	0.99±0.04	3.22±0.16	0.03±0.13	0.25	0.806±0.039
acetonitrile	1.70±0.01	308±5	0.62±0.07	2.01±0.23	1.23±0.23	0.25	0.503±0.057
N,N-dimethyl formamide	1.76±0.02	209±42	0.38±0.05	2.97±0.64	1.82±0.44	0.20	0.593±0.128
dimethyl sulfoxide	1.91±0.02	199±10	0.61±0.04	3.07±0.25	1.96±0.23	0.22	0.674±0.056

Table 4.2. Polar properties of the solvents used in this work.

solvent	*py* value ± 1σ	dielectric constant ε_0	dipole moment D
cyclohexane	0.56±0.01	2.02	0.00
n-hexane	0.56±0.01	1.89	0.08
toluene	1.03±0.01	2.38	0.45
tetrahydrofuran	1.27±0.02	7.60	1.75
methanol	1.30±0.01	32.6	1.70
methylene chloride	1.33±0.02	9.08	1.60
ethyl acetate	1.35±0.02	6.02	1.81
acetone	1.59±0.01	20.7	2.88
acetonitrile	1.70±0.01	37.5	3.92
N,N-dimethyl formamide	1.76±0.02	36.7	3.86
dimethyl sulfoxide	1.91±0.02	46.6	3.90

ratio M_{BO}/M_{HT} is predicted by Eq. 4.10 to be 0.41. We can *estimate* this same ratio from our experimental data. The slope of the $k_R^{0\text{-}0}$ polarity dependence (HT contributions) can be compared to the slope of the $k_R^{0\text{-}v}$ (HT-BO) polarity dependence, once the relative weighting factors for $k_R^{0\text{-}0}$ and $k_R^{0\text{-}v}$ are accounted for. We estimate that ~20% of the total emission response is accounted for by the 0-0 band, based on the cross section ratio data presented in Table 4.1. The slope of the $k_R^{0\text{-}0}$ polarity dependence is ~3.5 x 10^5 s^{-1}, (Figure 4.5, 20% contribution to the spectrum) and the slope of the $k_R^{0\text{-}v}$ dependence is ~6 x 10^5 s^{-1} (Figure 4.6, 80% contribution to the spectrum). Correcting for fractional contributions to the spectrum yields an effective slope of 1.75 x 10^6 s^{-1} if the total emission band response is determined by HT coupling. For $k_R^{0\text{-}v}$, the slope of the polarity dependence would be 7.5 x 10^5 s^{-1} if purely (HT-BO) contributions to vibronic coupling determine the response. These estimates yield an experimental ratio of $\sigma_{BO}/\sigma_{HT} \approx 0.57$ (Eq. 4.8). Because $\sigma \propto M^2$ (Eq. 4.9), $M_{BO}/M_{HT} \approx \sqrt{0.57} = 0.75$, somewhat larger than the theoretical prediction. We consider the agreement between the estimated and theoretical ratios to be quite good considering the uncertainty in our experimental data, the fact that we used several estimates in determinating this ratio, and the assumptions implicit in the derivation of Eq. 4.10.

A complicating factor that may give rise to the slight disagreement between experiment and theory lies in the inherent complexity of the pyrene vibrational response. Theories of vibronic coupling typically consider the coupling between electronic states to be mediated by a single vibrational mode that spans the coordinates of the two electronic states. Pyrene, however, has at least four b_{3g} modes in the frequency range of 1000 cm^{-1} - 1500 cm^{-1} that could participate in the coupling, with the dominant b_{3g} mode appearing

near 1100 cm^{-1}.[38,39] We present an exaggerated schematic of the nuclear motions associated with these vibrations in Figure 4.8. We determined these nuclear displacements using semi-empirical molecular orbital calculations,[40] and take them as instructive, rather than quantitative, representations of the relevant normal modes. Because of the complexity associated with relating the empirical *py* scale to vibronic coupling, we cannot speculate on what relative contribution each of these modes may have to the overall process.

Not all polycyclic aromatic hydrocarbons exhibit a measurable solvent polarity dependent emission response.[4-9] For example, perylene and pyrene are both peri-condensed fused ring systems. Perylene contains five fused rings and does not exhibit a solvent polarity dependent emission response, whereas pyrene, with four fused rings, does. Both of these molecules are of D_{2h} symmetry, but for perylene the $S_0 \rightarrow S_1$ transition is allowed, ($\varepsilon_{max} \sim 33{,}000\ cm^{-1}\ M^{-1}$) and for pyrene it is nominally forbidden, or at best only weakly allowed ($\varepsilon_{max} \sim 200\ cm^{-1}\ M^{-1}$). The reason for the fundamental difference between these two molecules lies in the correlation and electrostatic forces that determine state ordering in organic systems, and a discussion of several factors that relate to state ordering in cata- and peri-condensed systems has been reported by other authors.[41-43] Because the allowed $S_0 \rightarrow S_1$ transition in perylene is strong, it can be modeled effectively by separating the vibrational and electronic coordinates, and Franck-Condon transitions lead to nearly mirror image absorption and emission spectra.[44] For pyrene, because the $S_0 \rightarrow S_1$ transition is nominally forbidden, but fluorescence from the S_1 is observed, a simple Franck-Condon treatment does not describe its optical response adequately. The linear optical response of pyrene can be understood in terms of vibronic

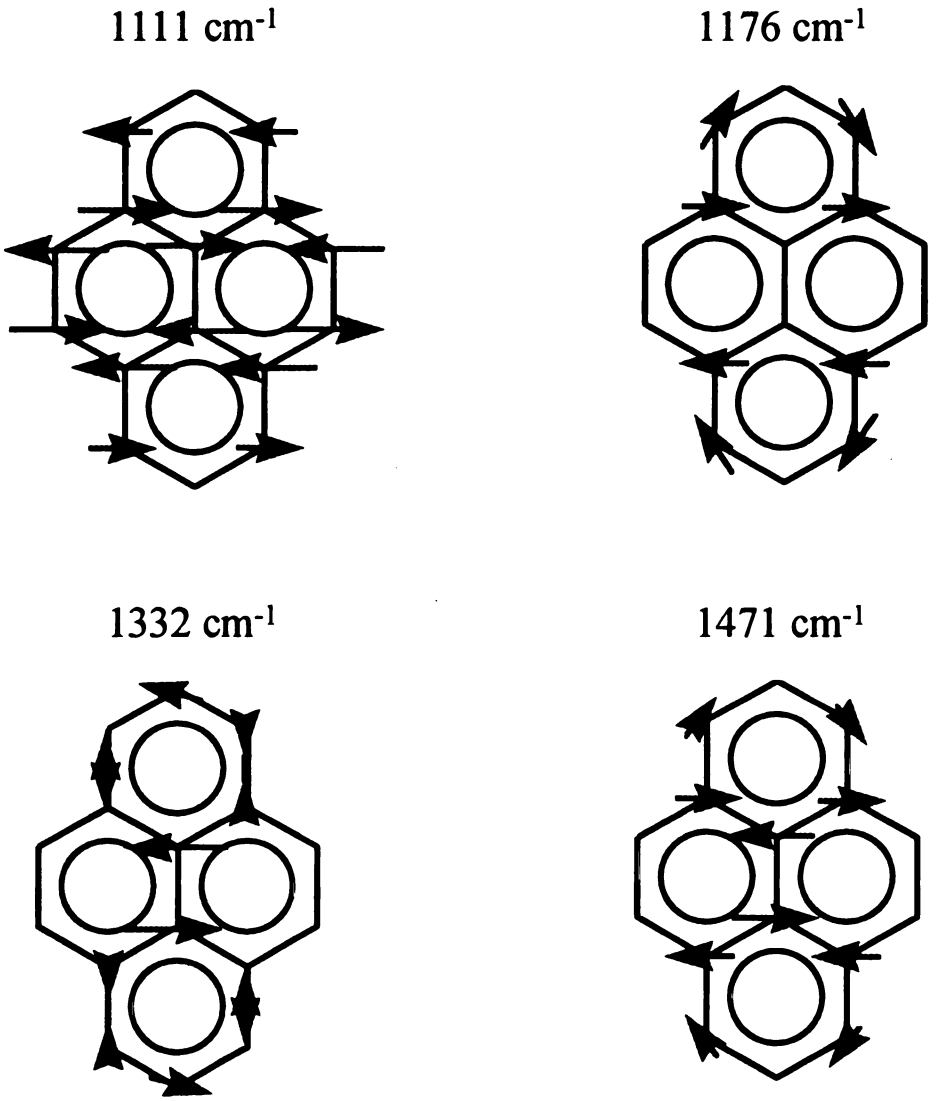

Figure 4.8. Representations of nuclear motions associated with the four b_{3g} vibrational modes in closest energetic proximity to the "III" band of pyrene. The frequencies reported for these modes were taken from references 38 and 39.

coupling between the S_1 and S_2 electronic states,[19] and we have argued that this coupling is the basis for the solvent polarity dependent emission response seen for pyrene.

It is important to test the validity of our hypothesis, that solvent polarity mediates vibronic coupling and therefore emission band intensities, in the context of its predictive power. We consider whether or not we can predict, based on the linear response of a given PAH, whether or not it will exhibit a solvent polarity-dependent emission response. If vibronic coupling gives rise to the solvent-dependent emission response seen for certain PAHs, we predict that PAHs having a strongly allowed $S_0 \leftrightarrow S_1$ transition and exhibiting a classical mirror image symmetry in their absorption and emission spectra will not display a solvent polarity-dependent emission response because vibronic coupling is too subtle an effect to contribute significantly to the intensities of strongly allowed transitions. If vibronic coupling is the operative mechanism for solvent polarity-dependent emission, then a PAH with a weakly allowed $S_0 \leftrightarrow S_1$ transition, and a more strongly allowed $S_0 \rightarrow S_2$ transition, should exhibit a solvent polarity-dependence, as is observed experimentally for benzene, coronene, benzo[*e*]pyrene, and benzo[*g,h,i*]perylene.[1,7] All of these molecules possess a weakly allowed $S_0 \leftrightarrow S_1$ transition ($\varepsilon_{max} \sim 250\ M^{-1}\ cm^{-1}$) and a strong $S_0 \rightarrow S_2$ transition within 2000 - 4000 cm^{-1} of the $S_0 \leftrightarrow S_1$. In contrast, perylene, benzo[*a*]pyrene and dibenzo[*a,e*]pyrene all possess a strongly allowed $S_0 \rightarrow S_1$ transition and none of these molecules exhibit a solvent polarity dependence.[7] While this is clearly a limited data set, largely because of a lack of experimental data, the strong correlation between weakly allowed $S_0 \leftrightarrow S_1$ / strongly allowed $S_0 \rightarrow S_2$ transitions and a solvent polarity-dependent emission response

indicates that, at least for the molecules listed above, vibronic coupling between excited electronic states S_1 and S_2 determines the presence (or not) of a solvent polarity-dependent emission response in polycyclic aromatic hydrocarbons.

4.4. Conclusions

We have examined the solvent polarity-dependent emission response of pyrene in a series of solvents that span the empirical *py* scale. Measurement of fundamental photophysical parameters such as radiative rate constant and fluorescence quantum yield have provided insight into the correlation between the empirical *py* scale and the efficiency of vibronic coupling between closely spaced electronic states. We assert based on the correlations we observe that the empirical *py* scale for pyrene can be explained in terms of vibronic coupling, and that the important intermolecular process that gives rise to the *py* scale is solvent dipole-solute induced dipole interactions. The dipolar nature of the solvent medium determines the extent to which of an induced dipole moment is formed in pyrene by vibrational distortion(s) of the nuclear coordinate of b_{3g} symmetry. Vibronic coupling in pyrene can be used to describe qualitatively the trends seen in the *py* scale, and can be used to predict the presence of a solvent polarity-dependent response in a given PAH.

4.5. Literature Cited

1. R. B. Cundall; L. C. Pereira; *Chem. Phys. Lett.*, **1973,** *18*, 371.

2. D. C. Dong; M. A. Winnik; *Can. J. Chem.*, **1984,** *62*, 2560.

3. D. C. Dong; M. A. Winnik; *Photochem. Photobiol.*, **1982,** *35*, 17.

4. W. E. Acree; S. A. Tucker; L .E. Cretella; A. I. Zvaigzne; K. W. Street; J. C. Fetzer; K. Nakasuji; I. Murata; *Appl. Spec.*, **1990,** *44*, 951.

5. S. A. Tucker, W. E. Acree; M. J. Tanga; *Appl. Spec.*, **1991,** *45,* 57.

6. R. Waris, K. W. Street, W. E. Acree, J. C. Fetzer; *Appl. Spec.*, **1989,** *43*, 845.

7. W. E. Acree; S. A. Tucker; A. I. Zvaigzne; K. W. Street; J. C. Fetzer; H.-F. Grutzmacher, *Appl. Spec.*, **1990,** *44*, 477.

8. S. A. Tucker; I.-L. Teng; W. E. Acree; J. C. Fetzer; *Appl. Spec.*, **1991,** *45*, 186.

9. S. A. Tucker; A. I. Zvaigzne; W. E. Acree; J. C. Fetzer; M. Zander; *Appl. Spec.*, **1991,** *45,* 424.

10. S.-H. Chen; V. L. McGuffin; *Appl. Spec.*, **1994,** ***48***, 596.

11. J. W. Carr; J. M. Harris; *Anal. Chem.*, **1986,** *58,* 626.

12. J. W. Carr; J. M. Harris; *J. Chromatog.*, **1989,** *481,* 135.

13. R. G. Bogar; J. C. Thomas; J. B. Callis; *Anal. Chem.*, **1984,** *56,* 1080.

14. E. Wistus; E. Mukhtar; M. Almgren; S.-E. Lindquist; *Langmuir*, **1992,** ***8,*** 1366.

15. Y. S. Liu; W. R. Ware; *J. Phys. Chem.*, **1993,** *97,* 5980.

16. Y. S. Liu; P. de Mayo; W. R. Ware; *J. Phys. Chem.*, **1993,** *97*, 5987.

17. Y. S. Liu; P. de Mayo; W. R. Ware; *J. Phys. Chem.*, **1993,** *97,* 5995.

18. A. Pellois; J. Ripoche; *Chem. Phys. Lett.*, **1969,** *3,* 280.

19. P. A. Geldof; R. P. H. Rettschnick; G. J. Hoytink; *Chem. Phys. Lett.*, **1971,** ***10***, 549.

20. G. Orlandi; W. Siebrand; *Chem. Phys. Lett.*, **1972,** *15,* 465.

21. G. Orlandi; W. Siebrand; *J. Chem. Phys.*, **1973,** *58*, 4513.

22. K. Cunningham; W. C. Brand; D. F. Williams; G. Orlandi; *Chem. Phys. Lett.*, **1973,** *20*, 496.

23. A. Nakajima; *Bull. Chem. Soc. Japan*, **1973,** *46*, 2602.

24. V. D. Tuan; U. P. Wild; M. Lamotte; A. M. Merle; *Chem. Phys. Lett.*, **1976,** *39*, 118.

25. T. Kobayashi; *J. Chem. Phys.*, **1978,** *69,* 3570.

26. K. Hara; W. R. Ware; *Chem. Phys.*, **1980,** *51,* 61.

27. A. Nakajima; *Spectrochimica Acta*, **1982,** *38A,* 693.

28. F. W. Langkilde; E. W. Thulstrup; J. Michl; *J. Chem. Phys.*, **1983,** *78,* 3372.

29. G. Marconi; P. R. Salvi; *Chem. Phys. Lett.*, **1986,** *123*, 254.

30. J. N. Demas, private communication.

31. J. N. Demas; G. A. Crosby; *J. Phys. Chem.*, **1971,** *75*, 991.

32. L. DeWitt; G. J. Blanchard; E. LeGoff; M. E. Benz; J. H. Liao; M. G. Kanatzidis; *J. Am. Chem. Soc.*, **1993,** *115*, 12158.

33. G. Herzberg, *Molecular Spectra and Molecular Structure, Vol. III*, Krieger, **1991**.

34. J. T. Edward; *J. Chem. Ed.*, **1970,** *47*, 261.

35. Y. Jiang; G. J. Blanchard; *J. Phys. Chem.*, **1994,** *98*, 6436.

36. Y. Jiang; G. J. Blanchard; *J. Phys. Chem.*, **1994,** *98,* 9411.

37. Y. Jiang; G. J. Blanchard; *J. Phys. Chem.*, **1994,** *98,* 9417.

38. A. Bree; V. V. B. Vilkos; *Spectrochimica Acta*, **1971,** *27A*, 2333.

39. E. A. Mangle; M. R. Topp; *J. Phys. Chem.*, **1986,** *90,* 802.

40. Calculations were performed using Spartan version 2.0 with AM1 parameterization.

41. H. B. Klevens; J. R. Platt; *J. Chem. Phys.*, **1949,** *17,* 470.

42. D. E. Mann; J. R. Platt; H. B. Klevens; *J. Chem. Phys.*, **1949,** *17*, 481.

43. J. R. Platt; *J. Chem. Phys.*, **1949**, *17*, 484.

44. I. B. Berlman, *Handbook of Fluorescence Spectra of Aromatic Molecules, 2nd Edition*, Academic Press, 1971, 399-400.

Chapter 5

Dynamics of a Tethered Chromophore Imbedded in a Self-Assembled Monolayer

Summary

We report the first measurements on the dynamical response of alkanethiol/gold monolayers using a depth-selective tethered probe molecule technique, where 5% of the monolayer is comprised of the probe. Our transient spectroscopic data indicate that, for the first ~10 CH_2 groups above the gold surface, the local environment is highly rigid and, from these same data, we recover an average tilt angle of 26°, in exact agreement with steady state measurements.

5.1. Introduction

Due to their numerous potential uses and nearly ideal properties as model systems, there is wide spread interest in the organization and dynamics of self-assembled monolayers, with particular interest on the alkanethiol/gold system because of its ease of formation and characteristically high degree of macroscopic order.[1-13] Self-assembled monolayers are used in interfacial electron transport research, micro-device patterning applications, and tribology.[14-19] In addition, there is growing interest in developing molecular shape-selective interfaces and in building patterned structures using self-assembled monolayers.[20,21] Although much is known about the macroscopic properties of self-assembled monolayers, little is known about their dynamics at the molecular level. The dynamical response of these monolayers will ultimately determine their applicability for patterning and sensor applications.

To understand these dynamics, we have performed probe molecule reorientation experiments using tethered pyrene within self-assembled monolayers. The rotational motion of a molecule is affected greatly by the shape and rigidity of its immediate environment, and these measurements allow us to determine the molecular-scale motional freedom and anisotropy characteristics of self-assembled monolayers. There are two approaches to such measurements; physisorption of chromophores onto the monolayer[22] and chemical incorporation into the layer[23,24]. We have chosen the latter route. By tethering the chromophores to the substrate, we minimize their translational freedom within the monolayer and sample only the rotational motion intrinsic to molecules bound to the surface. We present here our results on a 5% 4-(1-pyrenyl)-1-butanethiol /95% 1-octadecanthiol monolayer on gold (Figure 5.1).

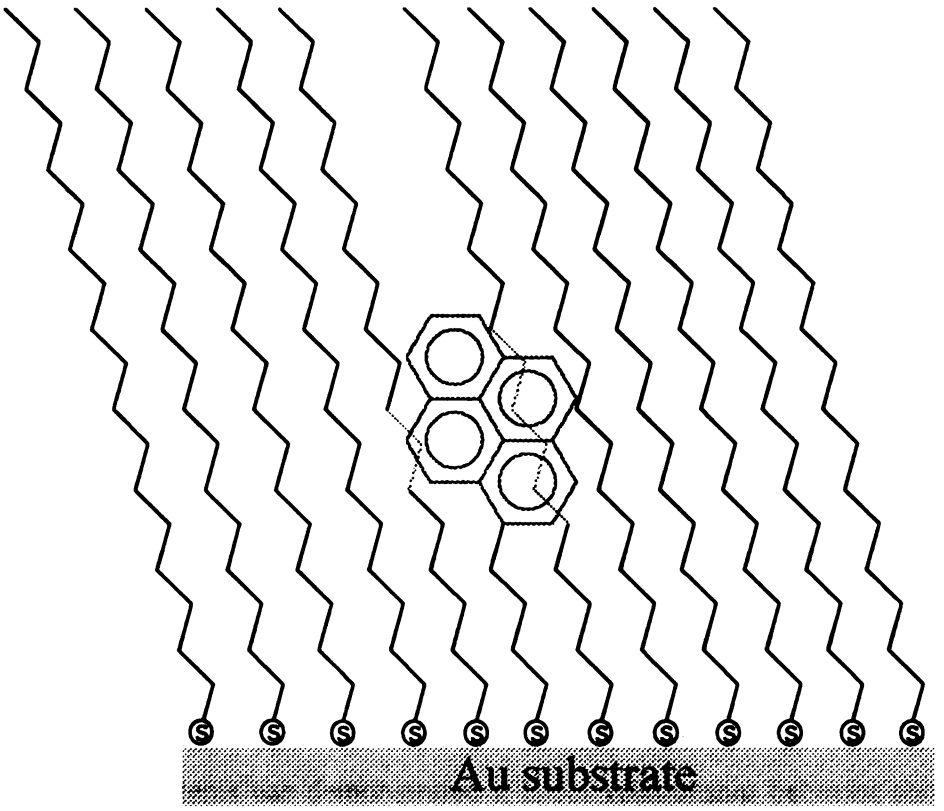

Figure 5.1. Qualitative schematic diagram of the alkanethiol/gold interface with the tethered 4-(1-pyrenyl)-1-butanethiol chromophore present.

5.2. Experimental

The substrates used were formed from evaporated gold that yields predominantly Au(111) microcrystalline domains.[9,10] The 4-(1-pyrenyl)-1-butanethiol was synthesized in our laboratories[25] by the reaction of 4-(1-pyrenyl)-1-butanol with thionyl chloride to form 4-(1-pyrenyl)-1-chlorobutane and, subsequently with thiourea to yield 4-(1-pyrenyl)-1-butanethiol.[26] 1-Octadecanethiol was purchased from Aldrich and used as received. The monolayers were formed from *n*-hexane solution, with $5x10^{-6}$ M 4-(1-pyrenyl)-1-butanethiol and $9.5x10^{-5}$ M 1-octadecanethiol concentrations. We characterized the thiol/gold monolayers with external reflectance FTIR (Nicolet 550, liquid nitrogen cooled MCT-A detector). The FTIR measurements indicated highly ordered structures characteristic of long chain alkanethiol/gold monolayer assemblies. Work on similar systems has demonstrated a linear relationship between chromophore fractional concentration in solution and in the formed monolayer.[27]

Time-correlated single photon counting (Chapter 4, Figure 4.1) was used to perform the time resolved emission measurements necessary for these studies.[28,29] We used a mode-locked CW Nd:YAG laser (Quantronix 416) to pump a cavity dumped dye laser (Coherent 702) operated at 630 nm using Kiton Red laser dye (Exciton). The output of the dye laser was typically 100 mW average power at 10 MHz repetition rate, with ~5 ps pulses. A fraction of the light is used as a reference beam, with the remaining light being frequency doubled to provide the 315 nm excitation of the pyrene chromophore. The polarization of the excitation beam is set to be vertical and, using a Glan-Taylor prism, emission polarization is selected either parallel or perpendicular to the excitation polarization. The instrument response function of this system is typically

30 ps FWHM. The dynamical information is obtained from the experimental data through R(t).

$$R(t) = \frac{I_{\parallel}(t) - I_{\perp}(t)}{I_{\parallel}(t) + 2I_{\perp}(t)} \qquad [5.1]$$

Where $I_{\parallel}(t)$ and $I_{\perp}(t)$ are experimental signal intensities for emission parallel and perpendicular to excitation polarizations. For all measurements, the samples were made just prior to measurement and the data were taken for the sample in air.

5.3. Results and Discussion

The tethered chromophore system we report here is modeled best as a hindered rotor according to Lipari and Szabo's treatment.[30] In this model, the motion of the chromophore is described as being confined within a cone of semi-angle $2\theta_0$ and with θ the average tilt angle of the chromophore within the cone (Figure 5.2). R(t) represents a re-randomization of the chromophore orientational distribution within the confining cone subsequent to the optical selection of a non-random subset of all chromophores within the monolayer.

$$R(t) = R(\infty) + \left[R(0) - R(\infty)\right]\exp(-t/\tau) \qquad [5.2]$$

The quantity R(0) is related to the angle between the excited and emitting transition moments of the probe. $R(\infty)$ is related to θ, the average tilt angle of the chromophore within the cone, and the quantity $R(\infty)/R(0)$ is related to θ_0, the maximum tilt angle within the cone.

We detect non-aggregated pyrene emission at 400 ± 30 nm. The use of a wide detection bandwidth was necessary owing to the weak signal recovered from our sample.

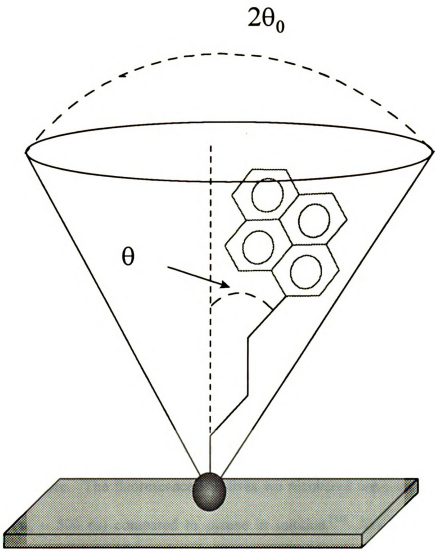

Figure 5.2. Schematic of the hindered rotor model used in interpretation of the R(t) data. The cone semi-angle $2\theta_0$ and the average chromophore tilt angle, θ, are indicated.

We sampled ~ 10^9 chromophore molecules in a typical experiment. The signal was attenuated significantly by chromophore-to-metal dipolar coupling, a well known quenching mechanism.[31,32] The emission near 400 nm is characteristic of individual pyrene molecules and not pyrene excimer (see Chapter 4). At the low chromophore concentrations we used, the chromophores are not expected to aggregate on the surface, but are dispersed within the alkanethiol monolayer. Even if undetectable aggregation is occurring in these monolayers, however, we are spectrally excluding any excimer contribution to our data because the monomer and excimer emission bands of the pyrene chromophore are well isolated from one another. We observe a non-exponential time decay of the fluorescence intensity (Figure 5.3) and attribute this behavior to heterogeneity of chromophore binding sites within the monolayer assembly.[33] Unfortunately, the limited signal-to-noise ratio of the data precludes the use of any detailed fitting analysis which could provide insight into the site distribution sampled by the chromophore. The fluorescence half-lives we recovered were very short for these systems ($\tau_{½}$ ~ 500 ps) compared to pyrene in solution.[34] We attribute the shorter lifetimes to at least three quenching mechanisms: Dipolar coupling of the chromophore to the metal, pyrene's sensitivity to the surrounding environment, and the possible presence of oxygen. We do not have the means to determine the relative importance of each of these quenching mechanisms at present, but note that the presence of O_2 may not be an important factor based on other experiments on alkylated pyrene that show only a limited sensitivity to this quenching agent.[35]

We have studied the linear optical response of pyrene previously,[34] and have found that the dominant absorption and emission transition moments are polarized

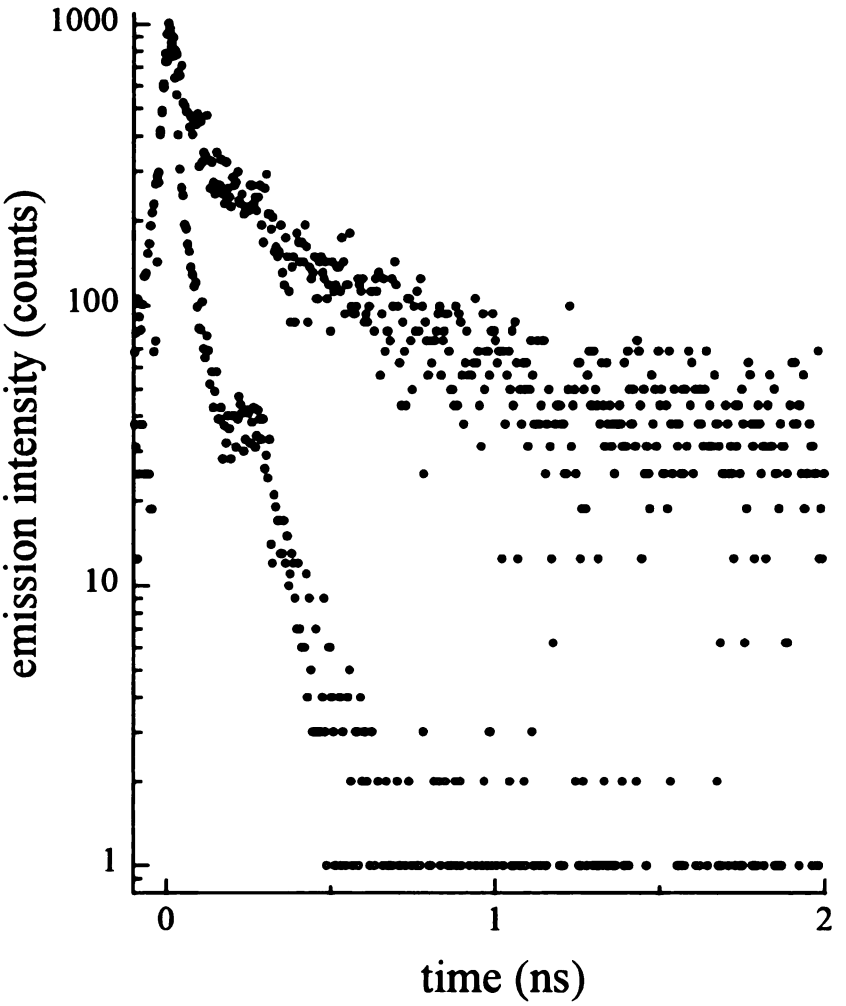

Figure 5.3. Experimental time resolved emission intensity data for a monolayer of 5% 4-(1-pyrenyl)-1-butanethiol and 95% 1-octadecanethiol on Au. The data (solid circles) are plotted on a $\log_{10}$ scale to underscore the non-exponential nature of the decay. The instrument response function is shown as open circles.

nominally perpendicular to each other, a condition which gives rise to the negative R(0) we observe experimentally. The dynamical response recovered from these monolayers revealed the absence of fast chromophore motion deep within the monolayer. The R(t) data (Figure 5.4) indicate that the intrinsic anisotropy in the system is constant over several probe lifetimes (nanoseconds), pointing to either a highly rigid system or an extremely free local environment, where the dynamics proceed within much less than the 30 ps response time of the spectrometer. We believe that the environment is rigid, based on the expected stick limit free-rotor reorientation time of τ_{OR} = 220 ps for 4-(1-pyrenyl)-1-butanethiol in *n*-hexadecane, a time regime that we can access easily. We attribute the rigidity of the alkanethiol/gold system to the efficient aliphatic chain packing of alkanethiol/gold monolayers about the tethered probe. We expect that, if we tethered the pyrene with a longer alkane chain, we would observe rotational motion since the pyrene would reside in a less rigid area of the alkane chain structure.[36] This assumption is consonant with simulations of these systems suggesting that the alkyl chains are rigid near the surface and less rigid near the ends of the monolayer.[37]

Despite the absence of measurable chromophore motion, we are able to apply the hindered rotor model to our data,

$$R(\infty) = -0.2\left\langle P_2(\cos\theta)\right\rangle^2 \qquad [5.3]$$

At t = 0, we detect the sum of the anisotropies present within the system, [R(0) + R(∞)], and from solution phase measurements of 4-(1-pyrenyl)-1-butanethiol, R(0) = -0.05.

From these data, the contribution to R(t) from the structural rigidity of the monolayer is R(∞) ≅ -0.10, yielding the average tilt angle of the chromophore within the

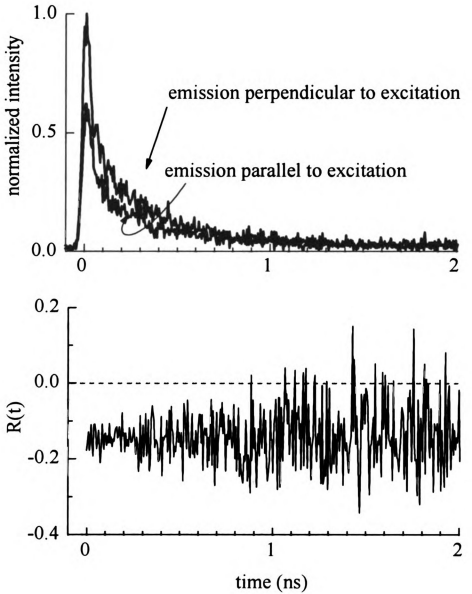

Figure 5.4. Top panel: Experimental emission intensity data for a monolayer comprised of 5% 4-(1-pyrenyl)-1-butanethiol and 95% 1-octadecanethiol on Au. Note that $I_{\perp}(t)$ is more intense than $I_{\parallel}(t)$, as is expected for pyrene. Bottom panel: R(t) data calc ulated from the raw experimental data using Eq. 5.1.

cone of $\theta = 26°$. This value correlates well to the accepted value of 30° for the tilt angle of alkane chains in alkanethiol/gold monolayers determined by external reflectance FTIR spectroscopy.

5.4. Conclusions

We have demonstrated, for the first time, a viable method for probing motional dynamics within monolayer assemblies that is sensitive to selected regions *within* the layer. The results we obtained are fully consistent with known properties of alkanethiol/gold monolayer systems. We have shown experimentally that alkanethiol/gold monolayers are quite rigid in the intermediate region between the substrate and the top on the interface, and measurements are underway to probe different regions of these monolayer assemblies.

5.5. Literature Cited

1. C.-J. Zhong, M. D. Porter, *Anal. Chem.*, **1995**, *67*, 709A.

2. N. Lewis, M. Tarlov, *J. Am. Chem. Soc.*, **1995**, *117*, 9574.

3. R. J. Willicut, R. L. McCarley, *Langmuir*, **1995**, *11*, 296.

4. L. H. Dubois, B. R. Zegarski, R. G. Nuzzo, *J. Am. Chem. Soc.*, **1990**, *112*, 570.

5. R. G. Nuzzo, E. M. Korenic, L. H. Dubois, *J. Chem. Phys.*, **1990**, *93*, 767.

6. E. B. Troughton, C. D. Bain, G. M. Whitesides, R. G. Nuzzo, D. L. Allara, M. D. Porter, *Langmuir*, **1988**, *4*, 365.

7. M. D. Porter, T. B. Bright, D. L. Allara, C. E. D. Chidsey, *J. Am. Chem. Soc.*, **1987**, *109*, 3559.

8. R. L. McCarley, Y.-T Kim, A. J. Bard, *J. Phys. Chem.*, **1993**, *97*, 211.

9. D. S. Karpovich, G. J. Blanchard, *Langmuir*, **1994**, *10*, 3315.

10. H. M. Schessler, D. S. Karpovich, G. J. Blanchard, *J. Am. Chem. Soc.*, in press.

11. C. A. Widrig, Chinkap Chung, M. D. Porter, *J. Electroanal. Chem.*, **1991**, *310*, 335.

12. C.-J. Zhong, M. D. Porter, *J. Am. Chem. Soc.*, **1994**, *116*, 11616.

13. D. E. Weishaar, M. M. Walczak, M. D. Porter, *Langmuir*, **1993**, *9*, 323.

14. C. D. Bain, G. M. Whitesides, *Science*, **1988**, *240*, 62.

15. J. L. Wilbur, H. A. Biebuyck, J. C. MacDonald, G. M. Whitesides, *Langmuir*, **1995**, *11*, 825.

16. R. A. Drawhorn, N. L. Abbott, *J. Phys. Chem.*, **1995**, *99*, 16511.

17. Y. Xia, X.-M. Zhao, E. Kim, G. M. Whitesides, *Chem. Mater.*, **1995**, *7*, 2332.

18. J. F. Ford, T. M. Vickers, C. K. Mann, J. B. Schlenoff, *Langmuir*, **1992**, *12*, 1944.

19. E. Kim, G. M. Whitesides, L. K. Lee, S. P. Smith, M. Prentiss, *Adv. Mater.*, **1996**, *8*, 139.

20. L. Sun, R. M. Crooks, *Langmuir*, **1993**, *9*, 1775.

21. L. Sun, L. J. Kepley, R. M. Crooks, *Langmuir*, **1992**, *8*, 2101.

22. M. J. Wirth, J. D. Burbage, Anal. Chem., **1991**, *63*, 1311.

23. J. W. Carr, J. M. Harris, Anal Chem., **1986**, *58*, 626.

24. J. W. Carr, J. M. Harris, *J. Chromatog.*, **1989**, *481*, 135.

25. M. Pallmer, private communication.

26. G. A. Page, D. S. Tarbell, *J. Am. Chem. Soc.*, **1953**, *75*, 2053.

27. J. C. Horne, G. J. Blanchard, *J. Am. Chem. Soc.*, in review.

28. G. R. Holtom, *Proc. SPIE*, **1990**, *1204*, 2.

29. L. DeWitt, G. J. Blanchard, E. LeGoff, M. E. Benz, J.-H. Liao, M. G. Kanatzidis, *J. Am. Chem. Soc.*, **1993**, *115*, 12158.

30. G. Lipari, A. Szabo, *Biophys. J.*; **1980**, *30*, 489.

31. R. R. Chance, A. Prock, R. Silbey, *J. Chem. Phys.*, **1975**, *62*, 2245.

32. R. R. Chance, A. Prock, R. Silbey, Adv. *Chem. Phys.*, **1978**, *37*, 1.

33. H. Wang, J. M. Harris, *J. Phys. Chem.*, **1995**, *99, 16999.*

34. D. S. Karpovich, G. J. Blanchard, *J. Phys. Chem.*, **1995**, *99*, 3951.

35. J. J. Tulock, G. J. Blanchard, *J. Phys. Chem.*, in preparation.

36. S. J. Klatte, T. L. Beck, *J. Phys. Chem.*, **1995**, *99*, 16024.

37. J. Hautman, M. L. Klein, *J. Chem. Phys.*, **1989**, *91*, 4994.

Chapter 6

Adsorption of Organic Molecules onto Metal and Modified Interfaces. Evidence for Site-Specific Adsorption

Summary

We have studied the adsorption of organic molecules from the vapor phase onto clean gold and thiol-modified gold surfaces using a controlled atmosphere chamber with an ellipsometer and a quartz crystal microbalance for simultaneous *in-situ* determinations of interfacial thickness and mass. Our results on maximum adsorbate mass uptake for each of the organic adsorbates are consistent with adsorption being dominated by dipole-induced dipole interactions for polar molecules and induced dipole-induced dipole interactions for non-polar molecules. For the thiol-modified surfaces, the extent of adsorption depends on the polarizability of the substrate. These data do not indicate the dominance of chemically selective interactions between the substrate and the adsorbate, but the relationship between interface thickness and adsorbed mass do indicate that the adsorbate layers are packed more densely than in their bulk liquid states. The packing densities we measure are consistent with site-specific adsorption, at least for the bare gold surface, where the data indicate adsorption to both types of three-fold sites present on the Au(111) surface.

6.1. Introduction

There has been considerable interest in designing chemically selective interfaces for use in sensing and separations applications. Organic-modified interfaces such as alkanethiol/gold monolayers have received extensive attention because they form readily, exhibit a high degree of order, and their structural and chemical properties (*e.g.* surface wettability, aliphatic chain ordering, electrochemical activity) have been determined.[1-48] Perhaps more important, their surface properties may be modified using thiol adsorbates with different ω-terminal functionalities.[1,10,49-52] Early studies of alkanethiol/gold monolayers used contact angle measurements to probe their wetting properties.[1,10] These studies gave intuitive insight into the interactions between the monolayers and macroscopic amounts of adsorbates (water and *n*-hexadecane), reinforcing the notion that interactions between adsorbates and interfaces can be understood within the same interpretive framework as intermolecular interactions in the liquid phase, where there are no restrictions on intermolecular alignment or distance. As interest in these systems has grown, monolayers with different terminal functionalities have been studied using these same approaches, and indications of chemical selectivity have been reported in certain cases. The Crooks group has focused on carboxylic acid terminated thiol/gold monolayers interacting with vapor-phase alkanoic acids, and they concluded from FTIR and ellipsometry data that hydrogen bonding played a dominant role in determining inter-layer attachment and organization.[50] Their subsequent work using Cu^{2+}-carboxylate terminated monolayers showed chemical selectivity for organophosphonates over simple organic solvents.[51] Crooks has also explored the use of nanoporous alkanethiol/gold monolayers where the porosity was induced by short hydroxyl terminated thiols.[53,54]

These systems exhibited size exclusion effects with a variety of redox-active molecules. These and other studies relate the selectivity of the monolayers to either chemically or structurally mediated interactions. These approaches to achieving chemical selectivity are based on the starting point that the interactions between adsorbates and interfaces can be understood in the same terms as solution phase intermolecular interactions. In this chapter, we present our studies on the interactions of organic vapor phase molecules with metal and thiol-modified substrates.

We have designed an apparatus that allows us to study both the mass and thickness change of interfacial films while adsorption of low molecular weight organic molecules from the vapor phase is proceeding. Our apparatus uses a controlled atmosphere chamber to house the sample. An optical ellipsometer is used for *in-situ* thickness measurement and a quartz crystal microbalance (QCM) is used as the substrate. This combination of measurement capabilities allows *in-situ* and real-time mass and thickness measurements to be made on the interfacial layers. We expose the substrates to an atmosphere of organic vapor and nitrogen gas and measure *in-situ* the mass and thickness of adlayers composed of the organic constituent. We used bare gold, 1-octadecanethiol/gold monolayers, 11-mercapto-1-undecanol (MUD)/gold layers and mixed MUD and 1-dodecanethiol/gold layers as substrates for adsorption of the selected organic species. From these studies we obtained two quantities; the maximum mass adsorbed and the relationship between adsorbed mass and adlayer thickness for each adsorbate/surface combination. The limiting mass data are related to the strength of adsorbate-surface interactions and the thickness versus mass data are related to the packing density of the adsorbed molecules at the surface. We used nonpolar (*n*-hexane

and cyclohexane), polar protic (methanol and water) and polar aprotic (acetonitrile and acetone) solvents as adsorbates. The data on these systems shed light on the dominant factors in the adsorbate-surface interactions and on the structural constraints imposed on the adlayers by the structure of the substrate. We find that chemically-specific interactions, such as hydrogen bonding, do not dominate the adsorption process but, rather, the efficiency of adsorption at these interfaces is determined primarily by the polarizability of the substrate. In addition, we find evidence that the atomic- or molecular-level structure intrinsic to the surface can affect the adsorbate layer packing density significantly.

6.2. Experimental

Controlled atmosphere chamber: The chamber used in this work is a stainless steel cube equipped with six 3.375" flange mounts (Huntington P/N VF-6-200). The chamber is mounted to an optical breadboard by one flange. The substrates we used were quartz crystal microbalances (QCMs) with polished, vapor deposited gold electrodes. The QCMs were suspended in the chamber from the top flange by a temperature controlled QCM holder (Maxtek). The temperature of the QCM was maintained at 1.0°C below the ambient (chamber) temperature for all experiments using a circulating bath. A BNC feed-through connector was used (top flange) to connect the QCM to its associated circuitry. The oscillator circuit (Maxtek P/N 124200-4) is powered by 5 VDC. We monitored the frequency with a universal frequency counter (Phillips PM 6673) equipped with an analog voltage output. This voltage was collected and stored electronically (IBM compatible PC).

Substrates: The QCMs (McCoy Electronics P/N 78-18-4, 6 MHz resonance frequency), were AT cut crystalline quartz and had polished, vapor deposited gold electrodes. The gold electrodes were cleaned using piranha solution (3:1 H_2O_2:H_2SO_4), rinsed with distilled water and dried before use. The electrodes were used either as bare gold surfaces or were modified with thiols. For these devices, the change in oscillation frequency depends on the mass adsorbed onto the crystal surface according to the Sauerbrey equation.[55]

$$\Delta f = \frac{-2\Delta m (f_o)^2 n}{A(\mu\rho)^{1/2}} \qquad [6.1]$$

Where n = the harmonic of the fundamental frequency (n = 1 here), ρ = the density of quartz (2.648 g/cm^3), μ = the shear modulus of quartz (2.947x10^{11}gcm^{-1}s^{-2}), A = the area of the deposit (0.33 cm^2), f_o = the fundamental frequency of the crystal (6 MHz), and Δm is the mass change of the crystal. For the QCMs that we use, we calculate the sensitivity to be 1 Hz decrease in frequency per 4 ng of adsorbed material, and this relationship is quantitative when using the QCM with gas phase adsorbates.[56,57] We note that slight variations in the QCM fundamental oscillation frequency result in a variation in sensitivity according the Eq. 6.1. We have determined that the slight variation in f_0 for the QCMs we use affects the sensitivity insignificantly when compared to other sources of uncertainty in our experiment.

Chamber optical and mechanical access. In two chamber faces, at right angles to one another, fused silica windows are mounted to permit the use of an optical ellipsometer. The windows are mounted with their surfaces at 25° with respect to the flange faces, such that the ellipsometer HeNe laser enters and exits the chamber normal

to the face of each window to preclude polarization changes associated with refraction. The ellipsometric angle of incidence is 70° with respect to the substrate surface normal. A vacuum system is connected to one flange for evacuation of the chamber. A butterfly valve isolates the chamber from the vacuum pump when not needed. One flange contains the inlet and outlet ports for the organic vapor/nitrogen gas stream. A schematic of the chamber is shown in Figure 6.1.

Adsorbate concentration control. We use a dynamic flow through approach to controlling the organic vapor atmosphere within the chamber (Figure 6.2). This method of atmospheric composition control ensures that the atmospheric composition within the chamber is not affected significantly by adventitious sources or sinks for organic adsorbates within the system. The nitrogen (AGA Gas, Inc.) is dried before its application to the gas blending system. The dry nitrogen line is split and sent to two adjustable flow meters (Cole Parmer P/N NO32-41). The maximum flow attainable with these meters is 148 cm^3/min N_2. One meter controls the flow of the dry nitrogen stream and the other meter is used to control the flow of the nitrogen stream through the gas washing bottle (the wet nitrogen source). The two gas streams are rejoined using a "T" fitting and sent through the chamber to a trap. The flow meters control the vapor concentration in the chamber atmosphere. We show in Table 6.1 the saturation concentration, expressed as mole fraction of adsorbate vapor in the wet nitrogen stream. These concentrations are, of course, proportional to the vapor pressures of the liquids used.

Adlayer thickness measurement: We used optical null ellipsometry for *in-situ* thickness measurements of adlayers.[58-61] The ellipsometer was constructed in-house

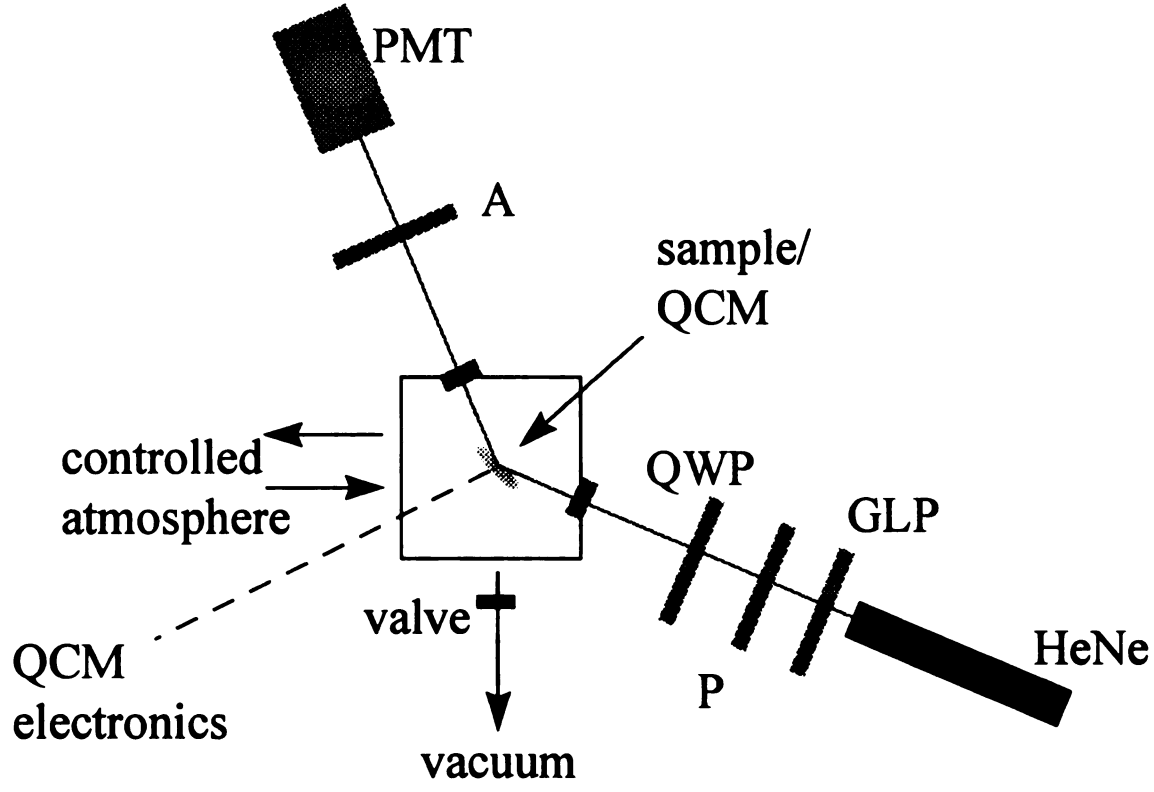

Figure 6.1. Top view schematic of the atmospheric chamber with incorporated ellipsometer. GLP = Glan-laser prism, P = polarizer, A = analyzer, QWP = quarter wave plate, PMT = photomultiplier detector and QCM = quartz crystal microbalance.

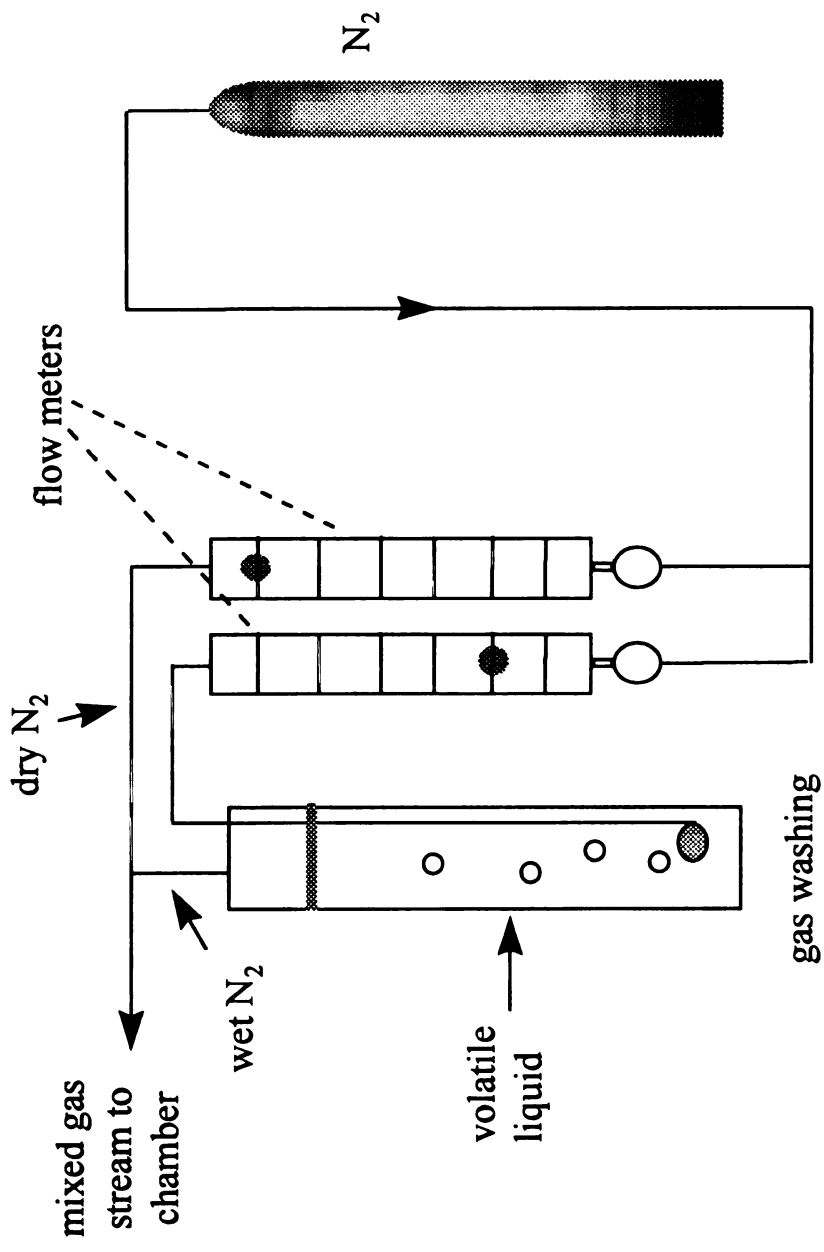

Figure 6.2. Schematic of the vapor generation and mixing system.

Table 6.1. Saturation concentrations of organic vapors in the "wet" nitrogen gas stream.

Adsorbate	mole fraction, X	vapor pressure at 20° C (Torr)
n-hexane	0.13	121
methanol	0.11	96
acetonitrile	0.09	73
cyclohexane	0.10	78
acetone	0.24	185
water	0.02	18

using discrete optical components as indicated in Figure 6.1. A linearly polarized HeNe laser (Melles-Griot, 1 mW) was used as the light source and a Glan-laser prism (Melles-Griot, extinction ratio 10^5) was used to ensure a linear polarization condition. A polarizer (P, CVI zero order $\lambda/2$ plate), and a $\lambda/4$ plate (CVI) are used to control the polarization condition of the light prior to its entrance into the chamber and reflection from the QCM. The light is incident on the sample at 70° with respect to the substrate normal. The polarization condition of the light is altered by reflection from the surface according to the optical constants of the substrate and the thickness and dielectric response of the adlayer(s). The reflected light passes through the analyzer (A, Melles-Griot Glan-laser prism) to a photomultiplier detector (RCA 1P28A). With the sample in place, the polarizer (P) and analyzer (A) are rotated until the minimum detector signal is achieved, and this set of readings is taken to be the optical null. The P and A readings are converted to the ellipsometric quantities Δ and ψ which are used to calculate the thickness of the adsorbed layer, given its refractive index. We use commercial software (Rudolph Research) for thickness calculations and a commercial automatic null ellipsometer (Rudolph Research AutoEL II) for calibration and comparison to our manual null ellipsometer. For all comparisons made, the data were identical. The commercial ellipsometer was used to measure the thickness of the thiol/gold monolayers directly after their formation due to the greater ease of sample manipulation with this system.

Chemicals and Materials: The thiol/gold monolayers were prepared by immersion of cleaned QCMs in 0.1 mM thiol (either 1-octadecanethiol or 11-mercapto-1-undecanol (MUD) solutions in *n*-hexane for 24 hours. We characterized the thiol/gold

monolayers with external reflectance FTIR using a Nicolet 550 FTIR with a liquid nitrogen cooled MCT-A detector. Mixed 1-dodecanethiol-MUD/gold layers were synthesized from 0.02 mM MUD, 0.08 mM 1-dodecanethiol in *n*-hexane solution. 1-Octadecanethiol and 1-dodecanethiol were purchased from Aldrich Chemical Co. and used as received. MUD was synthesized according to the method described by Frey *et al.*[49] The organic adsorbates *n*-hexane, methanol, acetone, acetonitrile, and cyclohexane were purchased from either Aldrich or Burdick and Jackson and were used as received. The water used in these experiments was in-house distilled water.

6.3. Results and Discussion

The principal foci of this work are understanding the forces that dominate adsorbate interactions with selected surfaces and the factors that are important to the organization of the adsorbate layers as they form. To address these two questions, we have determined saturation mass loadings of the adsorbates onto the surfaces and the relationship between adlayer mass and thickness up to the saturation mass loading. We studied adsorption to bare gold to establish a point of reference for the other substrates, and we consider the results for this surface first.

As can be seen from the data presented in Table 6.2, the maximum mass adsorbed onto the gold substrate was essentially constant for all adsorbates except water. The strength of interaction for the gold surface is dominated by the surface polarizability. We expect that the mass of adsorbed water achieved at maximum vapor concentration is substantially lower than that of the other adsorbates because of the limited vapor phase concentration of water in nitrogen. Earlier macroscopic wetting studies of gold surfaces

Table 6.2. Maximum mass and thickness uptake of adsorbates onto substrates.

adsorbate molecule	substrate	maximum mass (ng) ± 95% C.I.	maximum thickness (Å) ± 95% C.I.
n-hexane	gold	80 ± 10	14.3 ± 0.7
	1-octadecanethiol/gold	33 ± 2	8 ± 3
	MUD/gold	90 ± 1	15 ± 4
	mixed MUD and 1-dodecanethiol on gold	80 ± 20	17 ± 1
methanol	gold	90 ± 20	13 ± 2
	1-octadecanethiol/gold	24 ± 2	2 ± 1
	MUD/gold	110 ± 30	16 ± 5
	mixed MUD and 1-dodecanethiol on gold	110 ± 60	19 ± 4
acetonitrile	gold	60 ± 10	7 ± 2
	1-octadecanethiol/gold	20 ± 10	1.0 ± 0.5
	MUD/gold	50 ± 10	5 ± 1
	mixed MUD and 1-dodecanethiol on gold	60 ± 20	7 ± 2
acetone	gold	89 ± 9	12 ± 1
	1-octadecanethiol/gold	50 ± 10	1.3 ± 0.6
cyclohexane	gold	80 ± 20	12 ± 2
	1-octadecanethiol/gold	31 ± 4	31 ± 4
water	gold	30 ± 10	2 ± 2
	1-octadecanethiol/gold	not measurable	not measurable

indicated their hydrophilic nature.[1,10] A generally accepted implication of that work is that the gold surface will interact more strongly with polar adsorbates than with non-polar adsorbates. Our data do not support this broad implication, and we offer an explanation for this apparent inconsistency with intuition following consideration of the adsorption behavior of the selected other surfaces.

Compared to metallic gold, the 1-octadecanthiol/gold monolayer showed a much lower maximum mass uptake for all adsorbates. In addition, our data do not show any significant preference on the part of the 1-octadecanthiol/gold monolayer toward any adsorbate. We take from these data that the basic mechanism of interaction between adsorbate and surface is the same (equally non-selective) for both substrates, and that there is simply an absolute difference in the strength of adsorbate-surface interaction for the two substrates. A basic physico-chemical property that satisfies the constraint of non-selective interaction is the polarizability of the substrate. We expect that the metal surface is more polarizable than the aliphatic surface, and this expectation is in agreement with experimental data on strength of interaction.

While the postulation of adsorbate-surface interactions being dominated by the polarizability of the substrate is plausible, at least intuitively, we need to test this hypothesis using a substrate possessing a chemically selective functionality. Earlier studies by the Crooks group demonstrated hydrogen bonding interactions between vapor phase adsorbates and functionalized monolayer substrates.[50] Their data demonstrated adsorption of alkanoic acids a to carboxylic acid terminated thiol/gold layer, but not to an alkanethiol/gold monolayer. We have chosen to use hydroxyl-terminated monolayers (11-mercapto-1-undecanol, MUD) instead of carboxylic acid terminated monolayers as a

chemically selective surface. We made this choice based on the similar hydrodynamic radii of the -OH (1.60 Å) and -CH_3 (1.76 Å) groups,[62] in the hope that steric effects at the layer terminus would not affect overall ordering. Our data show that the interactions between all adsorbates and the full MUD/gold substrate are substantially the same, suggesting the same absence of chemical selectivity for this surface that we observed for both the clean gold and alkanethiol/gold surfaces. This is not necessarily a surprising result because adlayers of MUD on gold should exhibit significant intermolecular hydrogen bonding effects, precluding chemically selective interactions with adsorbates. In an effort to evaluate this possibility, we have compared data for adsorption to a full MUD/gold layer to that for a mixed MUD/1-dodecanethiol/gold interface. We observe no significant chemical selectivity on the part of the mixed surface for any of the adsorbates tested.

It is instructive at this point to consider the composition and structural properties of the full and mixed MUD surfaces. We have deliberately avoided referring to the MUD/gold systems as monolayers. Ellipsometric evidence suggests that MUD does not form simple monolayer structures. The measured thickness of a full MUD/gold assembly (23 Å) is essentially twice that of a 1-dodecanethiol/gold monolayer (12 Å). It is tempting, based on the integral relationship between these thickness values, to postulate that the MUD forms a bilayer structure spontaneously. Such a structure, however, would likely be accompanied by a significant level of organization within each layer. External reflectance FTIR measurements of these assemblies do not indicate a highly ordered structure compared to that observed for 1-dodecanethiol and 1-octadecanethiol monolayers on gold. These results leave open the possibility that the MUD adlayer

exists either as a disordered system in the form of a double layer or as an agglomerated multilayer and, in either case, it is not clear that the notion of discrete layers is appropriate. Attempts to remove overlayers of MUD by rinsing with excess methanol or ethanol were unsuccessful (*i.e.* no change in ellipsometric thickness), suggesting that interactions between MUD molecules in the assembly are chemical, not simply physical, in nature.

It is clear based on the ellipsometric data and washing experiments that hydrogen bonding between MUD molecules is important in determining the properties of the MUD/gold assemblies. Liquid alcohol hydrogen bonds are substantially the same strength as the thiol/gold interaction energy ($\Delta G_{ads} \sim -5.5$ kcal/mol).[18,63] It is likely that hydrogen bonding affects the formation and annealing of MUD/gold assemblies. The resulting structure will be held together by hydrogen bonds and attached to the surface by sulfur-gold bonds. Our results demonstrate that hydrogen bonding by the MUD assembly to adsorbates does not dominate the interactions we sense, indicating that the free energy of adsorption of small organic molecules is substantially less than -5 kcal/mol.

Our data for the MUD/gold systems indicate further the dominance of simple dipolar interactions in the adsorption process. Gold possesses a higher polarizability than aliphatic monolayer terminal CH_3 groups. In this model, both permanent and induced dipole moments mediate the strength of adsorbate-surface interactions. For the gold and alkanethiol substrates, there is no permanent dipole moment in the plane of the surface, and thus the polarizability of these media will determine their adsorption properties. For the MUD layers, it is not possible to distinguish the presence or absence

of a permanent dipole moment because of the comparatively limited information available on the mesoscopic structure of these assemblies. Thus for MUD/gold layers, either permanent or induced dipole moments may serve to mediate its interactions with polar and/or polarizable adsorbates.[64]

$$
\begin{aligned}
V &= -\frac{k}{r^6} \\
k &= \frac{2}{3k_B T}\left[\frac{\mu_a \mu_s}{4\pi\varepsilon_0}\right]^2 \qquad \text{(dipole-dipole interactions)} \\
k &= \frac{\mu_a^2 \alpha_s'}{4\pi\varepsilon_0} \qquad \text{(dipole-induced dipole interactions)} \\
k &= \frac{3\alpha_a' \alpha_s'}{2}\left[\frac{I_a I_s}{I_a + I_s}\right] \qquad \text{(induced dipole-induced dipole interactions)}
\end{aligned}
\qquad [6.2]
$$

The significance of Eqs. 6.2 is that all of these interactions operate over the same length scale, with the magnitude of the interaction potential being determined by the intrinsic properties of the substrate (*s*) and adsorbate (*a*), such as the polarizability (α'), permanent dipole moment (μ), and ionization energy (*I*). Because of their strong permanent dipole moments, methanol and acetonitrile can interact strongly with the polarizable surfaces. *n*-Hexane has a very small permanent dipole moment, and its interactions with the substrates will be mediated by the polarizabilities of both, implying the need for the interaction between several CH_x groups per adsorbate molecule and the substrate. The differences in substrate polarizabilities and/or dipole moments account for the high mass loading of all organic vapors on bare gold and hydroxyl-containing substrates compared to that achievable with the alkanethiol monolayers. Despite the strong interactions between adsorbates and the MUD/gold and the mixed MUD/gold

systems, we found no evidence for the dominance of hydrogen-bonding interactions over the less specific polar interactions described above.

To this point, we have considered the maximum mass loading of the various adsorbates onto the substrates. In addition, we have monitored the thickness change of the adlayers as a function of adsorbate mass. We determined these relationships by controlling the adsorbate concentration in the atmospheric chamber, as described in the Experimental section. We found a linear relationship between adlayer mass and thickness for all systems studied (Table 6.3 and Figure 6.3). The linear relationship between adlayer mass and thickness shows that adsorption to the surface is a statistical process, not affected significantly by aggregation. The relationship between mass and thickness is unique for each system, and there is chemical significance to these relationships, as we consider below.

In order to determine the adlayer densities, we must know the surface area of the QCM that is available for adsorption. The total surface area is the product of the macroscopic geometric surface area and the surface roughness factor, R (R = actual surface area/geometric surface area). Schlenoff *et al.* have reported surface roughness factors for gold surfaces made and treated in several different ways.[65] The values reported range from R = 1.2 for polished, annealed gold to R = 2.0 for gold sputtered onto glass; a perfectly smooth surface would have R = 1. The gold electrodes on our QCMs are vapor deposited and polished, and for this type of surface, Schlenoff *et al.* have reported that R = 1.44.[65] The geometric active area of the surfaces we use is 0.33 cm^2, and with the correction for surface roughness, the area available for adsorption onto the QCM surface is 0.48 cm^2. From the data presented in Table 6.3 and the active QCM

Table 6.3. Mass vs. thickness increase of adsorbates on substrates

adsorbate molecule	substrate	slope ± 95% C.I. mass/thickness (ng/Å)
n-hexane	gold	5.4 ± 0.4
	1-octadecanethiol/gold	5 ± 1
	MUD/gold	5.4 ± 0.8
	mixed MUD and 1-dodecanethiol on gold	5 ± 2
methanol	gold	6.5 ± 0.2
	1-octadecanethiol/gold	not measurable
	MUD/gold	6.7 ± 0.5
	mixed MUD and 1-dodecanethiol on gold	5 ± 2
acetonitrile	gold	8.0 ± 0.5
	1-octadecanethiol/gold	not measurable
	MUD/gold	8 ± 1
	mixed MUD and 1-dodecanethiol on gold	9 ± 2
acetone	gold	7.2 ± 0.8
	1-octadecanethiol/gold	not measurable
cyclohexane	gold	7.0 ± 0.6
	1-octadecanethiol/gold	7 ± 2
water	gold	not measurable
	1-octadecanethiol/gold	not measurable

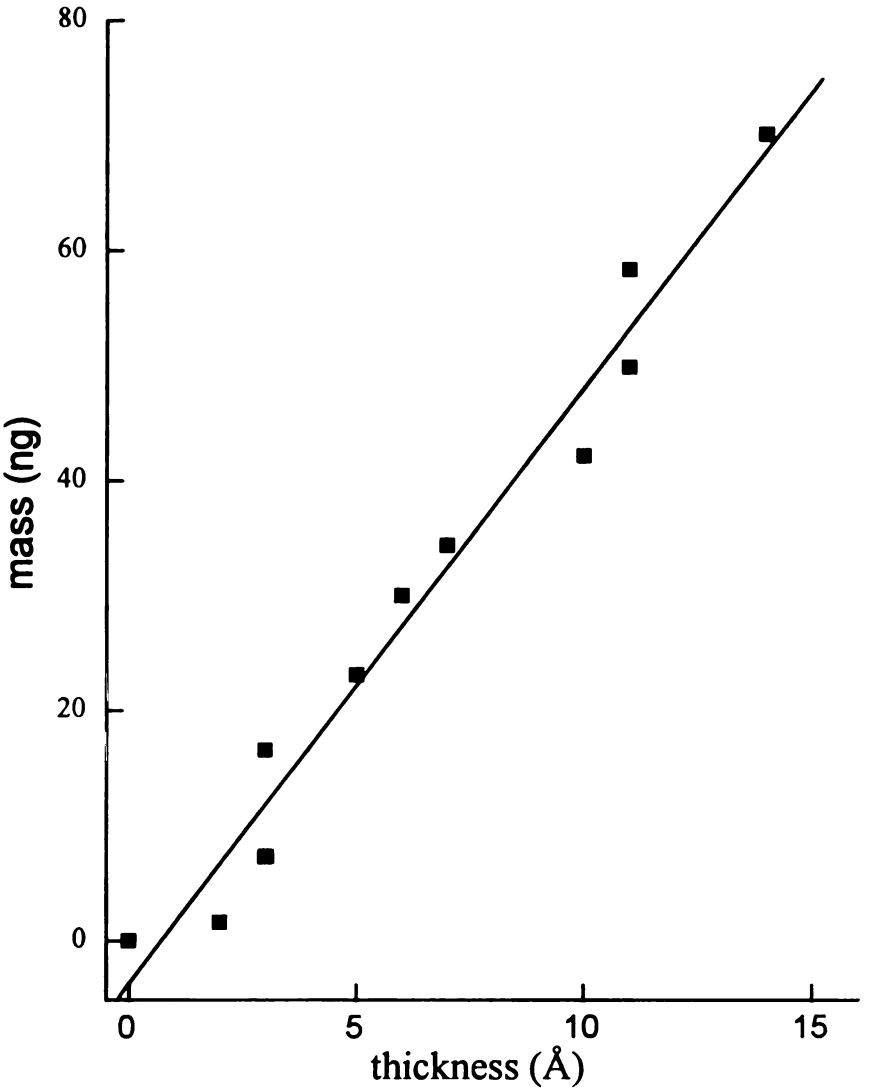

Figure 6.3. Plot of adsorbed mass vs. adlayer thickness of a gold surface while exposed to an atmosphere of *n*-hexane in nitrogen gas.

surface area, we calculate the densities of the adsorbed organic layers (Table 6.4). The values we obtain for the adlayer densities are substantially higher than densities of the corresponding bulk liquids, and these differences place important limits on the possible ways in which the adsorbates can interact with the substrates.

It is fair, of course, to consider that our ability to determine adlayer density is limited by our knowledge of the surface roughness factor, R. For the experimental densities to match the corresponding bulk liquid densities, we would have to adjust the surface roughness factor to be ~2.8, a quantity we believe to be unrealistically large given the optical and physical properties of the QCM electrodes. An R value of 2.8 implies a surface much rougher than sputtered gold on glass (R = 2.0) which is unlikely for polished, vapor deposited gold surfaces. Likewise, we recognize that our QCM surfaces are far from perfect (R = 1), and a value of R = 1.44 is entirely consistent with our knowledge of these surfaces. We believe the derived adlayer densities are approximately correct and, based on this starting point, consider the limits the density data place on adsorbate packing.

Using the calculated van der Waals volumes[62] and molecular weights, we calculate theoretical close-packed densities for the organic molecules (see Table 6.5) which are similar to our experimental densities. The volumes used for calculation of these densities do not include any free space between the molecules and therefore represent the extreme upper limit on densities attainable for these molecules. The theoretical close-packed densities are not, however, the preferred densities of the organic liquids, as indicated by comparison to experimental bulk liquid densities. The bulk liquid densities reflect the optimal intermolecular distances determined by the balance of

Table 6.4. Adsorbed layer densities calculated from mass/thickness values.

adsorbate molecule	substrate	density ± 95% C.I. (g/cm^3)
n-hexane	gold	1.13 ± 0.09
	1-octadecanethiol/gold	1.0 ± 0.3
	MUD/gold	1.1 ± 0.2
	mixed MUD and 1-dodecanethiol on gold	1.0 ± 0.4
methanol	gold	1.36 ± 0.05
	1-octadecanethiol/gold	not measurable
	MUD/gold	1.4 ± 0.1
	mixed MUD and 1-dodecanethiol on gold	1.1 ± 0.4
acetonitrile	gold	1.7 ± 0.1
	1-octadecanethiol/gold	not measurable
	MUD/gold	1.7 ± 0.3
	mixed MUD and 1-dodecanethiol on gold	1.9 ± 0.5
acetone	gold	1.5 ± 0.2
	1-octadecanethiol/gold	not measurable
cyclohexane	gold	1.5 ± 0.1
	1-octadecanethiol/gold	1.4 ± 0.4
water	gold	not measurable
	1-octadecanethiol/gold	not measurable

Table 6.5. Densities of adsorbates (g/cm^3).

adsorbate	bulk liquid density	Average experimental density[a] ± 95% C.I.	density from van der Waals volumes	density for site-specific model
n-hexane	0.66	1.1 ± 0.1	1.26	1.10
methanol	0.79	1.3 ± 0.2	1.33	0.58
acetonitrile	0.78	1.7 ± 0.2	1.45	0.70
acetone	0.79	1.5 ± 0.2	1.49	0.89
cyclohexane	0.78	1.4 ± 0.2	1.37	1.10

[a]Average for the adsorbates over all substrates

attractive and repulsive forces averaged over all orientations. To achieve a density different than that of the bulk liquid, an additional, external force must be exerted on the system. The attractive and repulsive forces between adsorbate molecules are nominally constant or, at worst, are altered only slightly by any molecular directionality enforced by adsorption. The external force responsible for this change in density must result from interactions of the adsorbates with the substrate. For the substrate to affect the inter-adsorbate distance, the adsorbate to substrate interactions must be site specific.

For simplicity, we treat the Au surface first, because it possesses the greatest surface order of the substrates we have used. We consider that the QCM surfaces are comprised of predominantly Au(111) and, thus it is possible to estimate the geometric constraints imposed by the adsorption sites. In the hexagonal close packed structure of Au(111), the spacing between each gold atom is 5 Å.[66] There are interstitial sites located at voids formed by three gold atoms, 2.89 Å apart from one another. There are two types of these interstitial sites; those where a gold atom resides directly beneath the void, and those in which there is no gold atom beneath. The nearest-neighbor spacing between identical interstitial sites is 5 Å. Based on our findings that indicate adsorbate and substrate polarizabilities mediate the attractive interactions, we expect substrate electron density to play an important role in determining the identities of the adsorption sites. The most polarizable site on the Au surface will be the interstitial site with a gold atom directly beneath the void, providing the adsorbate with at least partial access to four gold atoms. The next most favorable site is the interstitial site without a gold atom beneath. The least favorable site, in terms of available electron density is at the "top" of each gold atom.

Adsorption to one type of site will occur at a higher rate than that for the other types of sites and, while there may be an equilibrium between adsorption at each class of sites, the most electron-rich sites will be occupied most frequently. With an inter-site spacing of 5 Å for a given type of site, we calculate that the available QCM surface has ~2.2 x 10^{14} sites. Using this site density, adsorbate molecular mass, and the adsorbate radius extracted from its van der Waals volume, we calculate the density of adsorbate monolayers expected from site-specific adsorption. These calculated site-specific densities are shown in Table 6.5 along with the experimental and theoretical close-packed densities. The experimental monolayer densities are much higher than the bulk densities and are consistent with theoretical close packed densities. The site specific densities in Table 6.5 are also consistent for the larger adsorbate molecules cyclohexane and *n*-hexane, but are too small for the other adsorbate molecules. We have calculated the site specific densities assuming that only the most preferred site is occupied. In the case of methanol and acetonitrile, occupying only one type of site yields densities smaller than those of the corresponding bulk liquid. If methanol, acetonitrile, and acetone occupied both of the three-fold interstitial sites, the site-specific densities would be twice those shown in Table 6.5 and consistent with the experimental adlayer densities. We emphasize that, while our model is qualitative in nature, its predictions correspond remarkably well to the experimental data, lending credence to the notion that variations in substrate polarizability over molecular length scales determine the packing properties of physisorbed adlayers.

Our data indicate that the hexanes adsorb to only one type of site while the other adsorbates occupy both types of three-fold interstitial sites, consistent with the steric

constraints imposed by these comparatively large adsorbates. In addition, due to the comparatively small polarizabilities of these aliphatic molecules, it is likely that more than one CH_x group per molecule is involved in interactions with the substrate, a condition that would serve to obscure neighboring substrate sites.

We have applied the site-specific adsorption model to the gold substrate, and now consider its application to 1-octadecanethiol/gold monolayers. The terminal CH_3 groups of alkanethiol/gold monolayers have been shown to exhibit ordering that corresponds to the gold surface structure.[11,14] Based on this structural feature, we expect similar adsorbate alignment effects to be important for this non-polar monolayer, although its influence may not be as pronounced as it is for the gold surface. We do not know the exact structure of the MUD/gold systems, but we do know that the maximum achievable density of the hydroxyl groups is limited by gold surface structure. The hydroxyl groups possess lone pairs of electrons with which the adsorbates will interact. Our results show the same behavior on the mixed MUD/1-dodecanethiol/gold systems as the MUD/gold systems indicating similar structure. It is likely that during the formation of the substrates that the MUD molecules adsorbed preferentially to the 1-dodecanthiol molecules thus giving essentially a MUD/gold system with less 1-dodecanethiol content than in solution.

6.4. Conclusions

We have studied the interactions of organic molecules in the vapor phase to gold, polar thiol/gold monolayers and non-polar alkanethiol/gold monolayers. We find that the interactions between the adsorbates and substrates are dominated by their polarizabilities. We do not find evidence for chemical functionality-specific interactions in these systems, and these data place limitations on the utility of thiol/gold systems for selective chemical sensing applications. In addition, because the measurement scheme we have reported here yields information on the density of the adsorbate layers, we have been able to determine that the atomic- or molecular-scale organization of the substrate determines the packing density and organization of the first adsorbate layer.

6.5. Literature Cited

1. R. G. Nuzzo, L. H. Dubois, D. L. Allara, *J. Am. Chem. Soc.*, **1990**, *112*, 558.

2. L. H. Dubois, B. R. Zegarski, R. G. Nuzzo, *J. Am. Chem. Soc.*, **1990**, *112*, 570.

3. R. G. Nuzzo, E. M. Korenic, L, H. Dubois, *J. Chem. Phys.*, **1990**, *93*, 767.

4. C. E. D. Chidsey, D. N. Loiacono, *Langmuir*, **1990**, *6*, 682.

5. C. E. D. Chidsey, C. R. Bertozzi, T. M. Putvinski, A. M. Muscje, *J. Am. Chem. Soc.*, **1990**, *112*, 4301.

6. C. D. Bain, E. B. Troughton, Y. T. Tao, J. Evall, G. M. Whitesides, R. G. Nuzzo, *J. Am. Chem. Soc.*, **1989**, *111*, 321.

7. C. D. Bain, G. M. Whitesides, *J. Am. Chem. Soc.*, **1989**, *111*, 7155.

8. E. B. Troughton, C. D. Bain, G. M. Whitesides, R. G. Nuzzo, D. L. Allara, M. D. Porter, *Langmuir*, **1988**, *4*, 365.

9. M. D. Porter, T. B. Bright, D. L. Allara, C. E. D. Chidsey, *J. Am. Chem. Soc.*, **1987**, *109*, 3559.

10. G. M. Whitesides, P. E. Laibinis, *Langmuir*, **1990**, *6*, 87.

11. N. Camillone III, C. E. D. Chidsey, G.-Y. Liu, T. M. Putvinski, G. C. Scoles, J. Wang, *J. Chem. Phys.*, **1991**, *94*, 8493.

12. C. E. D. Chidsey, G.-Y. Liu, J. Wang, *Langmuir*, **1990**, *6*, 1804.

13. S. R. Wasserman, G. M. Whitesides, I. M. Tidswell, B. M. Ocko, P. S. Pershan, J. D. Axe, *J. Am. Chem. Soc.*, **1989**, *111*, 5852.

14. C. A. Widrig, C. A. Alves, M. D. Porter, *J. Am. Chem. Soc.*, **1991**, *113*, 2805.

15. G.-Y. Liu, M. B. Salmeron, *Langmuir*, **1994**, *10*, 367.

16. R. L. McCarley, Y.-T. Kim, A. J. Bard, *J. Phys. Chem.*, **1993**, *97*, 211.

17. R. L. McCarley, D. J. Dunnaway, R. J. Willicut, R. J.; *Langmuir*, **1993**, *9*, 2775.

18. D. S. Karpovich, G. J. Blanchard, *Langmuir*, **1994**, *10*, 3315.

19. C. A. Widrig, Chinkap Chung, M. D. Porter, *J. Electroanal. Chem.*, **1991**, *310*, 335.

20. C.-J. Zhong, M. D. Porter, *J. Am. Chem. Soc.*, **1994**, *116*, 11616.

21. D. E. Weishaar, M. M. Walczak, M. D. Porter, *Langmuir*, **1993**, *9*, 323.

22. C. A. Alves, E. L. Smith, M. D. Porter, *J. Am. Chem. Soc.*, **1992**, *114*, 1222.

23. D.-J. Zhong, M. D. Porter, *Anal. Chem.*, **1995**, *67*, 709A.

24. D. E. Weishaar, B. D. Lamp, M. D. Porter, *J. Am. Chem. Soc.*, **1992**, *114*, 5860.

25. E. L. Smith, C. A. Alves, J. W. Anderegg, M. D. Porter, L. M. Siperko, *Langmuir*, **1992**, *8*, 2707.

26. E. L. Smith, M. D. Porter, *J. Phys. Chem.*, **1993**, *97*, 8032.

27. M. O. Wolf, M. A. Fox, *Langmuir*, **1996**, *12*, 955.

28. J. M. Tour, L. Jones II, D. L. Pearson, J. J. S. Lamba, T. P. Burgin, G. M. Whitesides, D. L. Allara, A. N. Parikh, S. V. Atre, *J. Am. Chem. Soc.*, **1995**, *117*, 9529.

29. N. Lewis, M. Tarlov, *J. Am. Chem. Soc.*, **1995**, *117*, 9574.

30. R. J. Willicut, R. L. McCarley, *Langmuir*, **1995**, *11*, 296.

31. K. Sinniah, J. Cheng, S. Terrataz, J. E. Reutt-Robey, C. J. Miller, *J. Phys. Chem.*, **1995**, *99*, 14500.

32. R. L. Garrell, J. E. Chadwick, D. L. Severance, N. A. McDonald, D. C. Miles, *J. Am. Chem. Soc.*, **1995**, *117*, 11563.

33. J.-P. Bucher, L. Santesson, K. Kern, *Langmuir*, **1994**, *10*, 979.

34. E. Delamarche, B. Michel, H. Kang, Ch. Gerber, *Langmuir*, **1994**, *10*, 4103.

35. S.-C. Chang, I. Chao, Y.-T. Tao, *J. Am. Chem. Soc.*, **1994**, *116*, 6792.

36. P. Fenter, A. Eberhardt, P. Eisenberger, *Science*, **1994**, *266*, 1216.

37. N. Camillone III, P. Eisenberger, T. Y. B. Leung, P. Schwartz, G. Scoles, G. E. Poirier, M. J. Tarlov, *J. Chem. Phys.*, **1994**, *101*, 11031.

38. M. R. Anderson, M. Gatin, *Langmuir*, **1994**, *10*, 1638.

39. M. R. Anderson, M. N. Evaniak, M. Zhang, *Langmuir*, **1996**, *12*, 2327.

40. H. A. Biebuyck, C. D. Bain, G. M. Whitesides, *Langmuir*, **1994**, *10*, 1825.

41. H. Sellers, A. Ulman, Y. Shnidman, J. E. Eilers, *J. Am. Chem. Soc.*, **1993**, *115*, 9389.

42. Y.-T. Kim, R. L. McCarley, A. J. Bard, *Langmuir*, **1993**, *9*, 743.

43. S. E. Creager, L. A. Hockett, G. K. Rowe, *Langmuir*, **1992**, *8*, 854.

44. D. M. Collard, M. A. Fox, *Langmuir*, **1991**, *7*, 1192.

45. P. Krysinski, R. V. Chamberlain, M. M. Majda, *Langmuir*, **1994**, *10*, 4286.

46. O. Chailapakul, L. Sun, C. Xu, R. M. Crooks, *J. Am. Chem. Soc.*, **1993**, *115*, 12459.

47. L. Sun, R. M. Crooks, A. J. Ricco, *Langmuir*, **1993**, *9*, 1775.

48. R. C. Thomas, J. E. Houston, T. A. Michalske, R. M. Crooks, *Science*, **1993**, *259*, 1883.

49. B. L. Frey, D. G. Hanken, R. M. Corn, *Langmuir*, **1993**, *9*, 1815.

50. L. Sun, L. J. Kepley, R. M. Crooks, *Langmuir*, **1992**, *8*, 2101.

51. L. J. Kepley, R. M. Crooks, A. J. Ricco, *Anal. Chem.*, **1992**, *64*, 3191.

52. J-B. D. Green, M. T. McDermott, M. D. Porter, *J. Phys. Chem.*; **1996**, *100*, 13342.

53. O. Chailapakul, R. M. Crooks, *Langmuir*, **1993**, *9*, 884.

54. O. Chailapakul, R. M. Crooks, *Langmuir*, **1995**, *11*, 1329.

55. G. Z. Sauerbrey, *Z. Phys.*, **1959**, *155*, 206.

56. C.-S. Lu, *J. Vac. Sci. Tech.*, **1975**, *12*, 578.

57. J. Hlavay, G. G. Guilbault, *Anal. Chem.*, **1977**, *49*, 1890.

58. F. L. McCrackin, E. Passaglia, R. R. Stromberg, H. L. Steinberg, *J. Res. NBS*, **1963**, *67A*, 363.

59. R. W. Collins, Y. T. Kim, *Anal. Chem.*, **1990**, *62*, 887A.

60. H. G. Tompkins, A User's Guide to Ellipsometry, Academic Press, 1993.

61. R. M. A. Azzam, N. M. Bashara, Ellipsometry and Polarized Light, Elsevier, 1977.

62. J. T. Edward, *J. Chem. Ed.*, **1970**, *47*, 261.

63. H. M. Schessler, D. S. Karpovich, G. J. Blanchard, *J. Am. Chem. Soc.*, in press.

64. P. W. Atkins, Physical Chemistry, 4th Ed., W. H. Freeman and Co., 1990, pp. 655-660.

65. J. B. Schlenoff, M. Li, H. Ly, *J. Am. Chem. Soc.*, **1995**, *117*, 12528.

66. N. Camillone III, C. E. D. Chidsey, G.-Y. Liu, G. Scoles, *J. Chem. Phys.*, **1993**, *98*, 4234.

Chapter 7

Conclusions

When first discovered, self assembled monolayers appeared to posses ideal attributes for use in chemical sensor and microdevice patterning applications. Once made, their highly oriented structures were thought to be extremely stable and remain unchanged. However, the QCM formation studies described in Chapter 2 indicate that alkanethiol/gold monolayers are structurally dynamic in nature with the thiols exhibiting mobility mediated by desorption and re-adsorption. The existence of structural mobility limits the use of SAMs for applications such as patterning. The results reported in Chapter 3 support further the notion of structurally dynamic systems and provide a thermodynamic perspective by determination of ΔH and ΔS for adsorption. The small free energy for the adsorption of thiols onto gold was a result of the balance of favorable enthalpic and countering entropic terms. These findings have a broader application, beyond the scope of model alkanethiol/gold systems, since it is the balance of such forces that determines the strength of interactions of molecules with surfaces. These studies underscore the importance of entropy to any adsorption process

While alkanethiol mobility across gold may limit patterning applications of thiol/gold SAMs, it has limited bearing on the average structure of the SAMs. The average properties of model alkanethiol/gold monolayers can be used to study fundamental interfacial phenomena. The average structure at the molecular level is important in determining monolayer interactions with adsorbing molecules. A novel measurement scheme presented in Chapter 5 revealed information about the dynamics of

the aliphatic chains. It was found that local environment formed by the aliphatic chains is rigid on short, (picosecond to nanosecond) timescales. This apparent rigidity limits the possibilities of elastic interactions with other molecules. Because of this rigidity and the close packing of the aliphatic chains, it is also unlikely that molecules would be able to penetrate into the monolayers, thus limiting interactions to the terminal areas of the monolayers.

The interactions of gas phase adsorbate molecules with gold and thiol modified gold substrates were reported in Chapter 6. It was found that methyl terminated alkanethiol/gold monolayers did not interact as strongly with low molecular weight organic molecules as do gold or hydroxyl terminated thiol/gold layers. The differences in the strengths of interactions were correlated to the polarizabilities of substrates. Chemical specificity on the part of the substrates toward interactions with the adsorbates was not observed despite the similarity of some adsorbates to the substrates (alcohols with -OH terminated layers and *n*-hexane with aliphatic monolayers). The lack of chemical specificity is not surprising for the thiol/gold monolayers given their apparent rigidity (see Chapter 5). Adsorbates would only be able to interact with terminal methyl groups in the 1-octadecanethiol/gold monolayers, thus it is not surprising that *n*-hexane, for instance, did not adsorb preferentially to other adsorbates. It is evident, based on these studies, that true chemically selective substrates cannot be made without adding more complexity to the interface. In addition, the adsorbates formed adlayers that were more dense than their liquid counterparts. The densities of the adlayers were consistent with site specific adsorption. Thus adlayer packing is determined by the organization of the substrate.

It is evident that alkanethiol/gold monolayers are very useful, although for applications different than originally thought. They are useful model systems for studying adsorption processes and interfacial structural dynamics as demonstrated in this thesis. The fundamental knowledge gained from studying the formation of alkanethiol/gold monolayers can be used to design more robust structures. The reorientational dynamics measurements of the tethered pyrene within alkanethiol/gold monolayers demonstrate a novel technique useful for probing motional dynamics within interfacial systems. The studies of the interactions of gas phase organic adsorbates with the gold and thiol modified gold served to demonstrate *in-situ* mass and thickness measurements as well as provide fundamental information about the interaction of molecules with surfaces.